10 Agent-based cell modeling: application to breast cancer[1]

With P. Macklin and M.E. Edgerton

In Chapter 6, we discussed an agent-based cell model that can be applied to a variety of biological systems, with a particular emphasis on epithelial cancers. We now illustrate the model by applying it to breast cancer and demonstrating its use in obtaining theoretical biologic and clinical insight, including quantitative predictions that can be assessed using patient immunohistochemistry and histopathology data. Theoretical biologic and clinical significance are discussed.

10.1 Introduction

Ductal carcinoma in situ (DCIS) is the most prevalent precursor to invasive breast cancer (IC), the second-leading cause of death in women in the United States. The American Cancer Society predicted that 50,000 new cases of DCIS alone (excluding lobular carcinoma in situ) and 180,000 new cases of IC would be diagnosed in 2007 [348, 25]. Co-existing DCIS is expected in 80% of IC, or 144,000 cases [399]. Because DCIS is a known precursor to IC, this leads us to hypothesize that up to 75% of DCIS cases progress to invasion prior to detection by screening mammography. While DCIS itself is not life-threatening, it is a very important precursor to IC because (1) it can be treated and (2) if left untreated, it is likely to progress to IC, which is a deadly disease [518, 370, 585].

Women prefer breast conserving surgery (BCS), also known as lumpectomy, versus complete mastectomy to treat DCIS [620]; in the United States today, approximately two-thirds of women diagnosed with DCIS will opt for BCS over mastectomy. Women who undergo BCS face two problems. First, an estimated 38-72% of women seeking BCS will not have their entire tumor removed in one surgery and may require up to three surgeries (called re-excisions) for complete removal of the DCIS [136, 108, 180]. Second, DCIS recurs at the same location greater than 20% of the time in patients who undergo BCS alone [528]. To combat this recurrence, women are advised to undergo radiation therapy to the breast, which induces residual cells of DCIS to apoptose. Even in women who have been treated with surgery and radiation, DCIS recurs approximately 10% of the

[1] This chapter is an extension of the work by Macklin et al. (2009) [435], and an advance copy of the work to be submitted by Macklin et al. in [436] and Edgerton et al. in [196].

time [528]. Half of these recurrences already show progression to invasive cancer (IC). The single most important underlying problem that contributes to both re-excisions and to recurrences is DCIS that is left inside the breast [619].

Hence, predicting the size and shape of DCIS is critical to successfully eradicating the disease in patients and preventing recurrences that often progress to deadlier invasive carcinoma. In addition, understanding the progression from DCIS to IC key to developing future treatments to improve patient survival. Mathematical modeling can play a role in both these tasks. In this chapter, we apply the agent-based model from Chapter 6 to DCIS. The model is well-suited to patient-specific calibration, can be modularly extended to focus attention on specific aspects of biological interest, and can be used for generating testable scientific hypotheses. The model presented here can be incorporated into a broader, multiscale framework (such as that discussed in Chapter 7) capable of making patient-specific, clinical predictions of DCIS outcome [194, 195, 138, 436].

10.1.1 Biology of breast duct epithelium

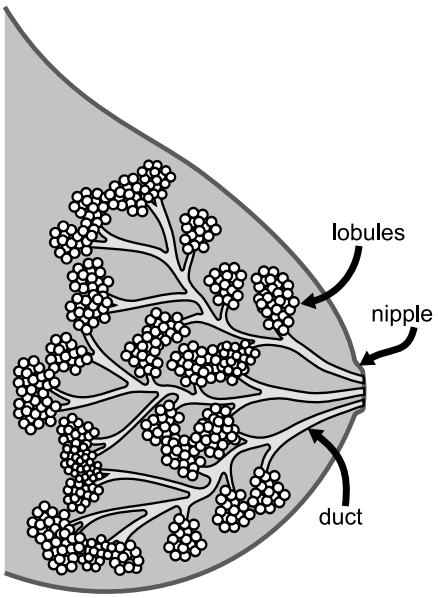

Figure 10.1 Breast duct tree architecture.

As an organ, the breast is organized as a system of 12-15 independent, largely parallel duct systems: clusters of milk-producing lobules that feed into a branched duct system that terminates at the nipple [690, 475, 506, 288]. See Figure 10.1. The duct systems are separated by supporting ligaments and fatty tissue and drained by the lymphatic system (not shown) [654]. The ducts have a well-characterized microarchitecture: each duct is a tubular arrangement of

epithelial cells, surrounded by myoepithelial cells (epithelial cells with muscle-like properties, such as contracting the duct to transport milk) and a basement membrane (hereafter BM). The center of the duct, known as the lumen, is filled with either milk (during lactation) or fluid. See Figure 10.2 (top left). Surrounding and supporting the duct is the stroma: a scaffolding of collagen and other fibers (collectively called the extracellular matrix, or ECM) that is secreted and maintained by fibroblasts. The stroma also contains blood vessels that supply oxygen, glucose, and growth factors to the tissue. A key aspect of this architecture is that the epithelial cells in the breast duct have no direct access to oxygen and nutrients; instead, these must diffuse into the duct through the BM.

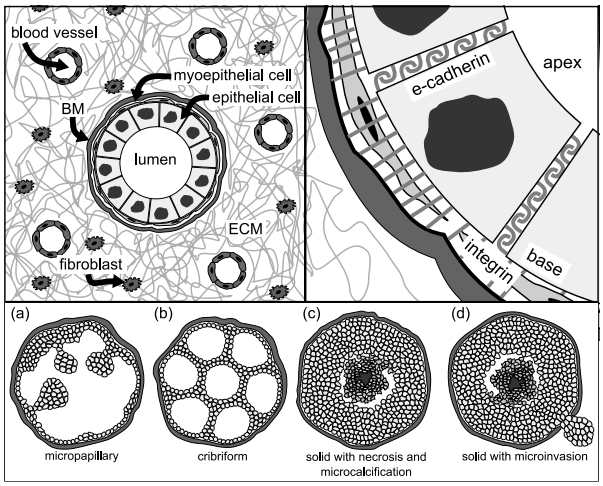

Figure 10.2 **Top Left:** Typical breast duct micro- anatomy. **Top Right:** Breast duct epithelial cell polarization. **Bottom:** Major DCIS types and IDC. Reprinted with permission from [436].

The arrangement of the epithelial cells in the duct depends upon the polarization of the cells and the anisotropic distribution of different surface adhesion molecules. Integrins line the cell base and adhere to several ligands (generally laminin and fibronectin) on the basement membrane; E-cadherin molecules cover the cell surface between the base and apex and adhere to E-cadherin molecules on neighboring cells [92]. See Figure 10.2 (top right). The careful orchestration of integrin-mediated cell-BM adhesion and E-cadherin-mediated cell-cell adhesion helps determine the tissue geometry [303, 688]. While the epithelial cell population oscillates with the menstrual cycle (e.g., [376, 377]), on average it is maintained in homeostasis by carefully balancing cell proliferation and apoptosis. Microenvironmental changes can trigger internal signaling responses in the epithelial cells that lead to either proliferation or apoptosis as warranted by the proper maintenance of the tissue architecture. After apoptotic cells disintegrate

into apoptotic bodies, they are either absorbed by surrounding epithelial cells or digested by macrophages that travel through and along the BM [371, 391].

The integrin signaling pathway allows the cells to detect detachment from the basement membrane: when integrins are adhered to their ligands on the BM, they send signals within the cell that trigger the production of survival proteins (e.g., FAK) that inhibit p53-mediated apoptosis [332, 680]. Loss of attachment to the BM therefore allows apoptosis to occur, thus preventing overgrowth of cells into the lumen [164]. E-cadherin signaling helps the cells to detect the presence or absence of neighbors: when E-cadherin is bound to E-cadherin on neighboring cells, its intracellular domain binds to and sequesters β-catenin near the cell membrane. This prevents β-catenin from transcribing Cyclin D1, c-myc, and Axin2—proteins that are associated with cell cycle progression. (See Section 2.1.5.) As a result, cell cycling is thus inhibited [71, 600, 430, 315]. When a neighboring cell dies, E-cadherin signaling is reduced, thereby allowing the cell cycle to progress. This results in the production of a new daughter cell to fill in the gap in the duct epithelium. The epithelial cells also respond to hormones (intercellular signaling molecules) that bind to surface receptors. Estrogen, progesterone, androgen, prolactin, and epidermal growth factor all affect epithelial cell proliferation and apoptosis decisions, such as increased proliferation prior to lacation (to enlarge the breast duct system and prepare the lobules [33]) and increased apoptosis during breast involution (the "shutdown" process after lactation [56]).

10.1.2 Biology of DCIS

Overexpressed oncogenes and underexpressed tumor suppressor genes can disrupt the balance of epithelial cell proliferation and apoptosis, leading to cell overproliferation. This can occur either by the accumulation of DNA mutations (genetic damage) [622] or epigenetic anomalies (e.g., alterations in heritable CH_3 methyl groups that suppress key oncogenes) [8]. The transformation from regular breast epithelium to carcinoma is thought to occur in stages. For simplicity, we neglect the benign, precursor transformations (e.g., atypical ductal hyperplasia, or ADH [622]) and focus on DCIS.

In the most well-differentiated classes of DCIS, the epithelial cells maintain their basic polarity and anisotropic surface adhesion receptor distributions, resulting in partial recapitulation of the non-pathological duct structure within the lumen. These demonstrate either finger-like growths into the lumen (micropapillary: see Figure 10.2 (bottom:a)), or arrangements of duct-like structures (cribriform: see Figure 10.2 (bottom:b)) [621]. The cells in solid type DCIS lack polarity and do not develop these microstructures. Instead, the cells proliferate until they fill the entire lumen (Figure 10.2 (bottom:c)) [164]. The proliferating cells uptake oxygen and nutrients as they diffuse into the duct through the basement membrane, leading to oxygen and nutrient gradients (decreasing oxygen/nutrient concentrations with distance from the BM). If the central oxygen is

sufficiently depleted, the interior tumor cells die and form a necrotic core of cellular debris (comedo-type solid DCIS: see Figure 10.2 (bottom:c)) [621]. These cells are typically not phagocytosed by non-apoptotic epithelial cells (none nearby) and macrophages (too far from the BM). Instead, they swell and burst [51], and their solid (i.e., non-water) components are slowly calcified [641]. In fact, mammograms generally rely upon these calcifications for DCIS detection [139].

While it is tempting to regard DCIS as a progression from regular epithelium to cribriform or micropapillary ("partially transformed") to solid type ("fully transformed"), there is insufficient evidence to support such a linear progression, and indeed, the mutation pathway from noncancerous epithelium to DCIS is currently an open question [206, 568]. The dominant type of DCIS in any particular case may well depend upon which genes are mutated; for example, the cribriform DCIS microarchitecture could be due to hyperproliferation in cells whose genes regulating polarization (particularly of E-cadherin) are intact. Due to the current difficulty in fully characterizing DCIS carcinogenesis, there is an excellent opportunity for mathematical modeling to test competing theories by generating testable, quantitative hypotheses.

DCIS is a pre-malignant cancer because the basement membrane confines it to the duct system, blocking metastasis. However, it is an important precursor stage of invasive ductal carcinoma (IDC), where further genetic or epigenetic mutations lead to tumor cell motility along the BM, secretion of matrix metalloproteinases that degrade the BM, and subsequent invasion into the surrounding stroma (Figure 10.2 (bottom:d)) [618, 6]. An estimated 3/4 of all DCIS cases are already invasive at the time of detection [399, 348, 25]. Thus, there is substantial risk that an undetected DCIS precursor (e.g., ADH) can progress to IDC between annual mammograms [194]. Predicting the behavior of DCIS is important to understanding and hopefully preventing progression to IDC.

10.2 Adaptation of the Agent Model

We now adapt the agent model from Chapter 6 to the geometry and biology of solid-type, non-motile DCIS: tumor cells in the viable rim can be quiescent ($\mathcal{Q}$), apoptotic ($\mathcal{A}$) or proliferative ($\mathcal{P}$). For simplicity, cells in hypoxic regions ($\sigma < \sigma_H$) bypass the hypoxic state (i.e., we neglect $\mathcal{H}$), immediately enter the necrotic state ($\mathcal{N}$), and eventually become calcified debris ($\mathcal{C}$).[2] Thus, $\beta_H = \infty$. Because the cells are assumed non-motile, we neglect the motile state $\mathcal{M}$ and set $\mathbf{F}_{\text{loc}}$ to zero. We assume that there is no extracellular matrix in the duct lumen, and so $\mathbf{F}_{\text{cma}} = \mathbf{0}$. Cell-cell adhesion is assumed homophilic between E-cadherin molecules, and cell-BM adhesion is heterophilic between integrins and

[2] In Chapters 6 and 10, σ and g denote oxygen and glucose, which are generalized by the substrate n in the remainder of the book. In these chapters, n denotes an integer.

uniformly-distributed ligands on the BM. In the simulations below, we neglect the presence of non-cancerous epithelial cells lining the duct.

Parameter	Physical Meaning	Data Source
σ_H	hypoxic threshold	literature [682]
λ_p	oxygen uptake rate by proliferating tumor cells	[682, 221] and analysis [436]
λ_n	oxygen uptake rate by non-proliferating tumor cells	[682, 221] and analysis [436]
λ_t	oxygen uptake rate by all tumor cells	see discussion in the text
λ_b	background oxygen decay rate	analysis [436]
$\langle\lambda\rangle$	mean oxygen uptake rate in viable rim	literature [221]
L	oxygen diffusion length scale	literature [221]
$\ell_{\rm duct}$	length of breast duct segment	set at 1 mm
$r_{\rm duct}$	breast duct radius	histopathology measurement
β_H^{-1}	hypoxic survival time	simplified to 0
β_N^{-1} $(=\beta_C^{-1})$	time to necrose and calcify	parameter study [436]
β_P^{-1}	mean cell cycle time	literature [515]
β_A^{-1}	time to complete apoptosis	analysis [436] of lit. data [408]
α_A^{-1}	mean time to enter apoptosis	Cleaved Caspase-3 immunostain
$\overline{\alpha}_P^{-1}$	mean time to enter proliferative state	Ki-67 immunostain
$R_{\rm cca}$	cell-cell adhesion interaction distance	analysis [436] of cell deformation data [298]
$R_{\rm cba}$	cell-BM adhesion interaction distance	analysis [436] of cell deformation data [298]
V_S/V	solid fraction of individual cell	analysis [436] of literature data [442]
$n_{\rm cca}$, $n_{\rm cba}$	cell-cell and cell-BM adhesion powers in the potential function in Section 6.2.2	set equal to 1
$n_{\rm ccr}$, $n_{\rm cbr}$	cell-cell and cell-BM repulsion powers in the potential function in Section 6.2.2	set equal to 1
$\alpha_{\rm cca}$	strength of cell-cell adhesion	cell density in viable rim
$\alpha_{\rm ccr}$	strength of cell-cell repulsion	cell density in viable rim
$\alpha_{\rm cba}$	strength of cell-BM adhesion	set equal to $\alpha_{\rm cca}$
$\alpha_{\rm cbr}$	strength of cell-BM repulsion	set equal to $5\alpha_{\rm cba}$

Table 10.1. Main parameters for the agent-based model of DCIS.

10.2.1 Oxygen and Metabolism

In the DCIS model, we assume that oxygen σ is uptaken at a rate λ_p by proliferating cells and λ_n by non-proliferating cells (including quiescent and apoptotic cells), and oxygen decays with rate λ_b in the necrotic core (containing necrotic

cells and calcified debris) and the duct lumen. In regions containing a mixture of viable and non-viable tissue and lumen, we assign a volume-averaged uptake rate. We discuss the orders of magnitude for λ_p, λ_n, and λ_b in Section 10.3.1.

10.2.2 Duct Geometry

We denote the duct lumen by Ω and the duct boundary (BM) by $\partial\Omega$. In this chapter, we treat the duct as a rectangular region (a longitudinal cross-section of a cylinder) of radius r_{duct} and length ℓ_{duct}. We terminate the left side of the duct with a semicircle, as an initial approximation to a lobule. (See Figure 10.3 for a typical simulation view.) We introduce a framework that allows us to simulate DCIS growth in arbitrary duct geometries, such as near a branch point in the duct tree. We represent the duct wall implicitly by introducing an auxilliary signed distance function d (a *level set function*) satisfying

$$\begin{cases} d(\mathbf{x}) > 0 & \mathbf{x} \in \Omega \\ d(\mathbf{x}) = 0 & \mathbf{x} \in \partial\Omega \\ d(\mathbf{x}) < 0 & \mathbf{x} \notin \overline{\Omega} = \Omega \cup \partial\Omega \\ |\nabla d(\mathbf{x})| \equiv 1. \end{cases} \tag{10.1}$$

The gradient of the distance function gives the normal vector $\mathbf{n}$ (oriented into the lumen) to the interior duct surface. See [437, 438, 439, 440, 230, 441], where the method is used to describe moving tumor boundaries.

Level set methods were first developed by Osher and Sethian [511] and have been used to study moving surfaces that experience frequent topology changes (e.g., merger of regions and fragmentation), especially in the contexts of fluid mechanics and computer graphics. (See the books by Sethian [605] and Osher [510] and the references [511, 509, 606].) For more information on the level set method and its application to fluid mechanics, please see [511, 649, 449, 450, 4, 605, 509, 510, 606].

10.2.3 Intraductal Oxygen Diffusion

We model the release of oxygen by blood vessels outside the duct, its diffusion through the duct wall $\partial\Omega$ and within the duct lumen Ω, and its cellular uptake and decay (e.g., by reacting with molecules in the interstitial fluid), by

$$\begin{cases} \frac{\partial\sigma}{\partial t} = D\nabla^2\sigma - \lambda\sigma & \text{if } \mathbf{x} \in \Omega \\ \sigma = \sigma_B & \text{if } \mathbf{x} \in \partial\Omega, \end{cases} \tag{10.2}$$

where σ is the nondimensional oxygen level (scaled by the oxygen concentration σ_∞ in well-oxygenated tissue near the blood vessels in the stroma), D is the oxygen diffusion coefficient, λ is the local oxygen uptake/decay rate (generally λ averages 0.1 min^{-1} [515], currently assumed equal for all cell types for simplicity), and σ_B is the (nondimensional) oxygen level on the basement membrane.

The oxygen diffusion equation admits an intrinsic length scale $L = \sqrt{D/\overline{\lambda}}$ that we use to nondimensionalize space in Eq. (10.2). Here, $\overline{\lambda}$ is a characteristic value of λ. By the literature, $\overline{\lambda} \approx 0.1 \ \text{min}^{-1}$ and $L \approx 100\,\mu\text{m}$ [515].

10.2.4 Numerical Method

We introduce an independent computational mesh for oxygen that discretizes the duct lumen with spacing $\Delta x = \Delta y = 0.1$ (approximately 10 μm spacing in dimensional space) to resolve oxygen gradients. We use a cell interaction mesh with 1 μm spacing to avoid directly testing each cell for iteraction with every other cell, hence avoiding an $\mathcal{O}\left(\#\ \text{cells}^2\right)$ computational cost.

We use an object-oriented C++ framework, where each cell is an instance of a `Cell` class and endowed with instances of `Cell_properties` (proliferation and apoptosis parameters, initial radius and volume, etc.) and `Cell_state` (cell state, position, velocity) classes. We order the cells with a doubly-linked list structure, which allows us to easily delete apoptosed cells and insert new daughter cells.

To update our agent-based model at time t to the next simulation time $t + \Delta t$:

1. Update the oxygen solution on the oxygen mesh using standard explicit forward Euler finite difference methods; see Chapter 8 and [436].
2. Iterate through all the cells to update the interaction mesh.
3. Iterate through all the cells to update their states according to Section 6.2.3. Update the necrosing cells' radii, volumes, and calcification as described.
4. Iterate through all the cells to update their velocities as described above.
5. Iterate through all the cells to determine $\max |\mathbf{v}_i|$. Use this to determine the new Δt using the stability criterion $\Delta t < \frac{1}{\max|\mathbf{v}_i|}$.
6. Iterate through all the cells to update their positions according to their new velocities. We use forward Euler stepping ($\mathbf{x}_i(t + \Delta t) = \mathbf{x}_i(t) + \Delta t \mathbf{v}_i(t)$), although improved (e.g., Runge-Kutta) methods are straightforward.

These steps require at most cycling through all the cells. If interaction testing can be made similarly efficient, then the overall simulation requires computational effort that is linear in the number of cells.

Efficient Interaction Testing

With spatial resolution given by the interaction mesh (1 micron spacing), we create an array of linked lists of interactions as follows:

1. Let $R = 2 \max_i \left\{r^i_{\text{cca}}\right\}$
2. Initialize the array such that each pointer is NULL.
3. For each cell i, append its memory address to the list for each mesh point within a distance R of its center $\mathbf{x}_i$.

Once complete, at any mesh point (i, j), we have a linked list of cells which are allowed to interact with a cell centered at or near (x_i, y_j).

We use this list whenever we compute a quantity of the form

$$\sum_j f\left(\text{cell}_i, \text{cell}_j\right)\left(x_k, y_\ell\right) \tag{10.3}$$

by contracting the sum to the members of the linked list at (x_k, y_ℓ). Because the number of points written to the array is fixed for each cell, this reduces the computational cost of cell-cell interaction testing to $\mathcal{O}\left(\#\text{ cells}\right)$, rather than the more typical $\mathcal{O}\left(\#\text{ cells}^2\right)$. Furthermore, this interaction data structure still allows arbitrary cell-cell interactions. Notice that this computational gain relies upon the fact that cells can only interact over finite distances.

10.3 Patient-Specific Calibration with Patient Data

To make the model predictive we must constrain the non-patient-specific parameters as much as possible (e.g., by literature searches and analysis of the mathematical model behavior across the parameter space) and calibrate the undetermined parameters using available patient-specific data. We now summarize key parameter estimates made by [436] and follow with a calibration protocol. In this discussion, we neglect hypoxia and motility, and take $\beta_N = \beta_{NL} = \beta_{NS} = \beta_C$.

10.3.1 Estimating "Universal" Parameters

We first estimate parameters that are common to all patients, based upon literature searches of theoretical/experimental biology and prior modeling efforts.

Cell Cycle, Apoptosis, and Necrosis/Calcification Times

We estimate that the cell cycle time β_P^{-1} is 18 hours by the modeling literature (e.g., see [515]). We estimate $\beta_A^{-1} \approx 8.6$ h below in Section 10.4.1, and we estimate $\beta_N^{-1} \approx 30$ days in Section 10.4.1.

Oxygen Parameters

By the literature, the mean cellular oxygen uptake rate is $\langle\lambda\rangle = 0.1\ \text{min}^{-1}$ (in the viable rim), and $L = 100\ \mu$m. To estimate the hypoxic threshold σ_H, we examine the mitosis function $k_m(\sigma)$ in [682], which is the basis of the breast cancer model in [221]. Ward and King found that at the step function limit, $k_m(\sigma) \propto H(\sigma - \sigma_c)$; they determined that $\sigma_c \approx 0.2$ experimentally when σ is nondimensionalized by σ_∞, the far-field nutrient value in non-pathologic, well-vascularized tissue [682]. Because the step function limit is similar to our α_P parameter, our σ_H is analogous to σ_c in [682], and as we have nondimensionalized oxygen by the nutrient value in well-vascularized, non-pathologic breast tissue, we set $\sigma_H = 0.2$ as well. We observe in our immunohistochemical and histological images that the quiescent and proliferating viable tumor cells have the same general size; this suggests that the quiescent tumor cells are relatively metabolically

active compared to non-cancerous, long-term quiescent cells that generally are smaller with condensed nuclei (relates to lack of transcriptional activity), reduced mitochondrial populations [227], and less cytosol. Hence, we estimate that λ_p and λ_n are of similar orders of magnitude. In [436], a parameter study found that $\lambda_p \gg \lambda_n$ was inconsistent with the population dynamic and morphologic characteristics of DCIS observed in our immunohistochemistry and histologic data. For simplicity, we set $\lambda_p = \lambda_n = \lambda_t$ and $\lambda_t = \lambda_b$ and investigate the more general case in [436]. A statistical analysis of the viable rim thickness and tumor cell density in multiple breast ducts also supported our approximation that $\lambda_p \approx \lambda_n$ [115, 434].

Cell Mechanics

We estimate the cells' solid volume fraction (V_S/V) at approximately 10% by combining the published data of [442] with the assumption that the solid component is one-to-ten times denser than water [435, 436]. We estimate the maximum cell-cell and cell-BM interaction distances R_{cca} and R_{cba} using published measurements of breast cancer cell deformations. Byers et al. [93] found the deformation of MCF-7 (an adhesive, moderately agressive breast cancer cell line) and MCF-10A (a benign cell line) breast epithelial cells to be bounded around 50% to 70% of the cell radius in shear flow conditions; this is an upper bound on R_{cca} and R_{cba}. Gucke et al. [298] measured breast epithelial cell deformability (defined as additional stretched length over relaxed length) after 60 seconds of stress. Deformability was found to increase with malignant transformation: MCF10 deformed 10.5%, MCF7 deformed 21.4%, MCF7 deformed 30.4% after weakening the cytoskeleton, and MDA-MB-231 (an aggressive cancer cell line) deformed 33.7%. Because DCIS is moderately aggressive, we use the MCF7 estimate and thus set $R^i_{\text{cca}} = R^i_{\text{cba}} = 1.214 r_i$. It is likely that the cell-cell and cell-BM adhesive forces decrease rapidly with distance, and so we used the lowest (simplest) adhesion powers that capture a smooth decrease at the maximum interaction distances: $n_{\text{cca}} = n_{\text{cba}} = 1$. For simplicity, we also set $n_{\text{ccr}} = n_{\text{cbr}} = 1$.

10.3.2 Calibrating Patient-Specific Parameters

We now present the patient-specific portion of the calibration protocol, as detailed in [436]. The following patient-specific data are available:

- Average duct radius $\langle R \rangle$ and average viable rim thickness $\langle T \rangle$, measured directly on the IHC images.
- Average cell density $\langle \rho \rangle$ in the viable rim, measured by counting nuclei and computing the viable rim size;
- Cell confluence f in the viable rim, defined to be the area fraction of the viable region occupied by cell nuclei and cytoplasm;

- Proliferating index PI, measured by staining images for Ki-67, (a nuclear protein marker for cell cycling), and then counting the total number of Ki-67-positive nuclei versus the total number of nuclei; and
- Apoptotic index AI, measured by staining images for cleaved Caspase-3, an "executioner" caspase involved throughout most of the apoptosis process. Because Caspase-3 is a cytosolic protein, we identify cleaved Caspase-3 positive cells by comparing the whole cell staining intensities. The apoptotic index is then computed across the viable rim as with PI.

Geometry:
We match the simulated duct radius to the mean measured duct radius $\langle R\rangle$. We obtain the average (equivalent) cell radius from the mean viable rim cell density $\langle\rho\rangle$ and measured confluence f $(0 \le f \le 1)$ by the relation:

$$f = \langle\rho\rangle\pi r^2. \tag{10.4}$$

Oxygen:
For the special case we consider here, $\lambda_p = \lambda_n = \langle\lambda\rangle$; we assume that λ_b is stipulated as an additional constraint $\Lambda_b = \lambda_b/\langle\lambda\rangle$. The more general case is considered by separating the viable rim into fluid, proliferating cells, and non-proliferating cells and applying additional constraints on both $\lambda_n/\langle\lambda\rangle$ and $\lambda_b/\langle\lambda\rangle$ to uniquely determine the oxygen uptake rate [436].

Next, we use the mean viable rim thickness $\langle T\rangle$ as an indicator of oxygenation and thus determine the boundary oxygen value σ_B. In 2D (the 3-D results are in Section 10.4.2), the steady-state oxygen profile away from the leading edge reduces to a simple 1-D equation

$$0 = \begin{cases} D\sigma'' - \langle\lambda\rangle\sigma & 0 < x < \langle T\rangle \\ D\sigma'' - \Lambda_b\langle\lambda\rangle\sigma & \langle T\rangle < x < \langle R\rangle \end{cases} \tag{10.5}$$

with the boundary and matching conditions

$$\sigma(0) = \sigma_B, \quad \sigma(\langle T\rangle) = \sigma_H, \quad \sigma'(\langle R\rangle) = 0 \tag{10.6}$$

$$D \lim_{x\uparrow\langle T\rangle} \sigma'(x) \qquad = \qquad D \lim_{x\downarrow\langle T\rangle} \sigma'(x). \tag{10.7}$$

Here, x is the distance from the duct wall.

After applying all conditions except $\sigma(0) = \sigma_B$, we have

$$\sigma(x) = \sigma_H \begin{cases} \left[\cosh\left(\frac{x-\langle T\rangle}{L}\right) - \sqrt{\Lambda_b}\tanh\left(\frac{\langle R\rangle-\langle T\rangle}{L/\sqrt{\Lambda_b}}\right)\sinh\left(\frac{x-\langle T\rangle}{L}\right)\right] & 0 < x < \langle T\rangle \\ \left[\cosh\left(\frac{x-\langle T\rangle}{L/\sqrt{\Lambda_b}}\right) - \tanh\left(\frac{\langle R\rangle-\langle T\rangle}{L/\sqrt{\Lambda_b}}\right)\sinh\left(\frac{x-\langle T\rangle}{L/\sqrt{\Lambda_b}}\right)\right] & \langle T\rangle < x < \langle R\rangle. \end{cases}$$

We evaluate at $x = 0$ to determine σ_B:

$$\sigma_B = \sigma_H\left[\cosh\frac{\langle T\rangle}{L} + \sqrt{\Lambda_b}\tanh\left(\frac{\langle R\rangle - \langle T\rangle}{L/\sqrt{\Lambda_b}}\right)\sinh\frac{\langle T\rangle}{L}\right] \tag{10.8}$$

Lastly, we compute the mean oxygen value across the viable rim:

$$\langle\sigma\rangle = \sigma_H \frac{L}{\langle T\rangle}\left[\sqrt{\Lambda_b}\tanh\left(\frac{\langle R\rangle - \langle T\rangle}{L/\sqrt{\Lambda_b}}\right)\left(\cosh\frac{\langle T\rangle}{L} - 1\right) + \sinh\frac{\langle T\rangle}{L}\right]. \quad (10.9)$$

Population Dynamics:
By the analysis in Section 6.5, given β_P, β_A, and measurements of PI and AI, we solve Eqs. (6.51)-(6.52) to steady state to determine $\langle\alpha_P\rangle$ and α_A:

$$\langle\alpha_P\rangle = \frac{\beta_P\left(\mathrm{PI} + \mathrm{PI}^2\right) - \beta_A \mathrm{AI}\cdot\mathrm{PI}}{1 - \mathrm{AI} - \mathrm{PI}} \quad (10.10)$$

$$\alpha_A = \frac{\beta_A\left(\mathrm{AI} - \mathrm{AI}^2\right) + \beta_P \mathrm{AI}\cdot\mathrm{PI}}{1 - \mathrm{AI} - \mathrm{PI}}. \quad (10.11)$$

We calibrate the functional form for α_P by combining this result with the computed mean oxygen in the previous step and solving for $\overline{\alpha}_P$:

$$\langle\alpha_P\rangle = \overline{\alpha}_P \frac{\langle\sigma\rangle - \sigma_H}{1 - \sigma_H}. \quad (10.12)$$

Cell-Cell Mechanics:
For confluent cells in solid-type DCIS ($f = 1$), we convert the mean density $\langle\rho\rangle$ to an equivalent cell spacing s (between cell centers) via

$$s = \sqrt{\frac{2}{\sqrt{3}\langle\rho\rangle}}, \quad (10.13)$$

which is based upon matching the mean cell density to a hexagonal cell packing. We balance the cell-cell adhesive and repulsive forces at this equilibrium spacing.

If $n_{\mathrm{cca}} = n_{\mathrm{nccr}} = 1$ and $R_{\mathrm{cca}} = 1.14r$, and $\langle R\rangle_{ccr} = r$, and $\mathcal{E} = 1$, then

$$\frac{\alpha_{\mathrm{cca}}}{\alpha_{\mathrm{ccr}}} = \frac{\varphi'\left(s; 2r, n_{\mathrm{ccr}}\right)}{\varphi'\left(s; 2R\mathrm{cca}, n_{\mathrm{cca}}\right)} = \frac{\left(1 - \frac{s}{2r}\right)^{n_{\mathrm{ccr}}+1}}{\left(1 - \frac{s}{2.428r}\right)^{n_{\mathrm{cca}}+1}}. \quad (10.14)$$

This leaves a free parameter: in effect, the density determines the equilibrium spacing but does not stipulate how *strictly* that density is enforced. It may be possible to to fully constrain the mechanics by matching the simulation to the variance in ρ; this is the subject of ongoing research. In the meantime, we have found that setting $\alpha_{\mathrm{ccr}} = 8$ sufficiently enforces the density [436].

Cell-BM Mechanics:
Because we have no direct data on the cell-BM mechanical interactions, we choose the parameters to prevent cells from penetrating the duct wall; $\alpha_{\mathrm{cbr}} = 5$ suffices when $\alpha_{\mathrm{cba}} = \alpha_{\mathrm{cca}}$. It should be possible to further constrain the parameter values by comparing patient data to the simulated tumor propogation speed and leading edge morphology as α_{cba} and α_{cca} are varied; such parameter studies are the topic of ongoing research [436].

10.3.3 Sample Patient Calibration and Verification

Quantity	Measured Mean	Units
Duct Radius r_{duct}	170.10	μm
Viable Rim thickness T	76.92	μm
PI	17.43	%
raw AI	0.638	%
corrected AI	0.831	%
Cell density ρ	0.003213	cells/μm^2

Table 10.2. Key data for a de-identified patient.

We demonstrate the calibration protocol on IHC and histopathology material from a de-identified mastectomy patient from the M.D. Anderson Cancer Center (de-identified case number 100019). The measurements for this patient are given in Table 10.2. Because the cells are nearly confluent in the viable rim, we estimate $f \approx 1$. By the cell-cell mechanics calibration above (Eq. (10.4)), $r_{\text{cell}} = \sqrt{1/(\rho\pi)} \approx 9.953\,\mu$m. By the estimates of cell deformability above, we set $R_{\text{cca}} = R_{\text{cba}} = 1.21 r_{\text{cell}} \approx 12.0834$.

By the oxygen protocol (with $\lambda_p = \lambda_n = \lambda_b = 0.1$), we estimate the boundary condition at $\sigma_B \approx 0.3861$ (Eq. (10.8)), and $\langle\sigma\rangle \approx 0.2794$ (Eq. (10.9)). We further investigate the impact of $\lambda_p \neq \lambda_n$ and $\lambda_p \neq \lambda_b$ in [436].

Using the measured AI and PI, along with $\beta_P^{-1} = 18$ h and $\beta_A^{-1} = 8.6$ h (see Section 10.4.1), we estimate population dynamic parameters at

$$\alpha_A^{-1} \approx 47196.349 \text{ min}, \qquad \text{and} \qquad \overline{\alpha}_P^{-1} \approx 434.527 \text{ min}.$$

See Eqs. (10.11)-(10.12).

For the mechanics, the protocol gives $s \approx 18.957\,\mu$m (Eq. (10.13) $\alpha_{\text{ccr}} = 8$, and $\alpha_{\text{cca}} \approx 0.3915$ (Eq. (10.14)). We set $\alpha_{\text{cba}} = \alpha_{\text{cca}}$ and $\alpha_{\text{cbr}} = 5$, although we are currently investigating the impact of the balance between α_{cca} and α_{cba} in [436].

Verification of Calibration

All figures given as mean ± standard deviation		
Quantity	Patient Data	Simulated
PI (%)	17.43 ± 10.48	17.193 ± 7.216
AI (%)	0.831 ± 0.572	1.447 ± 3.680
Viable rim thickness (μm)	76.92 ± 13.70	80.615 ± 4.454
Cell density (cells/μm^2)	0.003213 ± 6.89e-4	0.003336

Table 10.3. Verification of the Patient-Specific Calibration: Note that there is no standard deviation for the simulated cell density because it was calculated over the entire viable rim.

To verify the calibration, we seeded a small section of a 1 mm virtual duct with tumor with AI and PI matching the IHC measurements. We then ran the simulation to time $t = 30$ days and checked the model's predictions of AI, PI,

viable rim thickness, and density in the viable rim. (See Section 6.6.1 for the fully dynamic simulation.) We sliced the computational domain at time $t = 30$ days into 6 μm-thick slices and performed virtual immunohistochemistry on those slices. We calculated the viable rim thickness in each slice, and the average cell density over the entire viable tumor region. See Table 10.3. The proliferative index matches extremely well, and the apoptotic index is within error tolerances. Because apoptosis is a rare stochastic event ($< 1\%$) in a region with fewer than 500 cells, we expect considerable noise; indeed, this is observed in the patient AI as well. The viable rim thickness is within the error bounds, and the cell density is in excellent agreement. Because all the numerical targets (outlined in Table 10.2) are within the error bounds, the calibration was a success.

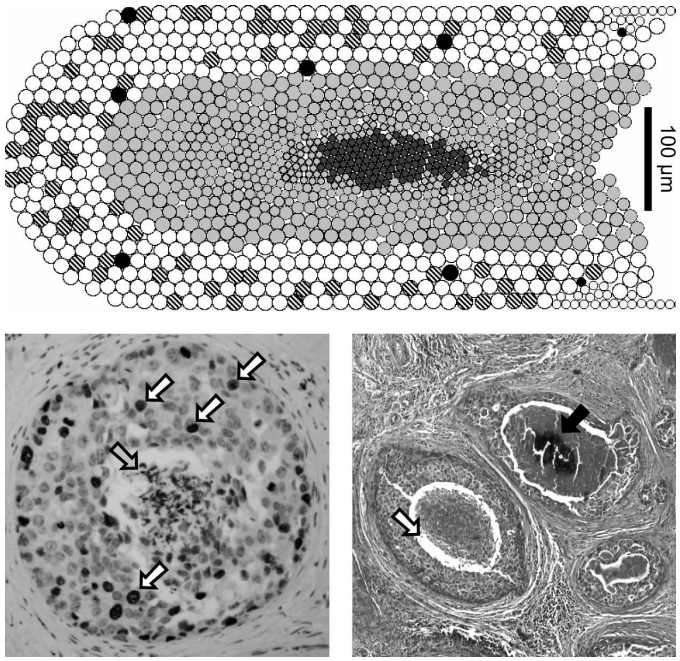

Figure 10.3 Verification of the morphological features of the calibrated simulation. **Top:** Simulation at time 30 days. White cells are quiescent, striped cells are proliferating (virtual Ki-67), black cells are apoptotic (virtual cleaved Caspase-3), medium gray cells are necrotic, and central dark gray cells are calcified debris. Small cells along the BM are noncancerous epithelium. **Bottom Left:** Ki-67 immunohistochemistry of a duct cross-section. White arrows show Ki-67 positive nuclei. The gray arrow shows necrotic debris. **Bottom Right:** H&E staining showing calcifications (black arrow) and the gap between the viable rim and necrotic core (white arrow). Reprinted with permission from [436].

We also compared the general tumor morphology to H&E stains (Figure 10.3: bottom right) and the spatial distribution of proliferating cells to Ki-67 immunostains (Figure 10.3: bottom left) from the patient. The virtual DCIS reproduced

the expected tumor microarchitecture: a viable rim closest to the duct wall, an interior necrotic core, and sporadic interior microcalcifications. The simulation also recapitulated the general distribution of proliferating cells across the viable rim: in both the simulation and the Ki-67 imaging, cycling tumor cells were observed most frequently along the duct wall where oxygen is most plentiful, and almost never at the peri-necrotic boundary where substrate levels are lowest. This evidence supports our model of α_P depending upon σ. This theme is discussed in greater detail in Section 10.4.2.

10.4 Case Studies

We close the chapter with three case studies using the agent model to facilitate predictive breast cancer research. First, we illustrate the utility of the model in estimating biological parameters that are difficult or impossible to measure experimentally. Second, we use the analytical volume-averaged behavior of the model to generate testable biological hypotheses of DCIS behavior, test those hypotheses using actual DCIS data, and use the results to refine and extend our model. Lastly, we demonstrate the use of the agent model in calibrating multi-scale cancer simulation frameworks, and compare the framework's predictions of tumor size to actual clinical data. We discuss the clinical signifigance of this last application and discuss future work.

10.4.1 Estimating Difficult Physical Parameters

Apoptosis Time β_A^{-1}

The time course from the initial signal to commence apoptosis to final cell lysis has been difficult to quantify [329]. Early reviews by key apoptosis researchers estimated the early cellular events in apoptosis comprise a fast process on the order of minutes, with digestion of apoptotic bodies occuring within hours of phagocytosis [371]. Hu et al. [329] conducted a detailed *in vivo* observation of apoptosis of epithelial cells in the rat hippocampus, observing cells breaking up in 12-24 hours and the complete elimination of apoptotic bodies within 72 hours. Experimental work in [595] similarly observed most apoptotic processes on the order of hours. This provides a bound for $\beta_A^{-1} \leq 24$ h. It also suggests that apoptotic bodies are absorbed by surrounding cells in under 48 hours after cell lysis. In total, the experimental observations in the literature lead us to estimate $\beta_A^{-1} \approx \mathcal{O}(10\text{h})$.

To estimate β_A for breast epithelial cells, we build on our working hypothesis that cancer cells use the same basic mechanisms of proliferation and apoptotis as noncancerous cells, only with altered frequency [302]. Hence, we postulate that β_A and β_P are the same for DCIS cells lines and noncancerous breast epithelial cells. Eq. (6.50) in Section 6.5 gives us a means to estimate β_A: assuming that on average, noncancerous breast epithelial tissue is in homeostasis (when averaged

through the duration of the menstrual cycle), then $\dot{N} = 0$, and we find

$$\beta_A = \beta_P \frac{P}{A} = \beta_P \frac{\text{PI}}{\text{AI}}. \tag{10.15}$$

In [408], the average proliferative and apoptotic indices of noncancerous breast epithelial cells in several hundred pre-menopausal (aged under 50 years old) women were measured at 0.0252 ± 0.0067 and 0.0080 ± 0.0006, respectively. While the AI and PI can vary considerably in time due to hormone cycling in the mestrual cycle [495], when averaged over many women (who fall at different points in this cycle), the effects of the monthly variation should be cancelled out. Based upon a cell cycle time $\beta_P^{-1} = 18$ h, we estimate $\beta_A = 0.175$ h^{-1}, giving an estimated time for apoptotis of approximately 5.7 h. This is consistent with our estimated order of magnitude.

In the same study, the PI and AI were measured over several hundred post-menopausal women (aged over 50 years old) at 0.0138 ± 0.0069 and 0.0043 ± 0.0007, respectively. Using these figures gives a similar estimate $\beta_A \approx 0.178$ h^{-1}. The similarity of the figures in pre-menopausal and post-menopausal women supports our working hypothesis that β_A and β_P are relatively fixed for the cell type, even when apoptosis and proliferation occur with differing frequencies and in different hormonal environments. We also note that conducting the same calculation with the data from [495] gives $\beta_A \approx 0.26$ h^{-1} and an estimated apoptosis time of 3.9 h. This work used a much smaller sample size, but nonetheless is generally consistent with our estimate.

We now attempt to improve our estimate to account for detection shortcomings in the immunostaining. (See the introduction in [190] for a good overview of the current methods of detecting apoptotic cells in histologic tissue cultures.) The AI measurements in [408] were obtained by TUNEL assay, which relies upon detecting DNA fragmentation. According to the detailed work on Jurkat cell apoptosis in [595], there was approximately a 3 hour lag between the inducement of apoptosis (observable by rapid changes in mitochondrial membrane potential voltage and the ratio of ATP to ADP) and the detection of DNA laddering and chromatin condensation. Cleaved Caspase-3 activity was neglibible for the first 60 minutes and steadily climbed thereafter, peaking after 180 minutes and reaching approximtely 10% of that peak in 50-60 minutes. On this basis, we would expect that TUNEL-assay-based AI figures fail to detect approximately the first 3 hours of apoptosis, and cleaved Caspase-3-based AI stain should fail to detect the first one-to-two hours. Thus, we increase our estimate for β_A^{-1} to 8.6 hours. This also gives "correction factors" to account for undetected apoptotic cells by TUNEL assay and cleaved-Caspase-3 immunostaining:

$$\text{AI}_{\text{actual}} \approx \frac{8.6}{5.6} \text{AI}_{\text{TUNEL}}, \qquad \text{and} \tag{10.16}$$

$$\frac{8.6}{7.6} \text{AI}_{\text{Caspase-3}} \leq \text{AI}_{\text{actual}} \leq \frac{8.6}{6.6} \text{AI}_{\text{Caspase-3}}. \tag{10.17}$$

Calcification time β_C^{-1}

There are little-to-no literature data available on the time to complete necrosis and calcify the breast tumor cells. The best available experimental data are generally animal time course studies of arterial calcification; we use these to estimate the order of magnitude of β_C^{-1}. Time course studies on *post mortem* cardiac valves by [350] observed significant tissue calcification between 7 days (10% increase in Ca incorporation) and 14 days (40% increase) after injection by TGF-β1. Lee et al. [407] examined a related process (elastin calcification) using a rat subdermal model, demonstrating calcification to occur gradually over the course of two-to-three weeks. Gadeau et al. [251] measured calcium accumulation in rabbit aortas following oversized balloon angioplasty injury. Calcified deposits appeared as soon as 2-4 days after the injury, increased over the course of 8 days, and approached a steady state between 8 and 30 days. Hence, we estimate β_C^{-1} is on the order of days to weeks.

To sharpen our estimate, we conducted a parameter study on the calcification time parameter β_C^{-1} using the fully dynamic model (See Section 6.6.1) that we calibrated in Section 10.3.3. We varied β_C^{-1} from 12 hours to 30 days and simulated our calibrated DCIS model to 30 days; the results are in Table 10.4. We found that calcification times under 15 days lead to necrotic cores that were nearly entirely calcified; this is not observed in H&E image data. See Figure 10.3, bottom right, black arrow. On the other hand, the 30-day calcification time lead (as expected) to a complete absence of microcalcifications in the core at time 30 days. Because DCIS tumors are hypothesized to grow to steady state in as little as two-to-three months [194, 195, 138], we expect microcalcifications by this time. Hence, our sharpened estimate of β_C^{-1} is 15 days, consistent with the literature. Parameter studies such as these are significant, because they allow us to estimate physical quantities that are difficult or impossible to determine experimentally.

β_C^{-1}	12 hours	1 day	5 days	15 days	30 days
% of core calcified	94.0%	83.7%	51.1%	6.9%	0%

Table 10.4. Parameter study on the calcification time.

10.4.2 Generating and Testing Hypotheses

Recall that when the agent model behavior is averaged across the entire viable rim, we obtain a nonlinear system of ODEs in PI and AI:

$$\begin{aligned} \dot{\mathrm{PI}} &= \langle \alpha_P \rangle (1 - \mathrm{AI} - \mathrm{PI}) - \beta_P \left(\mathrm{PI} + \mathrm{PI}^2\right) + \beta_A \mathrm{AI} \cdot \mathrm{PI} \\ \dot{\mathrm{AI}} &= \alpha_A (1 - \mathrm{AI} - \mathrm{PI}) - \beta_A \left(\mathrm{AI} - \mathrm{AI}^2\right) - \beta_P \mathrm{AI} \cdot \mathrm{PI}. \end{aligned} \tag{10.18}$$

As detailed earlier, for fixed AI, PI, β_A, and β_P, this can be used to determine $\langle \alpha_P \rangle$ and α_A, and ultimately, $\overline{\alpha}_P$. If instead we regard α_A and $\overline{\alpha}_P$ as fixed and replace $\langle \alpha_P \rangle$ with $\alpha_P(\mathcal{S}, \sigma, \bullet)$, we obtain a nonlinear system for AI and PI that

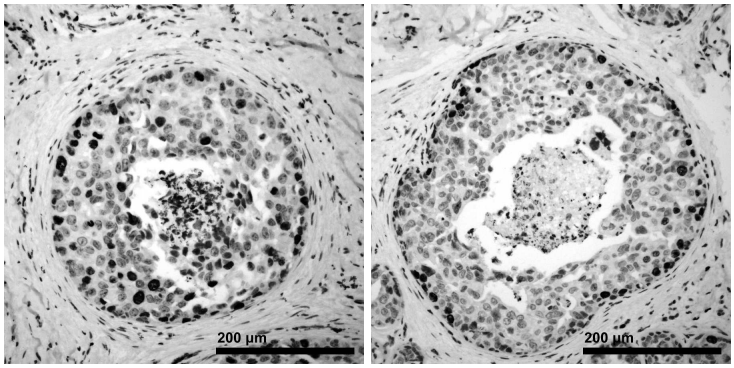

Figure 10.4 Ki-67 immunohistochemistry for ducts F3 (left) and F19 (right) for de-identified patient case 100019. Ki-67 positive nuclei stain darkly in the images. Reprinted with permission from [436].

varies with σ. If we solve the system to steady state for $\sigma_H < \sigma < 1$, we can use the model to predict the relationship between proliferation and oxygen availability. In [435], this analysis led us to hypothesize Michaelis-Menten population kinetics: for sufficient nutrient availability, proliferation saturates, indicating that oxygenation is no longer the primary growth-limiting factor.

We now test this hypothesis based upon a careful analysis of Ki-67 immunohistochemistry in two ducts (F3 and F19) for a DCIS patient (de-identified case 100019) [194, 195, 138]. See Figure 10.4. For each of these ducts, we calculate the distance of all nuclei and Ki-67 positive nuclei to the duct wall, the mean distance from the duct centroid to the duct wall (i.e., the radius R), and the mean duct viable rim thickness T. Next, we create a histogram of Ki-67-positive nucleus distances to the duct wall (Figure 10.5, first row), all nucleus distances to the duct wall *using the same histogram "bins"* (Figure 10.5, second row), and divide these to obtain the proliferative index (PI) versus distance from the duct wall (Figure 10.5, third row).

Next, we estimate the 3-D steady-state oxygen profile through the cylindrical ducts (assumed radially symmetric with no variation in the longitudinal direction):

$$0 = L^2 \left(\sigma'' + \frac{1}{r}\sigma' \right) - \sigma, \qquad 0 < r < R \tag{10.19}$$

with boundary conditions

$$\sigma(R - T) = \sigma_H, \qquad \sigma'(0) = 0, \tag{10.20}$$

The solution is

$$\sigma(r) = \frac{\sigma_H}{I_0\left(\frac{R-T}{L}\right)} I_0\left(\frac{r}{L}\right), \tag{10.21}$$

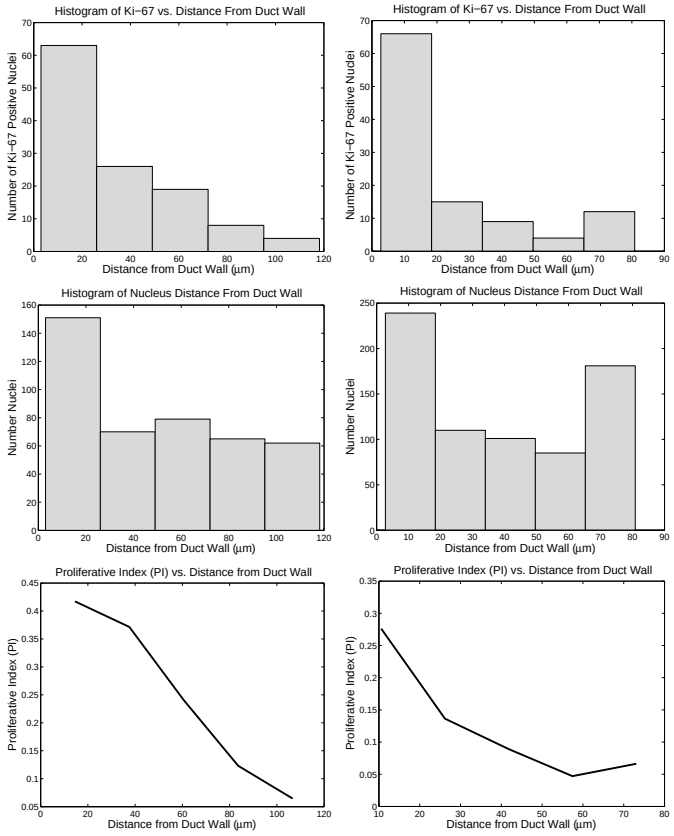

Figure 10.5 Histograms of Ki-67 positive nuclei vs. distance from duct wall (top row) and all nuclei vs. distance from duct wall (middle row), and proliferative index vs. distance from the duct wall (bottom row). These measurements are for ducts F3 (left column) and F19 (right column). Reprinted with permission from [436].

where L is the diffusion length scale (assumed 100 μm by [682, 221]), I_n is the n^{th}-order modifed Bessel function of the first kind, σ is nondimensionalized by the normoxic oxygen level in non-pathological tissue, and σ_H is the hypoxic threshold oxygen value (assumed 0.2 by [682, 221]). The mean value of the oxygen solution in the viable rim ($R - T < r < R$) is given explicitly by

$$\langle \sigma \rangle = \frac{\sigma_H}{I_0\left(\frac{R-T}{L}\right)} \frac{2L}{2RT - T^2} \left(RI_1\left(\frac{R}{L}\right) - (R-T)I_1\left(\frac{R-T}{L}\right)\right). \qquad (10.22)$$

For the duct in F3,

$$R \approx 188.4634\,\mu\text{m}, \qquad T \approx 119.0256\,\mu\text{m}, \qquad \text{and} \qquad \langle \sigma \rangle \approx 0.282145,$$

and for the duct in F19,

$$R \approx 217.5548\,\mu\text{m}, \qquad T \approx 97.9602\,\mu\text{m}, \qquad \text{and} \qquad \langle \sigma \rangle \approx 0.280459.$$

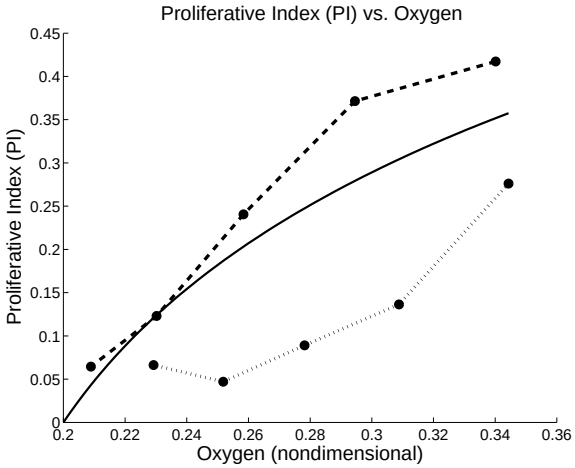

Figure 10.6 Comparison of the predicted PI curve (solid curve) with data from duct F3 (dashed curve) and duct F19 (dotted curve) for case 100019. Reprinted with permission from [436].

By correlating the oxygen solutions (not shown) with the PI profiles, we estimate the relationship between the measured PI and σ in the ducts. We plot these curves for F3 (dashed curve) and F19 (dotted curve) against the predicted curve (solid curve) from [436] in Figure 10.6. As we can see, the theoretical predictions and measurements agree qualitatively but not quantitatively. We conclude that while proliferation (given by PI) correlates with oxygen levels throughout the tumor, oxygenation alone cannot fully determine PI. Hence, we hypothesize that there must be additional heterogeneities in other microenvironmental factors (e.g., EGF), gene expression, or protein signaling across the tumor.

The next natural question is whether we can account for these hetergeneities with our current functional form by calibrating the agent model to the individual ducts. If we can, then this is further evidence that (i) we have chosen a suitable theoretical stochastic framework for the agent model, and (ii) future work must incorporate more sophisticated gene/protein signaling models. To address this question, we next calibrate the agent model for each duct to determine α_A and $\overline{\alpha_P}$. We use AI $= 0.008838$ in each duct as in [436], and PI, R, and T as measured separately for each duct above. For the duct in F3,

$$\mathrm{PI} = 0.281030, \qquad \alpha_A \approx 0.00162405\,\mathrm{h}^{-1},$$
$$\langle \alpha_P \rangle \approx 0.0277579\,\mathrm{h}^{-1}, \qquad \text{and} \qquad \overline{\alpha_P}(\mathcal{S}, \bullet) \approx 0.270331\,\mathrm{h}^{-1};$$

and for the duct in F19,

$$\mathrm{PI} = 0.148045, \qquad \alpha_A \approx 0.00129067\,\mathrm{h}^{-1},$$
$$\langle \alpha_P \rangle \approx 0.0110190\,\mathrm{h}^{-1}, \qquad \text{and} \qquad \overline{\alpha_P}(\mathcal{S}, \bullet) \approx 0.109562\,\mathrm{h}^{-1}.$$

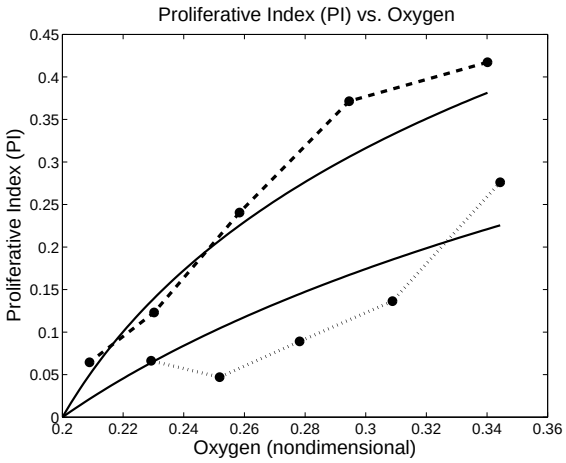

Figure 10.7 Comparison of the hypothesized (solid) and measured (dashed and dotted) PI vs. σ curves for duct F3 (dashed) duct F19 (dotted). Reprinted with permission from [436].

Using this, we generate PI-vs-σ curves for the individual ducts based upon Eq. (10.18) and compare them to the measured data in Figure 10.7. There is generally much improved quantitative agreement between the predicted (solid) and measured (dashed and dotted) curves. The difference in the predicted curves for the two ducts is due to the substantial difference in $\overline{\alpha}_P$: $\overline{\alpha}_P$ is much greater for F3, which has the overall higher PI curve.

We next examine the data in the ducts (Figure 10.4) within the context of our modeling framework and the predicted PI-vs-σ curves to generate additional biological hypotheses. Notice that the cell density is lower in F3 (Figure 10.4 left: larger nuclei and cells with greater spacing between cells) than in F19 (Figure 10.4 right: smaller nuclei and cells with less spacing between cells). These leads us to hypothesize that $\overline{\alpha}_P$ decreases with increasing cell density. E-cadherin/β-catenin signaling may be the physiological explanation of the phenomenon: when E-cadherin is bound to E-cadherin on a neighboring cell, β-catenin binds to the phosphorylated receptors, blocking its downstream pro-proliferative activity. (See Section 2.1.5.) For higher cell densities, more cell surfaces are in contact with one another, providing greater opportunities for E-cadherin binding; we consequently hypothesize that cell density correlates with cell cycle blockade by the E-cadherin/β-catenin pathway, resulting in the apparent relationship between cell density and $\overline{\alpha}_P$. Further evidence can be seen in duct F19 (Figure 10.4, right): the majority of the proliferation activity is in a single layer of cells along the duct wall. Because these cells are adhered to the basement membrane, they present less surface for E-cadherin binding activity (relative to the interior cells), resulting in reduced E-cadherin blockade of proliferation.

These hypotheses can be tested by correlating $\overline{\alpha}_P$ with cell density in a larger number of ducts, performing IHC for β-catenin activity, and correlating β-catenin-mediated transcription (indicated by presence of β-catenin in the cell nuclei) with cell density and distance from the duct wall. One could use these data to hypothesize, calibrate, and test new functional forms for α_P, such as:

$$\alpha_P(\mathcal{S}, \sigma, \bullet, \circ) = \overline{\alpha}_P(\bullet, \circ) \left(1 - \mathcal{E}\langle\mathcal{E}\rangle \frac{\rho}{\rho_{\max}}\right) \left(\frac{\sigma - \sigma_H}{1 - \sigma_H}\right), \tag{10.23}$$

where ρ is the local cell density, $\rho_{\max}$ is the density at which PI ≈ 0, $\mathcal{E}$ is the cell's (nondimensional) E-cadherin expression, and $\langle\mathcal{E}\rangle$ is the mean E-cadherin expression for the tumor. In such a formulation, $\overline{\alpha}_P(\bullet, \circ)$ determines the cell's $\mathcal{Q} \to \mathcal{P}$ transition rate in normoxic conditions with minimal E-cadherin signaling, and depends upon the cell's genetic profile $\bullet$ and potentially other signaling and/or microenvironmental factors $\circ$. These ideas are the topic of ongoing research by Macklin, Cristini, Edgerton, and others.

10.4.3 Calibrating Multiscale Modeling Frameworks: Preliminary Results

In Chapter 7, we discussed a multiscale modeling framework where data from various sources and scales (e.g., molecular data from IHC, cell-scale data from motility assays, and tissue-scale geometric data from MRI) are propogated throughout the framework through appropriate, dynamic upscaling and downscaling between the scales. The net result is a simulator that can simulate whole 3-D tumors in large microenvironments while efficiently incorporating molecular- and cell-scale dynamics (e.g., hypoxic signaling and cell motility) where needed.

Recall that the overall change in the number of cells N is given by

$$\dot{N} = (\beta_P \mathrm{PI}(\sigma) - \beta_A \mathrm{AI})\, N, \tag{10.24}$$

where we write PI(σ) to emphasize the dependency of PI on oxygen levels as demonstrated in Section 10.4.2. For the continuum model, the analogous form (neglecting cell transport) is given by

$$\dot{\rho} = (\lambda_M \sigma - \lambda_A)\, \rho. \tag{10.25}$$

By averaging across a fixed volume and equating these terms, we estimate that

$$\lambda_M \approx \frac{\beta_P \langle \mathrm{PI} \rangle}{\langle \sigma \rangle}, \qquad \text{and} \qquad \lambda_A \approx \beta_A \mathrm{AI}, \tag{10.26}$$

leading us to a preliminary upscaling between the agent and continuum models:

$$A = \frac{\lambda_A}{\lambda_M} = \langle \sigma \rangle \frac{\beta_A \mathrm{AI}}{\beta_P \langle \mathrm{PI} \rangle}, \tag{10.27}$$

or alternatively (by equating cell proliferation when $\sigma = 1$ in both models),

$$\lambda_M \approx \beta_P \mathrm{PI}(1) \Rightarrow A \approx \frac{\beta_A \mathrm{AI}}{\beta_P \mathrm{PI}(1)}. \tag{10.28}$$

Case ID	Subtype	Grade	A	L_0 (μm)	R (cm) (predicted)	R (cm) (geometric average of measured values***)	Model Prediction Accurate
14	Cribriform	2	0.004	171.83	34.63	0.58	-
19	Mixed**	3	0.0247	78.87	1.72	1.14	+
8	Cribriform	2	0.0342	183.22	5.52	0.46	-
28	Solid	3	0.0368	86.58	1.33	1.47	+
13	Solid	3	0.0373	96.43	1.51	1.64	+
22	Cribriform	3	0.0441	97.08	1.30	1.04	+
18(L)	Mixed**	3	0.0498	111.71	1.44	1.64	+
21	Cribriform	2	0.0601	113.11	1.17	1.03	+
23	Solid	3	0.120	134.78	0.75	0.58	+
15	Cribriform	1	0.132	147.77	0.75	0.48	+
17	Mixed**	2	0.223	108.92	0.28	0.56	+
18(R)	Cribriform	1	0.280	116.35	0.24	0.53	+

Table 10.5. Summary of pathological features with parameter values and predictions for index series*

* Volume density of 24.8% averaged over all cases was used for f

** Mixed Subtype denotes mixed solid and cribriform subtypes

*** Calculated geometric mean radius based upon measured dimensions

We applied the upscaling in Eq. (10.27) to the AI and PI data for 12 de-identified index cases obtained from archived mastectomy patient material at the M. D. Anderson Cancer Center. (See [196] for more information on how the cases were selected and the patient tissues were prepared and processed to obtain AI, PI, viable rim thickness, and viable volume fraction.) The data are given in Table 10.5. Applying Eq. (10.27) to this data, we obtained a patient-specific value of A for each case. See the fourth column of Table 10.5.

Next, we predicted the non-dimensional steady-state tumor size as a function of A, based upon solving the model in [151] (see Chapter 3) with spherical symmetry. The resulting curve is in Figure 10.8 (dashed curve). To properly compare this predicted relationship between A and the nondimensional tumor size R for the individual cases, we must properly determine the patient-specific length scale L to nondimensionalize the patients' measured tumor sizes (column 7 in Table 10.5). The diffusional length scale used by [151] (see Section 10.2.3) was formulated for solid tumors, whereas DCIS grows in ducts that comprise a fraction of the measured tumor volume. We modify the length scale by re-examining the nutrient transport equation. If f is the volume fraction of the breast tissue occupied by viable tumor, then the nutrient equation can be altered to describe the reduced uptake in the overall tissue:

$$0 = D\nabla^2\sigma - f\lambda\sigma, \tag{10.29}$$

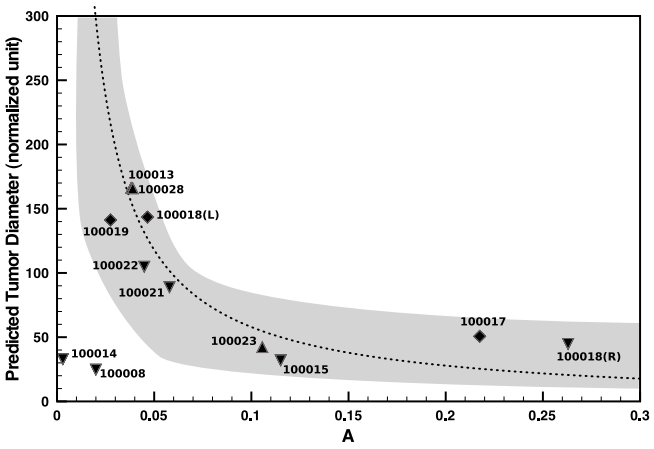

Figure 10.8 Validation of model predictions: Solid-type (▲), cribriform-type (▼), and mixed-type (◆) DCIS plotted against the model prediction (**dotted line**) from [151]. The **shaded region** gives the standard deviation in A (measured in individual duct spaces) for each case.

which admits the modified length scale

$$L = \sqrt{\frac{D}{f\lambda}} = \frac{1}{\sqrt{f}} L_0. \tag{10.30}$$

This scale now accounts for the depletion of oxygen across the entire cancerous region, rather than only within the solid tumor portion. We used an average value of $f = 0.248$ across all 12 index cases [196].

We used the measured viable rim thickness (Table 10.5: column 5) to estimate L_0 for each case; this takes into account the variability from patient to patient in the vascularity of the tissue between the ducts, differences in tumor cell density, as well as any differences in the cellular oxygen uptake rates. We nondimensionalized the measured tumor sizes using this length scale (Table 10.5: column 7). These predictions are presented as the labeled points in Figure 10.8. There was good qualitative and quantitative agreement between the predictions (dotted curve) and measurements (plotted points) for these index cases. To better quantify the quality of the predictions, we also estimated the measurement error (shaded region) based upon the standard deviation in AI and PI (horizontal breadth of the region). Ten of the twelve cases (83.33%: labeled '+' in Table 10.5: column 8) of the cases fell within the error estimate. The remaining two cases (16.67%) substantially over-estimated the tumor sizes.

Biological and modeling significance

The success of the model in predicting the tumor sizes serves to validate the biological modeling hypotheses at all scales, the calibration technique, and the upscaling linking the scales. Had any of these been invalid, then the model predictions would likely have been much less accurate.

At the cellular scale, the successful predictions validate the fundamental dependency of proliferation upon oxygen and nutrient availability, as well as the relative independence of apoptosis with respect to nutrient availability; the latter runs counter to the clear link between hypoxia and necrosis, underscoring the importance in properly modeling the nuances in cell death at the cellular scale. This theme was further explored in Section 6.6.3.

Given the successful upscaling, the work gives credence to the functional forms for the cell proliferation and apoptosis parameters λ_M and λ_A. This provides a concrete connection between cell-scale measurements (PI and AI) and macroscopic model quantities (λ_M and λ_A), allowing better physical interpretation of those macroscopic parameters. The parameter λ_M measures the rate of cell division in normoxic tissue, and its rate should be inversely proportional to cell cycle time β_P^{-1} plus the mean waiting time between cell cycles, here functionally encapsulated in PI. Similarly, the parameter λ_A gives the mean rate of cell death, which incorporates both the time scale of apoptosis (β_A^{-1}) and the mean waiting time to apoptosis (encapsulated in AI). Both parameters implicitly involve tumor genetics and proteomics through AI and PI.

These results and a similar analytical upscaling suggest a functional form for calibrating the necrosis volume loss parameter λ_N in our earlier continuum models in [432, 437, 438, 230, 439, 433, 440, 441] and Chapter 3: $\lambda_N \approx \beta_{NL}\,(1 - V_S/V)$, where β_{NL}^{-1} is the mean time for necrotic cells to lyse and lose their water content, and V_S/V is the non-water fraction of each cell. In Section 6.6.3, we estimated β_{NL}^{-1} is on the order of 1 to 5 days, and in Section 10.3.1, we estimated $V_S/V \approx 0.1$; hence, we estimate that λ_N is in the range $0.18\ \text{day}^{-1} \leq \lambda_N \leq 0.9\ \text{day}^{-1}$. This range is consistent with prior estimates using alternative approaches. In parameter studies on λ_N/λ_M conducted in [439], $0.1\ \text{day}^{-1} \leq \lambda_N \leq 1.0\ \text{day}^{-1}$ gave necrotic core sizes and morphologies consistent with *in vitro* tumor spheroids such as in [147]. Furthermore, calibration work on non-calcified glioblastoma multiforme in [228] estimated $\lambda_N \approx 0.7\ \text{day}^{-1}$.

At the whole-tumor scale, the good model predictions validate the nutrient and oxygen diffusional limit to tumor growth, even in vascularized tissue [151, 147]. In this case, the diffusional limit theory holds well once appropriately adapted to growth in a sparse duct microarchitecture, interspersed by well-vascularized breast stroma: at the macroscopic scale, this is completely analogous to growth of a well-vascularized tumor. The model success also validates the modification we made to the oxygen length scale to account for the breast tissue microarchitecture, and points to likely success when we more fully integrate this microarchitecture into the cell- and multicell-scale tumor behavior.

Lastly, this early success suggests that for short time scales or near steady state (when parameter values are relatively constant), we can calibrate and predict tumor growth based upon measurable physical quantities (proliferation and apoptosis rates, etc.) alone, without need for precise proteomic and genetic information that ultimately determine those physical quantitites. In effect, cancer be treated as an engineering problem determined by physical processes, without

regard for the genetic and molecular basis for those processes. However, as our work in Section 10.4.2 highlights, the molecular (and hence phenotypic) characteristics of a tumor can vary considerably even for fixed times. Hence, molecular- and cellular-scale modeling *are* required if we are to refine our modeling to accurately predict tumor morphology, motility, and other fine-scale details in patient-specific simulated tissues, as well as to understand a tumor's heterogeneous response to therapy. Indeed, this is the essence of multiscale modeling: to properly incorporate an increasing amount of data from various modeling scales to improve the predictivity of the modeling framework.

Clinical implications

The fact that ten of the twelve index cases could be accurately predicted using steady-state theory suggests that DCIS emerges quickly from an undetectable precursor state (e.g., ADH) betweeen annual mammograms. Indeed, in an exploration of the time to reach steady state, we noted that DCIS tumors reach 95% of their maximum size within three months of initiation for a physiological range of values of A, f and L_0 (results not shown). We therefore expect that 85% of DCIS should be at steady state for women undergoing yearly mammograms. For a sample size of 12, we should therefore expect one-to-two (on average: 1.8) cases to be smaller than the steady state predictions, fully consistent with the two overestimated cases above (denoted by '-' in column 8 of Table 10.5 above).

This has clear clinical implications. Given the relatively fast time scale of DCIS progression, at-risk populations (e.g., families with BRCA1 or BRCA2 mutations) may require more frequent surveillance than annual mammograms to adequately detect and treat breast cancer before it progresses to invasion. Indeed, an estimated 75% of all DCIS cases are already invasive at the time of detection [399, 348, 25]. Alternatively, low-dose chemotherapeutics could be prescribed for such high-risk groups to slow (undetected) DCIS progression to allow for adequate detection by annual mammograms.

Given the fast progression of DCIS to a steady state and the prevalence of hypoxia and necrosis when large or densely-packed ducts are involved, we see that tumor cells may be subject to hypoxic stress for substantial periods of time prior to detection by annual mammogram. This is consistent with the prevalence of co-existent invasive carcinoma in newly-detected DCIS cases [399]. Our simulations show that the extent of necrosis can be predicted by identifying regions of severe hypoxia. Based upon our simulations, necrosis occurs primarily in larger ducts with densely packed DCIS. Thus, the tumor's physical location, kinetic rates of proliferation and apoptosis, and local cell density are determinant predictors of extent of necrosis. Given that the peri-necrotic rim of a tumor represents the cell population that is at greatest risk for evolution to invasion, these measureable quantities could be better predictors of which DCIS cases are more likely to become invasive than grade or necrosis is today.

Our results also suggest new possible correlates for compromised margins (a predictor of tumor recurrence) and DCIS behavior. Several groups have studied

the relationship between the frequency with which residual DCIS is found in a re-excision and the margin status of the previous excision. For example, in a study of core biopsy predictors of compromised margins, [179] found that surface area involvement of cores by DCIS, solid type, high grade, presence of necrosis, and presence of calcifications all correlated with compromised margins in univariate analysis; surface area involvement persisted in multivariate analysis. This is consistent with our model's primary inputs: AI and PI correlate with grade, f is determined by the surface area DCIS density (and increases with solid-type DCIS). Furthermore, necrosis and calcification increase with hypoxia in our model, which scales roughly with tumor size and likelihood of invasion. Thus the morphological characteristics that [179] correlates with compromised margin are histological surrogates for parameter inputs in our mechanistic model; conversely, our mechanistic model should be able to use these quantifiable physical measurements to more specifically and accurately predict compromised margins. Thus, the model provides a mechanistic explanation for many of the morphological correlates that have been used to predict clinical outcomes in DCIS.

Similarly, high grade DCIS (especially solid-type) and DCIS with comedo-type necrosis are both considered to be correlates of higher risk for subsequent invasion. From the model we conclude that involvement of larger ducts, lower values of A, and more dense microarchitecture will result in more necrosis, and hence should correspond to higher risk of hypoxic stress and pro-invasion mutations. The interaction of physical location, growth and apoptosis rates, and local cell density are more specific predictors of extent of hypoxia and necrosis than the gross and morphologic parameters in typical use (grade, subtype, and comedonecrosis). Loss of p53 activity has also been suggested as a contributor to invasive potential in high grade DCIS (see e.g. [472]). Such loss would decrease native rates of apoptosis and decrease A. For high grade DCIS with its higher range of PI, the decrease in A could be even more significant, leading to rapid tumor growth and the evolution of extensive hypoxic stress zones. Thus, a decrease in A and the generation of more hypoxic stress could be a mechanism by which loss of p53 activity contributes to invasive potential in high grade DCIS.

Long-term vision: a surgical planning tool

In the longer term, a computational model of DCIS built upon these results could lead to better predictions of the tumor volume extent prior to treatment, thus providing a clinical tool to assist in (a) determining when a mastectomy is the preferred treatment over breast conserving surgery, (b) predicting an adequate tumor excision volume and geometry for breast conserving surgery, and (c) defining an optimal zone for radiation therapy. We have already demonstrated good predictive capability of the tumor volume; if we can additionally correlate mammographic or other imaging data to the tumor morphology (or predict it in near-real time based upon simulating growth in the duct system), we could overlay the predicted tumor morphology on real-time imaging during surgery.

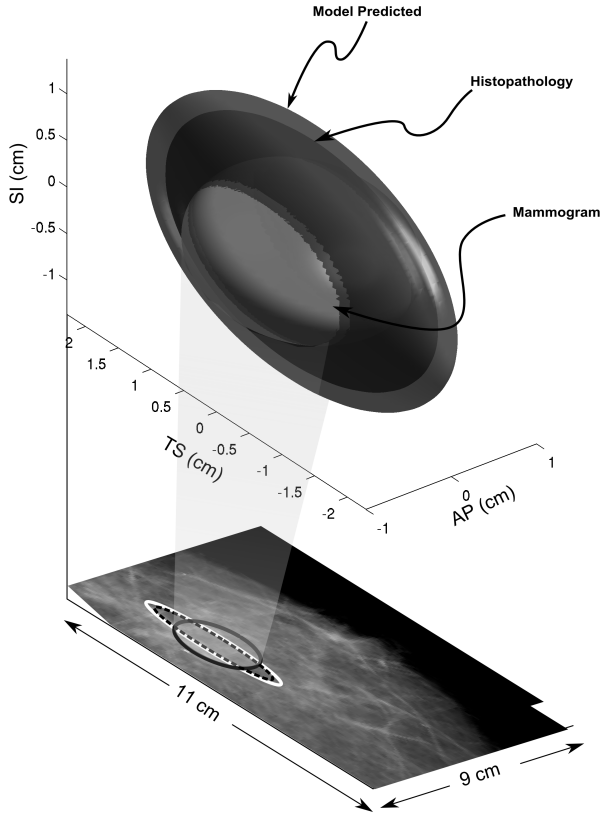

Figure 10.9 Comparison of mammography-based (innermost labeled volume), pathology-measured (intermediate volume labeled "histopathology"), and model-predicted (largest labeled volume) excision volumes. The model-predicted excision region uses the pathology-measured shape as a proof of concept. Reprinted from the submission [196].

In Figure 10.9, we show a mock-up of what such a tool might look like. Using the shape defined by the post-mastectomy pathology specimen as a proof of concept, along with the current volume prediction from Section 10.4.3, we show how a simulation result could be overlaid on medical imagery to plan a surgical excision. If the pathology-based shape estimate could be replaced by either a more detailed simulation geometry or better pre-surgical shape measurements, the such software (mock-up shown as largest labeled volume) could predict much more precise surgical margins than current mammographic measurements (innermost labeled volume), potentially allowing the patient to avoid re-excision.

In comparison, the volume predicted from measuring distances between calcifications in the mammogram is known to be inadequate (see e.g. [296]). While the model alone currently does not predict the tumor shape, this information could be obtained in near-real time using an imaging modality such as MRI. Thus, using the tumor shape defined by MRI, along with immunohistochemical

and histological inputs from the core biopsy, the model could be used to visualize the volume requiring resection rather than having to rely on viewing 2-D images of any kind (see e.g. [399]).

10.5 Concluding remarks

In this chapter, we adapted the agent-based model presented in Chapter 6 to ductal carcinoma in situ of the breast. After developing and testing a patient-specific calibration protocol, we surveyed several applications to test the model's predictive power.

We began by using the model to help estimate difficult biophysical parameters pertaining to cell death. By applying a volume-averaged version of the model to histopathologic data from normal breast epithelium, we were able to estimate the time duration of apoptosis at around 8.6 hours; this parameter can be difficult to observe experimentally. Furthermore, we arrived at the same estimate when using data from both pre- and post-menopausal women, thereby supporting the biological hypothesis that cancerous and non-cancerous cells use the same physical mechanisms (in this case apoptosis and proliferation), only with altered frequency. We applied a numerical implementation of the model to conduct a parameter study on the time duration of cell calcification, arriving at an estimate of approximately 15 days. Currently, cell calcification is difficult to study *in vitro*, and only limited, indirectly-available data exist for calcification *in vivo*.

We next examined the ability of the model to make testable predictions on cell biology. The model predicted a Michaelis-Menten-type response of cell proliferation to oxygen availability; subsequent analysis of patient immunohistochemistry verified the prediction with excellent quantitative agreement. However, this agreement came with an important caveat: the precise relationship between proliferation and oxygen availability can vary substantially across a single tumor even for fixed times–pointing to genetic and proteomic variation across a patient's tumor, such as in the E-cadherin/β-catenin signaling pathway.

Lastly, we conducted a preliminary study on the ability of the agent model to calibrate continuum-scale models (by upscaling) for patient-specific predictions of breast tumor volume. We found that the agent model, as part of a larger multiscale modeling framework, had success in predicting patient-specific tumor sizes in a small group of index cases. This success points to the multiscale model's potential as a tool that could be used in conjunction with an imaging modality to construct a volume around tumor axes and midpoints in MR and other imagery. This would help surgeons and pathologists to visualize DCIS tumors during surgery. We see the model as an important first step in understanding the physical changes that result from molecular alterations and contribute to the development of invasive breast cancer.

References

[1] A. C. Abajian and J. S. Lowengrug. An agent-based hybrid model for avascular tumor growth. *UCI Undergrad. Res. J.*, 11, 2008.

[2] R. Abbott, S. Forrest, and K. Pienta. Simulating the hallmarks of cancer. *Art. Lif*, 12(4):617–34, 2006.

[3] H. Acker, J. Carlsson, W. Mueller-Klieser, and R. Sutherland. Comparative po2 measurements in cell spheroids cultured with different techniques. *Br. J. Cancer*, 56:325–327, 1987.

[4] D. Adalsteinsson and J. A. Sethian. The Fast Construction of Extension Velocities in Level Set Methods. *J. Comput. Phys.*, 148(1):2–22, 1999.

[5] J. Adam. General aspects of modeling tumor growth and the immune response. In J. Adam and N. Bellomo, editors, *A Survey of Models on Tumor Immune Systems Dynamics*, pages 15–87. Birkhaeuser, Boston, 1996.

[6] T. L. Adamovich and R. M. Simmons. Ductal carcinoma in situ with microinvasion. *Am. J. Surg.*, 186(2):112–6, 2003.

[7] B. Addison-Smith, D. McElwain, and P. Maini. A simple mechanistic model of sprout spacing in tumour-associated angiogenesis. *J. Theor. Biol.*, 250:1–15, 2008.

[8] L. Ai, W.-J. Kim, T.-Y. Kim, C. R. Fields, N. A. Massoll, K. D. Robertson, and K. D. Brown. Epigenetic silencing of the tumor suppressor cystatin m occurs during breast cancer progression. *Canc. Res.*, 66:7899–909, 2006.

[9] T. Alarcón, H. Byrne, and P. Maini. A cellular automaton model for tumour growth in inhomogeneous environment. *J. Theor. Biol.*, 225:257–274, 2003.

[10] T. Alarcón, H. Byrne, and P. Maini. A multiple scale model for tumor growth. *Multiscale Model. Sim.*, 3:440–475, 2005.

[11] M. Alber, M. Kiskowski, J. Glazier, and Y. Jiang. On cellular automaton approaches to modeling biological cells. In R. Rosenthal and D. Gilliam, editors, *IMA Series on Mathematical systems theory in biology, communication and finance*, volume 142, pages 1–40. Springer, New York, 2002.

[12] B. Alberts, A. Johnson, J. Lewis, M. Raff, K. Roberts, and P. Walter. *Molecular Biology of the Cell*. Garland Science, New York, fifth edition, 2007.

[13] J. W. Allen, S. R. Khetani, R. S. Johnson, and S. Bhatia. *In Vitro* Liver Tissue Model Established from Transgenic Mice: Role of HIF-1alpha on Hypoxic Gene Expression. *Tissue Engineering*, 12(11):3135–47, 2006.

[14] M. Amar and A. Goriely. Growth and instability in soft tissues. *J. Mech. Phys. Solids*, 53:2284–2319, 2005.

[15] D. Ambrosi, F. Bussolino, and L. Preziosi. A review of vasculogenesis models. *Comp. Math. Meth. Med.*, 6:1–19, 2005.

[16] D. Ambrosi, A. Duperray, V. Peschetola, and C. Verdier. Traction patterns of tumor cells. *J. Math. Biol.*, 58(1-2):163–81, 2009.

[17] D. Ambrosi, A. Gamba, and G. Serini. Cell directional and chemotaxis in vascular morphogenesis. *Bull. Math. Biol.*, 66:1851–1873, 2004.

[18] D. Ambrosi and F. Guana. Mechanical aspects of growth in soft tissues. *Boll. Unione Mat. Ital.*, 7:775–781, 2004.

[19] D. Ambrosi and F. Guana. Stress-modulated growth. *Math. Mech. Solids*, 12:319–343, 2007.

[20] D. Ambrosi, A. Guillou, and E. DiMartino. Stress-modulated remodeling of a non-homogeneous body. *Biomech. Model. Mechanobiol.*, 7:63–76, 2008.

[21] D. Ambrosi and F. Mollica. On the mechanics of a growing tumor. *Int. J. Eng. Sci.*, 40:1297–1316, 2002.

[22] D. Ambrosi and F. Mollica. The role of stress in the growth of a multicell spheroid. *J. Math. Biol.*, 48:477–499, 2004.

[23] D. Ambrosi and L. Preziosi. On the closure of mass balance models for tumor growth. *Math. Mod. Meth. Appl. Sci.*, 12:737–754, 2002.

[24] D. Ambrosi and L. Preziosi. Cell adhesion mechanisms and elasto-viscoplastic mechanics of tumours. *Mech. Model. Mechanobiol.*, 8:397–413, 2009. 10.1007/s10237-008-145-y.

[25] American Cancer Society. American cancer society breast cancer facts and figures 2007-2008. *Atlanta: American Cancer Society, Inc.*, 2007. http://www.cancer.org/downloads/STT/BCFF-Final.pdf.

[26] A. Anderson. A hybrid mathematical model of solid tumour invasion: The importance of cell adhesion. *Math. Med. Biol.*, 22:163–186, 2005.

[27] A. Anderson and M. Chaplain. Continuous and discrete mathematical models of tumor-induced angiogenesis. *Bull. Math. Biol.*, 60:857–900, 1998.

[28] A. Anderson, M. Chaplain, E. Newman, R. Steele, and A. Thompson. Mathematical modeling of tumour invasion and metastasis. *J. Theor. Med.*, 2:129–154, 2000.

[29] A. Anderson, M. Chaplain, K. Rejniak, and J. Fozard. Single-cell based models in biology and medicine. *Math. Med. Biol.*, 25(2):185–6, 2008.

[30] A. Anderson and V. Quaranta. Integrative mathematical oncology. *Nature Reviews Cancer*, 8:227–244, 2008.

[31] A. Anderson, K. Rejniak, P. Gerlee, and V. Quaranta. Microenvironment driven invasion: a multiscale multimodel investigation. *J. Math. Biol.*, 58:579–624, 2009.

[32] A. Anderson, A. Weaver, P. Commmings, and V. Quaranta. Tumor morphology and phenotypic evolution driven by selective pressure from the microenvironment. *Cell*, 127:905–915, 2006.

[33] E. Anderson. Cellular homeostasis and the breast. *Maturitas*, 48(S1):13–7, 2004.

[34] M. Anderson, D. Srolovitz, G. Grest, and P. Sahini. Computer simulation of grain growth- i. kinetics. *Acta Metall.*, 32:783–791, 1984.

[35] E. D. Angelis and L. Preziosi. Advection-diffusion models for solid tumour evolution in vivo and related free boundary problem. *Math. Models Meth. Appl. Sci.*, 10:379–407, 2000.

[36] R. Araujo and D. McElwain. A history of the study of solid tumour growth: The contribution of mathematical modelling. *Bull. Math. Biol.*, 66:1039–1091, 2004.

[37] R. Araujo and D. McElwain. A linear-elastic model of anisotropic tumor growth. *Eur. J. Appl. Math.*, 15:365–384, 2004.

[38] R. Araujo and D. McElwain. New insights into vascular collapse and growth dynamics in solid tumors. *J. Theor. Biol.*, 228:335–346, 2004.

[39] R. Araujo and D. McElwain. A mixture theory for the genesis of residual stresses in growing tissues I: A general formulation. *SIAM J. Appl. Math.*, 65:1261–1284, 2005.

[40] R. Araujo and D. McElwain. A mixture theory for the genesis of residual stresses in growing tissues II: Solutions to the biphasic equations for a multicell spheroid. *SIAM J. Appl. Math.*, 66:447–467, 2005.

[41] R. Araujo and D. McElwain. The nature of the stresses induced during tissue growth. *Appl. Math. Lett.*, 18:1081–1088, 2005.

[42] N. Armstrong, K. Painter, and J. Sherratt. A continuum approach to modeling cell-cell adhesion. *J. Theor. Biol.*, 243:98–113, 2006.

[43] P. Armstrong. Light and electron microscope studies of cell sorting in combinations of chick embryo and neural retina and retinal pigment epithelium. *Willhelm Roux Archiv.*, 168:125–141, 1971.

[44] S. Astanin and L. Preziosi. Multiphase models of tumour growth. In N. Bellomo, M. Chaplain, and E. DeAngelis, editors, *Selected Topics on Cancer Modelling: Genesis - Evolution - Immune Competition - Therapy*. Birkhaeuser, Boston, 2007.

[45] C. Athale and T. Deisboeck. The effects of egf-receptor density on multiscale tumor growth patterns. *J. Theor. Biol.*, 238:771–779, 2006.

[46] C. Athale, Y. Mansury, and T. Deisboeck. Simulating the impact of a molecular 'decision-process' on cellular phenotype and multicellular patterns in brain tumors. *J. Theor. Biol.*, 233:469–481, 2005.

[47] H. Augustin. Tubes, branches, and pillars: The many ways of forming a new vasculature. *Circ. Research*, 89:645–647, 2001.

[48] D. H. Ausprunk and J. Folkman. Migration and proliferation of endothelial cells in preformed and newly formed blood vessels during tumour angiogenesis. *Microvasc. Res.*, 14(1):53–65, 1977.

[49] D. Balding and D. McElwain. A mathematical model of tumor-induced capillary growth. *J. Theor. Biol.*, 114:53–73, 1985.

[50] A. Bardelli, M. Basile, E. Audero, S. Giordano, S. Wennström, S. Ménard, P. Comoglio, and C. Ponzetto. Concomitant activation of pathways downstream of grb2 and pi 3-kinase is required for met-mediated metastasis. *Oncogene*, 18:1139–1146, 1999.

[51] L. F. Barros, T. Hermosilla, and J. Castro. Necrotic volume increase and the early physiology of necrosis. *Comp. Biochem. Physiol. A. Mol. Integr. Physiol.*, 130:401–9, 2001.

[52] U. Bartels, C. Hawkins, M. Jing, M. Ho, P. Dirks, J. Rutka, D. Stephens, and E. Bouffet. Vascularity and angiogenesis as predictors of growth in optic pathway/hypothalamic gliomas. *J. Neurosurg.*, 104:314–320, 2006.

[53] K. Bartha and H. Rieger. Vascular network remodeling via vessel cooption, regression and growth in tumors. *J. Theor. Biol.*, 241:903–918, 2006.

[54] R. J. Basaraba, H. Bielefeldt-Ohmann, E. K. Eschelbach, C. Reisenhauer, A. E. Tolnay, L. C. Taraba, C. A. Shanley, E. A. Smith, C. L. Bedwell, E. A. Chlipala, and I. A. Orme. Increased expression of host iron-binding proteins precedes iron accumulation and calcification of primary lung lesions in experimental tuberculosis in the guinea pig. *Tuberculosis*, 88(1):69–79, 2008.

[55] A. Bauer, T. Jackson, and Y. Jiang. A cell-based model exhibiting branching and anastomosis during tumor-induced angiogenesis. *Biophys. J.*, 92:3105–3121, 2007.

[56] F. O. Baxter, K. Neoh, and M. C. Tevendale. The beginning of the end: Death signaling in early involution. *J. Mamm. Gland Biol. Neoplas.*, 12(1):3–13, 2007.

[57] B. Bazaliy and A. Friedman. A free boundary problem for an elliptic-parabolic system: Application to a model of tumor growth. *Comm. Partial Diff. Eq.*, 28:517–560, 2003.

[58] P. A. Beachy, S. S. Karhadkar, and D. M. Berman. Tissue repair and stem cell renewal in carcinogenesis. *Nature*, 432(7015):324–331, 2004.

[59] E. Bearer, J. Lowengrub, Y. Chuang, H. Frieboes, F. Jin, S. Wise, M. Ferrari, D. Agus, and V. Cristini. Multiparameter computational modeling of tumor invasion. *Cancer Res.*, 69:4493–4501, 2009.

[60] L. Bello, V. Lucini, F. Costa, M. Pluderi, C. Giussani, F. Acerbi, G. Carrabba, M. Pannacci, D. Caronzolo, S. Grosso, S. Shinkaruk, F. Colleoni, X. Canron, G. Tomei, G. Deleris, and A. Bikfalvi. Combinatorial administration of molecules that simultaneously inhibit angiogenesis and invasion leads to increased therapeutic efficacy in mouse models of malignant glioma. *Clin. Cancer Res.*, 10:4527–4537, 2004.

[61] N. Bellomo, E. de Angelis, and L. Preziosi. Multiscale modeling and mathematical problems related to tumor evolution and medical therapy. *J. Theor. Medicine*, 5:111–136, 2003.

[62] N. Bellomo, N. Li, and P. Maini. On the foundations of cancer modelling: selected topics, speculations, and perspectives. *Math. Models Meth. Appl. Sci.*, 4:593–646, 2008.

[63] N. Bellomo and L. Preziosi. Modelling and mathematical problems related to tumor evolution and its interaction with the immune system. *Math. Comput. Modelling*, 32:413–542, 2000.

[64] M. Ben-Amar and A. Gorielly. Growth and instability in elastic tissues. *J. Mech. Phys. Solids*, 53:2284–2319, 2005.

[65] R. Benjamin, J. Capparella, and A. Brown. Classification of glioblastoma multiforme in adults by molecular genetics. *The Cancer Journal*, 9:82–90, 2003.

[66] J. R. Berenson, L. Rajdev, and M. Broder. Pathophysiology of Bone Metastases. *Cancer Biol. Ther.*, 5(9):1078–1081, 2006.

[67] M. Berger and I. Rigoutsos. An algorithm for point clustering and grid generation. *IEEE Trans. Syst. Man. Cybern.*, 21:1278–1286, 1991.

[68] H. Bernsen and A. van der Kogel. Antiangiogenic therapy in brain tumor models. *J. Neuro-oncology*, 45:247–255, 1999.

[69] R. Betteridge, M. Owen, H. Byrne, T. Alarcón, and P. Maini. The impact of cell crowding and active cell movement on vascular tumour growth. *Networks Heterogen. Media*, 1:515–535, 2006.

[70] Y. Bi, C. H. Stuelten, T. Kilts, S. Wadhwa, R. V. Iozzo, P. G. Robey, X.-D. Chen, and M. F. Young. Extracellular matrix proteoglycans control the fate of bone marrow stromal cells. *J. Biol. Chem.*, 280:30481–9, 2005.

[71] M. Bienz and H. Clevers. Linking colorectal cancer to Wnt signaling. *Cell*, 103:311–20, 2000.

[72] M. V. Blagosklonny and A. B. Pardee. The restriction point of the cell cycle. *Cell Cycle*, 1(2):103–110, 2002.

[73] C. Blanpain and E. Fuchs. Epidermal Stem Cells of the Skin. *Annu. Rev. Cell Dev. Biol.*, 22:339–73, 2006.

[74] H. Bloemendal, T. Logtenberg, and E. Voest. New strategies in anti-vascular cancer therapy. *Euro J. Clin. Invest.*, 29:802–809, 1999.

[75] C. Boccaccio, M.Andò, L. Tamagnone, A. Bardelli, P. Michieli, C. Battistini, and P. Comoglio. Induction of epithelial tubules by growth factor hgf depends on the stat pathway. *Nature*, 391:285–288, 1998.

[76] K. Bold, Y. Zou, I. Kevrekidis, and M. Henson. An equation-free approach to analyzing heterogeneous cell population dynamics. *J. Math. Biol.*, 55:331–352, 2007.

[77] A. Brandt. Multi-level adaptive solutions to boundary-value problems. *Math. Comput.*, 31:333–390, 1977.

[78] B. Brandt, D. Kemming, J. Packeisen, R. Simon, M. Helms, U. Feldmann, A. Matuschek, C. Kersting, B. Hinrichs, J.-M. Midart, D. Bellet, K. Bartkowiak, N. Dankbar, T. Dittmar, G. Sauter, W. Boecker, and H. Buerger. Expression of early placenta insulin-like growth factor in breast cancer cells provides an autocrine loop that preodominantly enhances invasiveness and motility. *Endocrine-Related Canc.*, 12(4):823–7, 2005.

[79] A. Bredel-Geissler, U. Karbach, S. Walenta, L. Vollrath, and W. Mueller-Klieser. Proliferation-associated oxygen consumption and morphology of tumor cells in monolayer and spheroid culture. *J. Cell Phys.*, 153:44–52, 1992.

[80] D. Bresch, T. Colin, E. Grenier, and B. Ribba. A viscoelastic model for avascular tumor growth. inria-00267292, version 2, 2008.

[81] D. Bresch, T. Colin, E. Grenier, B. Ribba, and O. Saut. Computational modeling of solid tumor growth: the avascular stage. unpublished, 2007.

[82] C. Breward, H. Byrne, and C. Lewis. The role of cell-cell interactions in a two-phase model for avascular tumour growth. *J. Math. Biol.*, 45:125–152, 2002.

[83] C. Breward, H. Byrne, and C. Lewis. A multiphase model describing vascular tumor growth. *Bull. Math. Biol.*, 65:609–640, 2003.

[84] D. Brizel, S. Scully, J. Harrelson, L. Layfield, J. Bean, L. Prosnitz, and M. Dewhirst. Tumor oxygenation predicts for the likelihood of distant metastases in human soft tissue sarcoma. *Cancer Res.*, 56:941–943, 1996.

[85] D. Brizel, G. Sibley, L. Prosnitz, R. Scher, and M. Dewhirst. Tumor hypoxia adversely affects the prognosis of carcinoma of the head and neck. *Int. J. Radiat. Oncol. Biol. Phys.*, 38:285–289, 1997.

[86] J. Brown and L. Lowe. Multigrid elliptic equation solver with adaptive mesh refinement. *J. Comput. Phys.*, 209:582–598, 2005.

[87] R. K. Bruick and S. L. McKnight. A conserved family of Prolyl-4-Hydroxylases that modify HIF. *Science*, 294(5545):1337–40, 2001.

[88] H. Bueno, G. Ercole, and A. Zumpano. Asymptotic behaviour of quasi-stationary solutions of a nonlinear problem modelling the growth of tumours. *Nonlinearity*, 18:1629–1642, 2005.

[89] E. Bullitt, D. Zeng, G. Gerig, S. Aylward, S. Joshi, J. Smith, W. Lin, and M. Ewend. Vessel tortuosity and brain tumor malignance: a blinded study. *Acad. Radiol.*, 12:1232–1240, 2005.

[90] A. Burton. Rate of growth of solid tumours as a problem of diffusion. *Growth*, 30:157–176, 1966.

[91] F. Bussolino, M. Arese, E. Audero, E. Giraudo, S. Marchiò, S. Mitola, L. Primo, and G. Serini. *Cancer Modelling and Simulation*, chapter 1: Biological Aspects of Tumour Angiogenesis, pages 1–22. Chapman and Hall/CRC, London, 2003.

[92] L. M. Butler, S. Khan, G. E. Rainger, and G. B. Nash. Effects of endothelial basement membrane on neutrophil adhesion and migration. *Cell. Immun.*, 251:56–61, 2008.

[93] S. Byers, C. Sommers, B. Hoxter, A. Mercurio, and A. Tozeren. Role of e-cadherin in the response of tumor cell aggregates to lymphatic, venous and arterial flow: measurement of cell-cell adhesion strength. *J. Cell Sci.*, 108:2053–2064, 1995.

[94] H. Byrne. The effect of time delays on the dynamics of avascular tumor growth. *Math. Biosci.*, 144:83–117, 1997.

[95] H. Byrne. The importance of intercellular adhesion in the development of carcinomas. *IMA J. Math. Med. Biol.*, 14:305–323, 1997.

[96] H. Byrne. A comparison of the roles of localized and nonlocalised growth factors in solid tumour growth. *Math. Models Meth. Appl. Sci.*, 9:541–568, 1999.

[97] H. Byrne. A weakly nonlinear analysis of a model of avascular solid tumour growth. *J. Math. Biol.*, 39:59–89, 1999.

[98] H. Byrne, T. Alarcón, M. Owen, S. Webb, and P. Maini. Modeling aspects of cancer dynamics: A review. *Phi. Trans. R. Soc. A*, 364:1563–1578, 2006.

[99] H. Byrne and M. Chaplain. Growth of nonnecrotic tumors in the presence and absence of inhibitors. *Mathl. Biosci.*, 130:151–181, 1995.

[100] H. Byrne and M. Chaplain. Mathematical models for tumour angiogenesis: Numerical simulations and nonlinear wave solutions. *Bull. Math. Biol.*, 57:461–486, 1995.

[101] H. Byrne and M. Chaplain. Growth of necrotic tumors in the presence and absence of inhibitors. *Mathl. Biosci.*, 135:187–216, 1996.

[102] H. Byrne and M. Chaplain. Modelling the role of cell-cell adhesion in the growth and development of carcinomas. *Mathl. Comput. Modelling*, 24:1–17, 1996.

[103] H. Byrne and M. Chaplain. Free boundary value problems associated with the growth and development of multicellular spheroids. *Eur. J. Appl. Math.*, 8:639–658, 1997.

[104] H. Byrne and D. Drasdo. Individual-based and continuum models of growing cell populations: A comparison. *J. Math. Biol.*, 58(4-5):657–87, 2009.

[105] H. Byrne, J. King, D. McElwain, and L. Preziosi. A two-phase model of solid tumour growth. *Appl. Math. Letters*, 16:567–573, 2003.

[106] H. Byrne and P. Matthews. Asymmetric growth of models of avascular solid tumors: exploiting symmetries. *IMA J. Math. Appl. Med. Biol.*, 19:1–29, 2002.

[107] H. Byrne and L. Preziosi. Modelling solid tumour growth using the theory of mixtures. *Math. Med. Biol.*, 20:341–366, 2003.

[108] N. Cabioglu, K. K. Hunt, A. A. Sahin, H. M. Kuerer, G. V. Babiera, S. E. Singletary, G. J. Whitman, M. I. Ross, F. C. Ames, B. W. Feig, T. A. Buchholz, and F. Meric-Bernstam. Role for intraoperative margin assessment in patients undergoing breast-conserving surgery. *Ann. Surg. Oncol.*, 14(4):1458–71, 2007.

[109] J. Cahn and J. Hilliard. Free energy of a nonuniform system. i. interfacial free energy. *J. Chem. Phys.*, 28:258–267, 1958.

[110] R. Cairns, T. Kalliomaki, and R. Hill. Acute (cyclic) hypoxia enhances spontaneous metastasis of kht murine tumors. *Cancer Res.*, 61:8903–8908, 2001.

[111] D. Q. Calcagno, M. F. Leal, A. D. Seabra, A. S. Khayat, E. S. Chen, S. Demachki, P. P. Assumpcao, M. H. G. Faria, S. H. B. Rabenhorst, M. V. P. Ferreira, M. D. C. Smith, and R. R. Burbano. Interrelationship between chromosome 8 aneuploidy, C-MYC amplification and increased expression in individuals from northern Brazil with gastric adenocarcinoma. *World J. Gastroenterol.*, 12(38):6027–211, 2006.

[112] V. Capasso and D. Morale. Stochastic modelling of tumour-induced angiogenesis. *J. Math. Biol.*, 58:219–233, 2009.

[113] J. Carlsson and H. Acker. Relations ph, oxygen partial pressure and growth in cultured cell spheroids. *Int. J. Cancer*, 42:715–720, 1988.

[114] P. Carmeliot and R. Jain. Angiogenesis in cancer and other diseases. *Nature*, 407:249–257, 2000.

[115] L. Carreras, P. Macklin, J. Kim, S. Sanga, V. Cristini, and M. E. Edgerton. Oxygen uptake in quiescent versus cycling cells in a model of DCIS. *U.S. Canadian Acad. Path.*, 2010 Annual Meeting, 2010. (submitted).

[116] J. Casciari, S. Sotirchos, and R. Sutherland. Glucose diffusivity in multicellular tumor spheroids. *Cancer Res.*, 48:3905–3909, 1988.

[117] J. Casciari, S. Sotirchos, and R. Sutherland. Variations in tumor cell growth rates and metabolism with oxygen concentration, glucose concentration, and extracellular ph. *J. Cell. Physiol.*, 151:386–394, 1992.

[118] M. Castro, C. Molina-Paris, and T. Deisboeck. Tumor growth instability and the onset of invasion. *Phys. Rev. E*, 72:041907, 2005.

[119] P. Castro, P. Soares, L. Gusmo, R. Seruca, and M. Sobrinho-Simes. H-*RAS* 81 polymorphism is significantly associated with aneuploidy in follicular tumors of the thyroid. *Oncogene*, 25:4620–7, 2006.

[120] M. Chaplain. Reaction-diffusion prepatterning and its potential role in tumour invasion. *J. Biol. Sys.*, 3:929–936, 1995.

[121] M. Chaplain. Avascular growth, angiogenesis and vascular growth in solid tumours: The mathematical modelling of the stages of tumour development. *Mathl. Comput. Modelling*, 23:47–87, 1996.

[122] M. Chaplain. Pattern formation in cancer. In M. Chaplain, G. Singh, and J. MacLachlan, editors, *On Growth and Form: Spatio-Temporal Pattern Formation in Biology*. Wiley, New York, 2000.

[123] M. Chaplain, M. Ganesh, and I. Graham. Spatio-temporal pattern formation on spherical surfaces: numerical simulation and application to solid tumour growth. *J. Math. Biol.*, 42:387–423, 2001.

[124] M. Chaplain, L. Graziano, and L. Preziosi. Mathematical modelling of the loss of tissue compression responsiveness and its role in solid tumor development. *Math. Med. Biol.*, 23:197–229, 2006.

[125] M. Chaplain and G. Lolas. Mathematical modeling of cancer cell invasion of tissue: The role of the urokinase plasminogen activation system. *Math. Models Meth. Appl. Sci.*, 15:1685–1734, 2005.

[126] M. Chaplain, S. McDougall, and A. Anderson. Mathematical modeling of tumor-induced angiogenesis. *Ann. Rev. Biomed. Eng.*, 8:233–257, 2006.

[127] M. Chaplain and B. Sleeman. Modelling the growth of solid tumours and incorporating a method for their classification using nonlinear elasticity theory. *J. Math. Biol.*, 31:431–479, 1993.

[128] M. Chaplain and A. Stuart. A model mechanism for the chemotactic response of endothelial cells to tumor angiogenesis factor. *IMA J. Math. Appl. Med. Biol.*, 10:149–168, 1993.

[129] A. Chauvier and L. Preziosi. A mathematical framework to model migration of a cell population in the extracellular matrix. In A. Chauvier, L. Preziosi, and C. Verdier, editors, *Cell mechanics: From single cell scale-based models to multiscale modeling*. Chapman and Hall/CRC Press, Boca Raton, 2009.

[130] A. Chauviere, T. Hillen, and L. Preziosi. Modeling cell movement in anisotropic and heterogeneous tissues. *Networks Hetero. Media*, 2:333–357, 2007.

[131] A. Chauviere, L. Preziosi, and T. Hillen. Modeling the motion of a cell population in the extracellular matrix. *Discrete Cont. Dyn. Syst. B*, Supp:250–259, 2007.

[132] C. Chen, H. Byrne, and J. King. The influence of growth-induced stress from the surrounding medium on the development of multicell spheroids. *J. Math. Biol.*, 43:191–220, 2001.

[133] L. L. Chen, L. Zhang, J. Yoon, and T. S. Deisboeck. Cancer cell motility: optimizing spatial search strategies. *Biosys.*, 95(3):234–42, 2009.

[134] W. W. Chen, B. Schoeberl, P. J. Jasper, M. Niepel, D. A. Nielsen, U B andLauffenburger, et al. Input-output behavior of ErbB signaling pathways as revealed by a mass action model trained against dynamic data. *Mol. Syst. Biol.*, 5:239ff, 2009.

[135] X. Chen, S. Cui, and A. Friedman. A hyperbolic free boundary problem modeling tumor growth: asymptotic behavior. *Trans. Am. Math. Soc.*, 357:4771–4804, 2005.

[136] L. Cheng, N. K. Al-Kaisi, N. H. Gordon, A. Y. Liu, F. Gebrail, and R. R. Shenk. Relationship between the size and margin status of ductal carcinoma in situ of the breast and residual disease. *J. Natl. Cancer Inst.*, 89(18):1356–60, 1997.

[137] J. H. Choi, Y. Y. Jeong, S. S. Shin, H. S. Lim, and H. K. Kang. Primary calcified T-cell lymphoma of the urinary bladder: a case report. *Korean J. Radiol.*, 4(4):252–4, 2003.

[138] Y.-L. Chuang, M. E. Edgerton, P. Macklin, S. Wise, J. S. Lowengrub, and V. Cristini. Clinical predictions of bulk DCIS properties based on a duct-scale mixture model. (in preparation), 2009.

[139] S. Ciatto, S. Bianchi, and V. Vezzosi. Mammographic appearance of calcifications as a predictor of intraductal carcinoma histologic subtype. *Eur. Radiology*, 4(1):23–6, 1994.

[140] R. G. Clyde, J. L. Brown, T. R. Hupp, N. Zhelev, and J. W. Crawford. The role of modelling in identifying drug targets for diseases of the cell cycle. *J. R. Soc. Interface*, 3(10):617–627, 2006.

[141] D. Coffey. Self-organization, complexity and chaos: the new biology for medicine. *Nature Med.*, 4:882, 1998.

[142] P. Colella, D. T. Graves, T. J. Ligocki, D. F. Martin, D. Modiano, D. B. Serafini, and B. V. Straalen. CHOMBO software package for AMR applications: design document. Technical report, Lawrence Berkeley National Laboratory, Applied Numerical Algrithms Group; NERSC Division, Berkeley, CA, USA, 2003.

[143] B. Coleman and W. Noll. Thermodynamics of elastic materials with conduction and viscosity. *Arch. Rat. Mech.*, 13:167–178, 1963.

[144] M. Conacci-Sorrell, J. Zhurinsky, and A. Ben-Zeév. The cadherin-catenin adhesion system in signaling and cancer. *J. Clin. Invest.*, 109(8):987–91, 2002.

[145] J. Condeelis, R. Singer, and J. Segall. The great escape: When cancer cells hijack the genes for chemotaxis and motility. *Annu. Rev. Cell Dev. Biol.*, 21:695–718, 2005.

[146] A. Coniglio, A. deCandia, S. DiTalia, and A. Gamba. Percolation and burgers' dynamics in a model of capillary formation. *Phys. Rev. E*, 69:051910, 2004.

[147] V. Cristini, H. Frieboes, R. Gatenby, S. Caserta, M. Ferrari, and J. Sinek. Morphologic instability and cancer invasion. *Clin. Cancer Res.*, 11:6772–6779, 2005.

[148] V. Cristini, H. Frieboes, X. Li, J. Lowengrub, P. Macklin, S. Sanga, S. Wise, and X. Zheng. Nonlinear modeling and simulation of tumor growth. In N. Bellomo, M. Chaplain, and E. de Angelis, editors, *Modelling and simulation in science, engineering and technology*. Birkhäuser, Boston, 2008.

[149] V. Cristini, X. Li, J. Lowengrub, and S. Wise. Nonlinear simulations of solid tumor growth using a mixture model: invasion and branching. *J. Math. Biol.*, 58(4-5):723–763, 2009.

[150] V. Cristini and J. Lowengrub. Three-dimensional crystal growth. i. linear analysis and self-similar evolution. *J. Crystal Growth*, 240:267–276, 2002.

[151] V. Cristini, J. Lowengrub, and Q. Nie. Nonlinear simulation of tumor growth. *J. Math. Biol.*, 46:191–224, 2003.

[152] S. Cui. Analysis of a mathematical model for the growth of tumors under the action of external inhibitors. *J. Math. Biol.*, 44:395–426, 2002.

[153] S. Cui. Analysis of a free boundary problem modeling tumor growth. *Acta Math. Sinica*, 21:1071–1082, 2005.

[154] S. Cui. Well-posedness of a multidimensional free boundary problem modelling the growth of nonnecrotic tumors. *J. Func. Analysis*, 245:1–18, 2007.

[155] S. Cui. Lie group action and stability analysis of stationary solutions for a free boundary problem modelling tumor growth. *J. Diff. Eq.*, 246(5):1845–1882, 2009.

[156] S. Cui and J. Escher. Asymptotic behaviour of solutions of a multidimensional moving boundary problem modeling tumor growth. *Comm. Partial Diff. Equations*, 33:636–655, 2008.

[157] S. Cui and J. Escher. Well-posedness and stability of a multi-dimensional tumor growth model. *Arch. Rat. Mech. Analysis*, 191:173–193, 2009.

[158] S. Cui and A. Friedman. Analysis of a mathematical model of the effect of inhibitors on the growth of tumors. *Math. Biosci.*, 164:103–137, 2000.

[159] S. Cui and A. Friedman. A free boundary problem for a singular system of differential equations: An application to a model of tumor growth. *Trans. Amer. Math. Soc.*, 255:3537–3590, 2003.

[160] S. Cui and A. Friedman. Formation of necrotic cores in the growth of tumors: analytic results. *Acta Matematica Scientia*, 26:781–796, 2006.

[161] S. Cui and X. Wei. Global existence for a parabolic-hyperbolic free boundary problem modelling tumor growth. *Acta Math. Appl. Sinica*, 21:597–614, 2005.

[162] S. Cui and S. Xu. Analysis of mathematical models for the growth of tumors with time delays in cell proliferation. *J. Math. Analysis Appl.*, 336:523–541, 2007.

[163] J. Dallon and H. Othmer. How cellular movement determines the collective force generated by the dictyostelium discoideum slug. *J. Theor. Biol.*, 231:299–306, 2004.

[164] C. G. Danes, S. L. Wyszomierski, J. Lu, C. L. Neal, W. Yang, and D. Yu. 14-3-3ζ down-regulates p53 in mammary epithelial cells and confers luminal filling. *Canc. Res.*, 68:1760–7, 2008.

[165] K. Date, K. Matsumoto, K. Kuba, H. Shimura, M. Tanaka, and T. Nakamura. Inhibition of tumor growth and invasion by a four-kringle antagonist (hgf/nk4) for hepatocyte growth factor. *Oncogene*, 17:3045–3054, 1998.

[166] C. R. De Potter, I. Eeckhout, A.-M. Schelfhout, M.-L. Geerts, and H. J. Roelsh. Keratinocyte induced chemotaxis in the pathogenesis of Paget's disease of the breast. *Histopath.*, 24(4):349–56, 1994.

[167] J. Debnath and J. Brugge. Modelling glandular epithelial cancers in three-dimensional cultures. *Nature Rev. Cancer*, 5:675–688, 2005.

[168] J. Debnath, K. Mills, N. Collins, M. Reginato, S. Muthuswarmy, and J. Brugge. The role of apoptosis in creating and maintaining luminal space within normal and oncogene-expressing mammary acini. *Cell*, 111:29–40, 2002.

[169] T. Deisboeck, M. Berens, A. Kansal, S. Torquato, A. Stemmer-Rachamimov, and E. Chiocca. Pattern of self-organization in tumour systems: Complex growth dynamics in a novel brain tumour spherical model. *Cell Proliferation*, 34:115–134, 2001.

[170] T. Deisboeck, L. Zhang, J. Yoon, and J. Costa. In silico cancer modeling: is it ready for prime time? *Nature Clin. Practice Oncol.*, 6(1):34–42, 2009.

[171] K. DeJaeger, M. Kavanagh, and R. Hill. Relationship of hypoxia to metastatic ability in rodent tumors. *Br. J. Cancer*, 84:1280–1285, 2001.

[172] H. D. Dell. Milestone 1 (1889) Seed and soil hypothesis: Observations from a ploughman. *Nat. Rev. Cancer*, 6:S7, 1989. http://www.nature.com/milestones/milecancer/index.html.

[173] R. Demicheli, G. Pratesi, and R. Foroni. The exponential-gompertzian growth model : data from six tumor cell lines in vitro and in vivo. estimate of the transition point from exponential to gompertzian growth and potential clinical applications. *Tumori*, 77:189–195, 1991.

[174] B. Desai, T. Ma, and M. A. Chellaiah. Invadopodia and matrix degradation, a new property of prostate cancer cells during migration and invasion. *J. Biol. Chem.*, 283(20):13856–66, 2008.

[175] A. Deutsch and S. Dormann. *Cellular automaton modeling of biological pattern formation*. Birkhäuser, New York, 2005.

[176] A. E. DeWitt, J. Y. Dong, H. S. Wiley, and D. A. Lauffenburger. Quantitative analysis of the EGF receptor autocrine system reveals cryptic regulation of cell response by ligand capture. *J. Cell. Sci.*, 114(Pt 12):2301–13, 2001.

[177] J. Diaz and J. Tello. On the mathematical controllability in a simple growth tumors model by the internal localized action of inhibitors. *Nonlinear Analysis*, 4:109–125, 2003.

[178] A. DiCarlo and S. Quiligotti. Growth and balance. *Mech. Res. Comm.*, 29:449–456, 2002.

[179] M. F. Dillon, A. A. Maguire, E. W. McDermott, C. Myers, A. D. Hill, A. O'Doherty, and C. M. Quinn. Needle core biopsy characteristics identify patients at risk of compromised margins in breast conservation surgery. *Mod. Pathol.*, 21(1):39–45, 2008.

[180] M. F. Dillon, E. W. McDermott, A. O'Doherty, C. M. Quinn, A. D. Hill, and N. O'Higgins. Factors affecting successful breast conservation for ductal carcinoma in situ. *Ann. Surg. Oncol.*, 14(5):1618–28, 2007.

[181] R. Dillon, M. Owen, and K. Painter. A single-cell based model of multicellular growth using the immersed interface method. In B. Khoo, Z. Li, and P. Lin, editors, *Contemporary mathematics: Moving interface problems and applications in fluid dynamics*, volume 466, chapter 1, pages 1–15. AMS, Providence, 2008.

[182] S. Dormann and A. Deutsch. Modeling of self-organized avascular tumor growth with a hybrid cellular automaton. *In Silico Biology*, 2:393–406, 2002.

[183] D. Drasdo. On selected individual-based approaches to the dynamics of multicellular systems. In W. Alt, M. Chaplain, and M. Griebel, editors, *Multiscale modeling*. Birkhaeuser, Basel, 2003.

[184] D. Drasdo. Coarse graining in simulated cell populations. *Adv. Complex Sys.*, 8:319–363, 2005.

[185] D. Drasdo and S. Höhme. Individual-based approaches to birth and death in avascular tumors. *Math. Comput. Modelling*, 37:1163–1175, 2003.

[186] D. Drasdo and S. Höhme. A single-scale-based model of tumor growth in vitro: monolayers and spheroids. *Phys. Biol.*, 2:133–147, 2005.

[187] D. Drasdo and S. Höhme. On the role of physics in the growth and pattern of multicellular systems: What we learn from individual-cell based models? *J. Stat. Phys.*, 128:287–345, 2007.

[188] D. Drasdo, R. Kree, and J. McCaskill. Monte-carlo approach to tissue cell populations. *Phys. Rev. E*, 52:6635–6657, 1995.

[189] F. Drees, S. Pokutta, S. Yamada, W. J. Nelson, and W. T. Weis. Alpha-catenin is a molecular switch that binds E-cadherin-beta-catenin and regulates actin-filament assembly. *Cell*, 123:903–15, 2005.

[190] W. R. Duan, D. S. Garner, S. D. Williams, C. L. Funckes-Shippy, I. S. Spath, and E. A. G. Blomme. Comparison of immunohistochemistry for activated caspase-3 and cleaved cytokeratin 18 with the TUNEL method for quantification of apoptosis in histological sections of PC-3 subcutaneous xenografts. *J. Pathol.*, 199(2):221–8, 2003.

[191] M. Ducasse and M. A. Brown. Epigenetic aberrations and cancer. *Mol. Cancer*, 5:60, 2006.

[192] H. S. Earp, T. L. Dawson, X. Li, and H. Yu. Heterodimerization and functional interaction between EGF receptor family members: a new signaling paradigm with implications for breast cancer research. *Breast Canc. Res. Treat.*, 35(1):115–132, 1995.

[193] D. A. Eberhard, B. E. Johnson, L. C. Amler, et al. Mutations in the epidermal growth factor receptor and in KRAS are predictive and prognostic indicatorsin patients with non-small-cell lung cancer treated with chemotherapy alone and in combination with erlotinib. *J. Clin. Oncol.*, 23:5900–09, 2005.

[194] M. Edgerton, Y.-L. Chuang, J. Kim, G. Tomaiuolo, P. Macklin, S. Sanga, W. Yang, A. Broom, K.-A. Do, and V. Cristini. Using mathematical models to understand the time dependence of the growth of ductal carcinoma in situ. *31st Annual San Antonio Breast Cancer Symposium.*, Supplement to Volume 68(24):Abstract 1165, 2008.

[195] M. Edgerton, Y.-L. Chuang, J. Kim, G. Tomaiuolo, P. Macklin, S. Sanga, W. Yang, A. Broom, K.-A. Do, and V. Cristini. Using mathematical models to understand time-dependence of growth DCIS: Implications for clinical detection and IDC. (in preparation), 2009.

[196] M. Edgerton, P. Macklin, Y.-L. Chuang, G. Tomaiuolo, W. Yang, J. Kim, S. Sanga, A. Broom, K.-A. Do, and V. Cristini. A multiscale model of ductal carcinoma in situ. *Cancer Res.*, 2010. (submitted).

[197] A. W. El-Kareh and T. W. Secomb. A mathematical model for cisplatin cellular pharmacodynamics. *Neoplasia*, 5(2):161–9, 2003.

[198] A. W. El-Kareh and T. W. Secomb. Two-mechanism peak concentration model for cellular pharmacodynamics of doxorubicin. *Neoplasia*, 7(7):705–13, 2005.

[199] C. Elliot and S. Luckhaus. A generalized diffusion equation for phase separation of a multi-component mixture with interfacial free energy. Technical report, Univ. Sussex and Univ. Bonn, 1991. Inst. Math. Appl., report 887.

[200] Y. I. Elshimali and W. W. Grody. The Clinical Significance of Circulating Tumor Cells in the Peripheral Blood. *Diagn. Mol. Pathol.*, 15(4):187–194, 2006.

[201] P. Elvin and A. Garner. Tumour invasion and metastasis: challenges facing drug discovery. *Curr. Opin. Pharmacol.*, 5:374–381, 2005.

[202] S. Enam, M. Rosenblum, and K. Edvardsen. Role of extracellular matrix in tumor invasion: migration of glioma cells along fibronectinpositive mesenchymal cell processes.

Neurosurgery, 42:599–608, 1998.

[203] R. Erban, I. Kevrekidis, and H. Othmer. An equation-free computational approach for extracting population-level behavior from individual-based models of biological dispersal. *Physica D*, 215:1–24, 2006.

[204] R. Erban and H. Othmer. From individual to collective behavior in bacterial chemotaxis. *SIAM J. Appl. Math.*, 65:361–391, 2004.

[205] R. Erban and H. Othmer. From signal transduction to spatial pattern formation in *E. coli*: A paradigm for multi-scale modeling in biology. *Multiscale Model. Simul.*, 3:362–394, 2005.

[206] B. Erbas, E. Provenzano, J. Armes, and D. Gertig. The natural history of ductal carcinoma *in situ* of the breast: a review. *Breast Canc. Res. Treat.*, 97(2):135–44, 2006.

[207] J. Erler, K. Bennewith, M. Nicolau, N. Dornhoefer, C. Kong, Q.-T. Le, J.-T. Chi, S. Jeffrey, and A. Giaccia. Lysyl oxidase is essential for hypoxia-induced metastasis. *Nature*, 440:1222–1226, 2006.

[208] M. Esteban and P. Maxwell. If, a missing link between metabolism and cancer. *Nature Med.*, 11:1047–1048, 2005.

[209] J. Fang, R. Gillies, and R. Gatenby. Adaptation to hypoxia and acidosis in carcinogenesis and tumor progression. *Semin. Cancer Biol.*, 18:330–337, 2008.

[210] A. Fasano, A. Bertuzzi, and A. Gandolfi. *Complex systems in biomedicine*, chapter Mathematical modelling of tumour growth and treatment, pages 71–108. Springer, Milan, 2006.

[211] L. Ferrante, S. Bompadre, L. Possati, and L. Leone. Parameter estimation in a gompertzian stochastic model for tumor growth. *Biometrics*, 56:1076–1081, 2000.

[212] M. Ferrari. Cancer nanotechnology: opportunities and challenges. *Nature Rev. Cancer*, 5:161–171, 2005.

[213] R. Filion and A. Popel. A reaction-diffusion model of basic fibroblast growth factor interactions with cell surface receptors. *Annals Biomed. Eng.*, 32:645–663, 2004.

[214] I. Fischer, J.-p. Gagner, M. Law, E. W. Newcomb, and D. Zagzag. Angiogenesis in Gliomas: Biology and Molecular Pathophysiology. *Brain Pathol.*, 15(4):297–310, 2005.

[215] A. B. Fisher, S. Chien, A. I. Barakat, and R. M. Nerem. Endothelial cellular response to altered shear stress. *Am. J. Physiol. Heart Circ. Physiol.*, 281(3):L529–L533, 2001.

[216] B. Flaherty, J. P. McGarry, and P. E. McHugh. Mathematical models of cell motility. *Cell. Biochem. Biophys.*, 49(1):14–28, 2007.

[217] G. B. Fogarty, N. M. Conus, J. Chu, and G. McArthur. Characterization of the expression and activation of the epidermal growth factor receptor in squamous cell carcinoma of the skin. *Brit. J. Derm.*, 156(1):92–98, 2007.

[218] J. Folkman. Angiogenesis in cancer, vascular, rheumatoid and other disease. *Nat. Med.*, 1:27–30, 1995.

[219] J. Forsythe, B. Jiang, N. Iyer, S. L. F. Agani, R. Koos, and G. Semenza. Activation of vascular endothelial growth factor gene transcription by hypoxia-inducible factor 1. *Mol. Cell. Biol.*, 16:4604–4613, 1996.

[220] L. M. Franks and M. A. Knowles. What is Cancer? In Knowles and Selby [386], chapter 1, pages 1–24.

[221] S. Franks, H. Byrne, J. King, J. Underwood, and C. Lewis. Modeling the early growth of ductal carcinoma in situ of the breast. *J. Math. Biol.*, 47:424–452, 2003.

[222] S. Franks, H. Byrne, H. Mudhar, J. Underwood, and C. Lewis. Mathematical modeling of comedo ductal carcinoma in situ of the breast. *Math. Med. Biol.*, 20:277–308, 2003.

[223] S. Franks and J. King. Interactions between a uniformly proliferating tumor and its surrounding. uniform material properties. *Math. Med. Biol.*, 20:47–89, 2003.

[224] J. Freyer and R. Sutherland. Determination of diffusion constants for metabolites in multicell tumor spheroids. *Adv. Exp. Med. Biol.*, 159:463–475, 1983.

[225] J. Freyer and R. Sutherland. A reduction in the in situ rates of oxygen and glucose consumption of cells in emt6/ro spheroids during growth. *J. Cell. Physiol.*, 124:516–524, 1985.

[226] J. Freyer and R. Sutherland. Regulation of growth saturation and development of necrosis in emt6/ro multicellular spheroids by the glucose and oxygen supply. *Cancer Res.*, 46:3504–3512, 1986.

[227] J. P. Freyer. Decreased mitochondrial function in quiescent cells isolated from multicellular tumor spheroids. *J. Cell. Physiol.*, 176(1):138–49, 1998.

[228] H. Frieboes, M. Edgerton, J. Fruehauf, F. Rose, L. Worrall, R. Gatenby, M. Ferrari, and V. Cristini. Prediction of drug response in breast cancer using integrative experimental/computational modeling. *Cancer Research*, 69:4484–4492, 2009.

[229] H. Frieboes, J. Fang, Y.-L. Chuang, S. Wise, J. Lowengrub, and V. Cristini. Nonlinear simulations of three-dimensional multispecies tumor growth -ii: Tumor invasion and angiogenesis. *J. Theor. Biol.*, in review.

[230] H. Frieboes, J. Lowengrub, S. Wise, X. Zheng, P. Macklin, E. Bearer, and V. Cristini. Computer simulation of glioma growth and morphology. *NeuroImage*, 37:S59–S70, 2007.

[231] H. Frieboes, X. Zheng, C.-H. Sun, B. Tromberg, R. Gatenby, and V. Cristini. An integrated computational/experimental model of tumor invasion. *Cancer Res.*, 66:1597–1604, 2006.

[232] P. Friedl. Prespecification and plasticity: shifting mechanisms of cell migration. *Curr. Opin. Cell Biol.*, 16:14–23, 2004.

[233] P. Friedl, E. Brocker, and K. Zanker. Integrins, cell matrix interactions and cell migration strategies: fundamental differences in leukocytes and tumor cells. *Cell Adhes. Commun.*, 6:225–236, 1998.

[234] P. Friedl, Y. Hegerfeldt, and M. Tilisch. Collective cell migration in morphogenesis and cancer. *Int. J. Dev. Biol.*, 48:441–449, 2004.

[235] P. Friedl, P. Noble, P. Walton, D. Laird, P. Chauvin, R. Tabah, M. Black, and K. Zaenker. Migration of coordinated cell clusters in mesenchymal and epithelial cancer explants in vitro. *Cancer Res.*, 55:4557–4560, 1995.

[236] P. Friedl and A. Wolf. Tumor cell invasion and migration: diversity and escape mechanisms. *Nat. Rev. Cancer*, 3:362–374, 2003.

[237] A. Friedman. A hierarchy of cancer models and their mathematical challenges. *Discrete Cont. Dyn. Systems Ser. B*, 4:147–159, 2004.

[238] A. Friedman, N. Bellomo, and P. Maini. Mathematical analysis and challenges arising from models of tumor growth. *Math. Models Meth. Appl. Sci.*, 17:1751–1772, 2007.

[239] A. Friedman and B. Hu. Asymptotic stability for a free boundary problem arising in a tumor model. *J. Diff. Equations*, 227:598–639, 2005.

[240] A. Friedman and B. Hu. Bifurcation from stability to instability for a free boundary problem arising in a tumor model. *Arch. Rat. Mech. Analysis*, 180:293–330, 2006.

[241] A. Friedman and B. Hu. Bifurcation from stability to instability for a free boundary problem modeling tumor growth by stokes equation. *J. Math. Analysis Appl.*, 327:643–664, 2007.

[242] A. Friedman and F. Reitich. Analysis of a mathematical model for the growth of tumors. *J. Math. Biol.*, 38:262–284, 1999.

[243] A. Friedman and F. Reitich. On the existence of spatially patterned dormant malignancies in a model for the growth of non-necrotic vascular tumors. *Math. Models Meth. Appl. Sci.*, 11:601–625, 2001.

[244] A. Friedman and F. Reitich. Symmetry-breaking bifurcation of analytic solutions to free boundary problems: an application to a model of tumor growth. *Trans. Am. Math. Soc.*, 353:1587–1634, 2001.

[245] S. H. Friend, R. Bernards, S. Rogelj, R. A. Weinberg, J. M. Rapaport, D. M. Albert, and T. P. Dryja. A human DNA segment with properties of the gene that predisposes to retinoblastoma and osteosarcoma. *Nature*, 323:643–6, 1986.

[246] S. M. Frisch and H. Francis. Disruption of epithelial cell-matrix interactions induces apoptosis. *J. Cell Biol.*, 124:619–26, 1994.

[247] R. Fukuda, H. Zhang, J.-W. Kim, L. Shimoda, C. V. Dang, and G. L. Semenza. HIF-1 regulates cytochrome oxidase subunits to optimize efficiency of respiration in hypoxic cells. *Cell*, 129(1):111–22, 2007.

[248] D. Fukumura and R. Jain. Tumor microenvironment abnormalities: causes, consequences, and strategies to normalize. *J. Cell. Biochem.*, 101:937–949, 2007.

[249] Y. Fung. *Biomechanics: motion, flow, stress and growth*. Springer, New York, 1990.

[250] Y. Fung. *Biomechanics: material properties of living tissues*. Springer, New York, 1993.

[251] A.-P. Gadeau, H. Chaulet, D. Daret, M. Kockx, J.-M. Daniel-Lamaziè, and C. Desgranges. Time course of osteopontin, osteocalcin, and osteonectin accumulation and calcification after acute vessel wall injury. *J. Histochem. Cytochem.*, 49:79–86, 2001.

[252] D. Galaris, A. Barbouti, and P. Korantzopoulos. Oxidative stress in hepatic ischemia-reperfusion injury: The role of antioxidants and iron chelating compounds. *Curr. Pharma. Design*, 12:2875–2890, 2006.

[253] J. Galle, G. Aust, G. Schaller, T. Beyer, and D. Drasdo. Individual cell-based models of the spatial temporal organization of multicellular systems- achievements and limitations. *Cytometry*, 69A:704–710, 2006.

[254] J. Galle, M. Hoffmann, and G. Aust. From single cells to tissue architecture-a bottom-up approach to modeling the spatio-temporal organization of complex multicellular systems. *J. Math. Biol.*, 58:261–283, 2009.

[255] J. Galle, M. Loeffler, and D. Drasdo. Modeling the effect of deregulated proliferation and apoptosis on the growth dynamics of epithelial cell populations in vitro. *Biophys. J.*, 88:62–75, 2005.

[256] J. Galle, L. Preziosi, and A. Tosin. Contact inhibition of growth described using a multiphase model and an individual cell based model. *Appl. Math. Lett.*, 2009. in press.

[257] A. Gamba, D. Ambrosi, A. Coniglio, A. deCandia, S. DiTalia, E. Giraudo, G. Serini, L. Preziosi, and F. Bussolino. Percolation, morphogenesis and burgers dynamics in blood vessels formation. *Phys. Rev. Lett.*, 90:118101, 2003.

[258] J. Ganghoffer. Some issues related to growth and goal functions for continuum biological systems. *Phil. Mag.*, 85:4353–4391, 2005.

[259] M. Garbey and G. Zouridakis. Modeling tumor growth: from differential deformable models to growth prediction of tumors detected in pet images. *Eng. Med. Biol. Soc.*, 3:2687–2690, 2003.

[260] H. Garcke, M. Rumpf, and U. Weikard. The Cahn-Hilliard equation with elasticity: finite element approximation and qualitative studies. *Interfaces Free Bound*, pages 101–

118, 2001.

[261] M. Gardner. The fantastic combinations of john conway's new solitaire game "life". *Scientific American*, 223:120–3, Oct. 1970.

[262] K. Garikipati, E. Arruda, K. Grosh, H. Narayanan, and S. Calve. A continuum treatment of growth in biological tissue: the coupling of mass transport and mechanics. *J. Mech. Phys. Solids*, 52:1595–1625, 2004.

[263] L. Garner, Y. Lau, T. Jackson, M. Uhler, D. Jordan, and R. Gilgenbach. Incorporating spatial dependence into a multicellular tumor spheroid growth model. *J. Appl. Phys.*, 98:124701, 2005.

[264] R. Gatenby and E. Gawlinski. The glycolytic phenotype in carcinogenesis and tumor invasion: insights through mathematical models. *Cancer Res.*, 63:3847–3854, 2003.

[265] R. Gatenby, E. Gawlinski, A. Gmitro, B. Kaylor, and R. Gillies. Acid-mediated tumor invasion: a multidisciplinary study. *Cancer Res.*, 66:5216–5223, 2006.

[266] R. Gatenby and E. Gawlinsky. *The tumour microenvironment*, chapter Mathematical models of tumour invasion mediated by transformation-induced alteration of microenvironmental pH, pages 85–99. Wiley, London, 2003.

[267] R. Gatenby and R. Gillies. A microenvironmental model of carcinogenesis. *Nat. Rev. Cancer*, 8:56–61, 2008.

[268] R. Gatenby, K. Smallbone, P. Maini, F. Rose, J. Averill, R. Nagle, L. Worrall, and R. Gillies. Cellular adaptations to hypoxia and acidosis during somatic evolution of breast cancer. *Br. J. Cancer*, 97:646–653, 2007.

[269] R. Gatenby and T. Vincent. An evolutionary model of carcinogenesis. *Cancer Res.*, 63:6212–6220, 2003.

[270] C. W. Gear and I. G. Kevrekidis. Projective methods for stiff differential equations: problems with gaps in the eigenvalue spectrum. *SIAM J. Sci. Comput.*, 24:1091–1106, 2003.

[271] C. W. Gear, I. G. Kevrekidis, and C. Theodoropoulos. 'Coarse' integration/bifurcation analysis via microscopic simulators: micro-Galerkin methods. *Comput. Chem. Engineer.*, 26:941–963, 2002.

[272] A. Gerisch and M. Chaplain. Mathematical modelling of cancer cell invasion of tissue: local and non-local models and the effect of adhesion. *J. Theor. Biol.*, 250:684–704, 2008.

[273] P. Gerlee and A. Anderson. An evolutionary hybrid cellular automaton model of solid tumor growth. *J. Theor. Biol.*, 246:583–603, 2007.

[274] P. Gerlee and A. Anderson. Stability analysis of a hybrid cellular automaton model of cell colony growth. *Phys. Rev. E*, 75:051911, 2007.

[275] P. Gerlee and A. Anderson. A hybrid cellular automaton model of clonal evolution in cancer: The emergence of the glycolytic phenotype. *J. Theor. Biol.*, 250:705–722, 2008.

[276] P. Gerlee and A. Anderson. A hybrid cellular automaton model of clonal evolution in cancer: The emergence of the glycolytic phenotype. *J. Theor. Biol.*, 250:705–722, 2008.

[277] J. Gevertz and S. Torquato. Modeling the effects of vasculature evolution on early brain tumor growth. *J. Theor. Biol.*, 243:517–531, 2006.

[278] F. G. Giancotti and E. Ruoslahti. Integrin signaling. *Science*, 285(5430):1028–32, 1999.

[279] J. W. Gibbs. Fourier's series. *Nature*, 59:200–200, 1898.

[280] M. Z. Gilcrease. Integrin signaling in epithelial cells. *Canc. Lett.*, 247(1):1–25, 2007.

[281] R. Gillies and R. Gatenby. Adaptive landscapes and emergent phenotypes: why do cancers have high glycolysis? *J. Bioenerg. Biomem.*, 39:251–257, 2007.

[282] R. Gillies and R. Gatenby. Hypoxia and adaptive landscapes in the evolution of carcinogenesis. *Cancer Metastasis Rev.*, 26:311–317, 2007.

[283] R. Gillies, Z. Liu, and Z. Bhujwalla. 31p-mrs measurements of extracellular ph of tumors using 3- aminopropylphosphonate. *Am. J. Physiol.*, 267:195–203, 1994.

[284] R. Gillies, I. Robey, and R. Gatenby. Causes and consequences of increased glucose metabolism of cancers. *J. Nuclear Med.*, 49:24S–42S, 2008.

[285] M. Gimbrone, R. Cotran, S. Leapman, and J. Folkman. Tumor growth and neovascularization: an experimental model using the rabbit cornea. *J. Nat. Cancer Inst.*, 52:413–427, 1974.

[286] J. Glazier and F. Garner. Simulation of the differential adhesion driven rearrangement of biological cells. *Phys. Rev. E*, 47:2128–2154, 1993.

[287] R. Godde and H. Kurz. Structural and biophysical simulation of angiogenesis and vascular remodeling. *Dev. Dyn.*, 220(4):387–401, 2001.

[288] J. J. Going and T. J. Mohun. Human breast duct anatomy, the 'sick lobe' hypothesis and intraductal approaches to breast cancer. *Breast. Canc. Res. and Treat.*, 97(3):0167–6806, 2006.

[289] J. D. Gordan, J. A. Bertout, C.-J. Hu, J. A. Diehl, and M. C. Simon. HIF-2α promotes hypoxic cell proliferation by enhancing c-Myc transcriptional activity. *Canc. Cell*, 11(4):335–47, 2007.

[290] V. Gordon, M. Valentine, M. Gardel, D. Andor-Ardó, S. Dennison, A. Bogdanov, D. Weitz, and T. Deisboeck. Measuring the mechanical stress induced by an expanding multicellular tumor system: a case study. *Exp. Cell Res.*, 289:58–66, 2003.

[291] T. Graeber, C. Osmanian, T. Jacks, and *et al.* Hypoxia-mediated selection of cells with diminished apoptotic potential in solid tumors. *Nature*, 379:88–91, 1996.

[292] F. Graner and J. Glazier. Simulation of biological cell sorting using a two-dimensional extended potts model. *Phys. Rev. Lett.*, 69:2013–2016, 1992.

[293] L. Graziano and L. Preziosi. Mechanics in tumor growth. In F. Mollica, L. Preziosi, and K. Rajagopal, editors, *Modeling of Biological Materials*, pages 267–328. Birkhaeuser, New York, 2007.

[294] H. Greenspan. Models for the growth of a solid tumor by diffusion. *Stud. Appl. Math.*, 51:317–340, 1972.

[295] H. Greenspan. On the growth and stability of cell cultures and solid tumors. *J. Theor. Biol.*, 56:229–242, 1976.

[296] A. Grin, G. Horne, M. Ennis, and F. P. O'Malley. Measuring extent of ductal carcinoma in situ in breast excision specimens: a comparison of 4 methods. *Arch. Pathol. Lab. Med.*, 133:31–7, 2009.

[297] K. Groebe, S. Erz, and W. Mueller-Klieser. Glucose diffusion coefficients determined from concentration profiles in emt6 tumor spheroids incubated in radioactively labeled l-glucose. *Adv. Exp. Med. Biol.*, 361:619–625, 1994.

[298] J. Guck, S. Schinkinger, B. Lincoln, F. Wottawah, S. Ebert, M. Romeyke, D. Lenz, H. M. Erickson, R. Ananthakrishnan, D. Mitchell, J. Käs, S. Ulvick, and C. Bilby. Optical deformability as an inherent cell marker for testing malignant transformation and metastatic competence. *Biophys. J.*, 88(5):3689–98, 2005.

[299] C. Guiot, P. D. Santo, and T. Deisboeck. Morphological instability and cancer invasion: a 'splashing water drop' analogy. *Theor. Biol. Med. Model.*, 4:4, 2007.

[300] G. P. Gupta and J. Massagu. Cancer Metastasis: Building a Framework. *Cell*, 127(4):679–695, 2006.

[301] G. Hamilton. Multicellular spheroids as an in vitro tumor model. *Cancer Letters*, 131:29–34, 1998.

[302] D. Hanahan and R. Weinberg. The hallmarks of cancer. *Cell*, 100:57–70, 2000.

[303] R. K. Hansen and M. J. Bissell. Tissue architecture and breast cancer: the role of extracellular matrix and steroid hormones. *Endocrine-Related Cancer*, 7(2):95–113, 2000.

[304] B. D. Harms, G. M. Bassi, A. R. Horwitz, and D. A. Lauffenburger. Directional persistence of EGF-induced cell migration is associated with stabilization of lamellipodial protrusions. *Biophys. J.*, 88(2):1479–88, 2005.

[305] A. Harris. Hypoxia-a key regulatory factor in tumor growth. *Nat. Rev. Cancer*, 2:38–47, 2002.

[306] A. Harten, B. Engquist, S. Osher, and S. R. Chakravarthy. Uniformly high order accurate essentially non-oscilatory schemes, III. *J. Comput. Phys.*, 71:231–303, 1987.

[307] H. Hashizume, P. Baluk, S. Morikawa, J. McLean, G. Thurston, S. Roberge, R. Jain, and D. McDonald. Openings between defective endothelial cells explain tumor vessel leakiness. *Am. J. Pathol.*, 156:1363–1380, 2000.

[308] H. Hatzikirou, L. Brusch, and A. Deutsch. From cellular automaton rules to an effective macroscopic mean field description. *Math. Biosci.*, 2009. in review.

[309] H. Hatzikirou, A. Deutsch, C. Schaller, M. Simon, and K. Swanson. Mathematical modeling of glioblastoma tumour development: A review. *Math. Models Meth. Appl. Sci.*, 15:1779–1794, 2005.

[310] M. A. Hayat. *Methods of Cancer Diagnosis, Therapy, and Prognosis: Liver Cancer*. Springer, New York, fifth edition, 2009.

[311] Y. Hegerfeldt, M. Tusch, E. Brocker, and P. Friedl. Collective cell movement in primary melanoma explants: plasticity of cell-cell interaction, 1-integrin function, and migration strategies. *Cancer Res.*, 62:2125–2130, 2002.

[312] G. Helmlinger, P. Netti, H. Lichtenbeld, R. Melder, and R. Jain. Solid stress inhibits the growth of multicellular tumor spheroids. *Nat. Biotech.*, 15:778–783, 1997.

[313] G. Helmlinger, F. Yuan, M. Dellian, and R. Jain. Interstitial ph and po2 gradients in solid tumors in vivo: high-resolution measurements reveal a lack of correlation. *Nat. Med.*, 3:177–182, 1997.

[314] R. S. Herbst. Review of epidermal growth factor receptor biology. *Int. J. Rad. Oncol. Biol. Phys.*, 59(2 (S1)):S21–S26, 2004.

[315] S.-i. Hino, C. Tanji, K. I. Nakayama, and A. Kikuchi. Phosphorylation of β-catenin by cyclic AMP-dependent protein kinase stabilizes β-catenin through inhibition of its ubiquitination. *Molec. Cell. Biol.*, 25(20):9063–72, 2005.

[316] S. Hiratsuka, K. Nakamura, S. Iwai, M. Murakami, T. Itoh, H. Kijima, J. M. Shipley, R. M. Senior, and M. Shibuya. MMP9 induction by vascular endothelial growth factor receptor-1 is involved in lung-specific metastasis. *Cancer Cell*, 2(4):289–300, 2002.

[317] M. Höckel, K. Schlenger, B. Aral, M. Mitze, U. Schaffer, and P. Vaupel. Association between tumor hypoxia and malignant progression in advanced cancer of the uterine cervix. *Cancer Res.*, 56:4509–4515, 1996.

[318] M. Höckel, K. Schlenger, S. Hoeckel, and P. Vaupel. Hypoxic cervical cancers with low apoptotic index are highly aggressive. *Cancer Res.*, 59:4525–4528, 1999.

[319] M. Höckel, K. Schlenger, and P. Vaupel. Tumor hypoxia: definitions and current clinical, biologic, and molecular aspects. *J. Natl. Cancer Inst.*, 93:266–276, 2001.

[320] C. Hogea, B. Murray, and J. Sethian. Simulating complex tumor dynamics from avascular to vascular growth using a general level-set method. *J. Math. Biol.*, 53:86–134,

2006.

[321] P. Hogeweg. Evolving mechanisms of morphogenesis: On the interplay between differential adhesion and cell-differentiation. *J. Theor. Biol.*, 203:317–333, 2000.

[322] J. Holash, P. Maisonpierre, D. Compton, P. Boland, C. Alexander, D. Zagzag, G. Yancopoulos, and S. Wiegand. Vessel cooption, regression, and growth in tumors mediated by angiopoietins and vegf. *Science*, 284:1994–1998, 1999.

[323] J. Holash, S. Wiegand, and G. Yancopoulos. New model of tumor angiogenesis: dynamic balance between vessel regression and growth mediated by angiopoietins and vegf. *Oncogene*, 18:5356–5362, 1999.

[324] M. Holmes and B. Sleeman. A mathematical model of tumor angiogenesis incorporating cellular traction and viscoelastic effects. *J. Theor. Biol.*, 202:95–112, 2000.

[325] J. M. Horowitz, D. W. Yandell, S.-H. Park, S. Canning, P. Whyte, K. Buchkovich, E. Harlow, R. A. Weinberg, and T. P. Dryja. Point mutational inactivation of the retinoblastoma antioncogene. *Science*, 243(4893):937–940, 1989.

[326] D. Horstmann, K. Painter, and H. Othmer. Aggregation under local reinforcement: From lattice to continuum. *Eur. J. Appl. Math.*, 15:545–576, 2004.

[327] K. B. Hotary, E. D. Allen, P. C. Brooks, N. S. Datta, M. W. Long, and S. J. Weiss. Membrane type 1 matrix metalloproteinase usurps tumour growth control imposed by the three-dimensional extracellular matrix. *Cell*, 114(1):33–45, 2003.

[328] M. Hu, J. Yao, L. Cai, K. E. Bachman, F. van den Brle, V. Velculescu, and K. Polyak. Distinct epigenetic changes in the stromal cells of breast cancers. *Nat. Genet.*, 37(8):899–905, 2005.

[329] Z. Hu, K. Yuri, H. Ozawa, H. Lu, and M. Kawata. The *In Vivo* time course for elimination of adrenalectomy-induced apoptotic profiles from the granule cell layer of the rat hippocampus. *J. Neurosci.*, 17(11):3981–9, 1997.

[330] J. Humphrey. Continuum biomechanics of soft biological tissues. *Proc. Roy. Soc. London A*, 459:3–46, 2003.

[331] J. Humphrey and K. Rajagopal. A constrained mixture model for growth and remodeling of soft tissues. *Math. Mod. Meth. Appl. Sci.*, 12:407–430, 2002.

[332] D. Ilic, E. A. Almeida, D. D. Schlaepfer, P. Dazin, S. Aizawa, and C. H. Damsky. Extracellular matrix survival signals transduced by focal adhesion kinase suppress p53-mediated apoptosis. *J. Cell Biol.*, 143:547–60, 1998.

[333] J. H. Irving and J. G. Kirkwood. The statistical mechanical theory of transport processes. IV. The equations of hydrodynamics. *J. Chem. Phys.*, 18:817–829, 1950.

[334] N. Ishii, D. Maier, A. Merlo, M. Tada, Y. Sawamura, A. Diserens, and E. V. Meir. Frequent co-alterations of tp53, p16/cdkn2a, p14arf, pten tumor suppressor genes in human glioma cell lines. *Brain Pathol.*, 9:469–479, 1999.

[335] T. Ishii, J. Murakami, K. Notohara, H. M. Cullings, H. Sasamoto, T. Kambara, Y. Shirakawa, Y. Naomoto, M. Ouchida, K. Shimizu, N. Tanaka, J. R. Jass, and N. Matsubara. Oeophageal squamous cell carcinoma may develop within a background of accumulating DNA methylation in normal and dysplastic mucosa. *Gut*, 56(1):13–19, 2007.

[336] T. Ishikawa, Y. Kobayashi, A. Omoto, Y. Adachi, S. Nakagawa, T. Kaneko, K. Nishida, Y. Miyamoto, Y. Chimori, T. Yoshikawa, and M. Kondo. Calcification in untreated non-Hodgkin's lymphoma of the jejunum. *Acta Haematol.*, 102(4):185–9, 1999.

[337] T. Jackson. Intracellular accumulation and mechanism of action of doxorubicin in a spatio-temporal tumor model. *J. Theor. Biol.*, 220:201–213, 2003.

[338] T. Jackson. A mathematical investigation of the multiple pathways to recurrent prostate cancer: Comparison with experimental data. *Neoplasia*, 6:697–704, 2004.

[339] T. Jackson. A mathematical model of prostate tumor growth and androgen-independent relapse. *Disc. Cont. Dyn. Sys. B*, 4:187–201, 2004.

[340] T. Jackson and H. Byrne. A mechanical model of tumor encapsulation and transcapsular spread. *Math. Biosci.*, 180:307–328, 2002.

[341] R. Jain. Determinants of tumor blood flow: a review. *Cancer Res.*, 48:2641–2658, 1988.

[342] R. Jain. Physiological barriers to delivery of monoclonal antibodies and other macromolecules in tumors. *Cancer Res.*, 50:814s–819s, 1990.

[343] R. Jain. Delivery of molecular medicine to solid tumors: lessons from in vivo imaging of gene expression and function. *J. Control. Release*, 74:7–25, 2001.

[344] R. Jain. Normalizing tumor vasculature with anti-angiogenic therapy: a new paradigm for combination therapy. *Nat. Med.*, 7:987–989, 2001.

[345] R. Jain. Molecular regulation of vessel maturation. *Nature Med.*, 9:685–693, 2003.

[346] R. Jain. Normalization of tumor vasculature: An emerging concept in antiangiogenic therapy. *Science*, 307:58–62, 2005.

[347] K. A. Janes and D. A. Lauffenburger. A biological approach to computational models of proteomic networks. *Curr. Opin. Chem. Biol.*, 10(1):73–80, 2006.

[348] A. Jemal, R. Siegel, E. Ward, T. Murray, J. Xu, and M. J. Thun. Cancer statistics, 2007. *CA Cancer J. Clin.*, 57(1):43–66, 2007.

[349] R. Jensen. Hypoxia in the tumorigenesis of gliomas and as a potential target for therapeutic measures. *Neurosurg. Focus*, 20:E24, 2006.

[350] B. Jian, N. Narula, Q.-Y. Li, E. R. Mohler III, and R. J. Levy. Progression of aortic valve stenosis: TGF-β1 is present in calcified aortic valve cusps and promotes aortic valve interstitial cell calcification via apoptosis. *Ann. Thoracic Surg.*, 75(2):457–65, 2003.

[351] G.-S. Jiang and C.-W. Shu. Efficient implementation of weighted ENO schemes. *J. Comput. Phys.*, 126:202–228, 1996.

[352] T. X. Jiang and C. M. Chuong. Mechanism of skin morphogenesis I: Analyses with antibodies to adhesion molecules tenascin, NCAM, and integrin. *Dev. Biol.*, 150:82–98, 1992.

[353] Y. Jiang, J. Pjesivac-Grbovic, C. Cantrell, and J. Freyer. A multiscale model for avascular tumor growth. *Biophys. J.*, 89:3884–3894, 2005.

[354] A. Jones, H. Byrne, J. Gibson, and J. Dold. Mathematical model for the stress induced during avascular tumor growth. *J. Math. Biol.*, 40:473–499, 2000.

[355] P. Jones and B. Sleeman. Angiogenesis-understanding the mathematical challenge. *Angiogenesis*, 9:127–138, 2006.

[356] P. A. Jones and S. B. Baylin. The fundamental role of epigenetic events in cancer. *Nat. Rev. Genet*, 3(6):415–28, 2002.

[357] P. A. Jones and P. W. Laird. Cancer epigenetics comes of age. *Nat. Genet.*, 21(2):163–7, 1999.

[358] R. E. Jr., K. O'Connor, D. Lacks, D. Schwartz, and R. Dotson. Dynamics of spheroid self-assembly in liquid-overlay culture of du 145 human prostate cancer cells. *Biotech. Bioeng.*, 72:579–591, 2001.

[359] K. Kaibuchi, S. Kuroda, and M. Amano. Regulation of the cytoskeleton and cell adhesion by the Rho family GTPases in mammalian cells. *Annu. Rev. Biochem.*, 68:459–86, 1999.

[360] F. Kallinowski, P. Vaupel, S. Runkel, G. Berg, H. Fortmeyer, K. Baessler, K. Wagner, W. Mueller-Klieser, and S. Walenta. Glucose uptake, lactate release, ketone body turnover, metabolic milieu and ph distributions in human cancer xenografts in nude rats. *Cancer Res.*, 48:7264–7272, 1988.

[361] K. Kaneko, K. Satoh, and A. Masamune. T. myosin light chain kinase inhibitors can block invasion and adhesion of human pancreatic cancer cell lines. *Pancreas*, 24:34–41, 2002.

[362] R. N. Kaplan, S. Rafii, and D. Lyden. Preparing the "Soil": The Premetastatic Niche. *Cancer Res.*, 66(23):11089–93, 2006.

[363] P. I. Karecla, S. J. Green, S. J. Bowden, J. Coadwell, and P. J. Kilshaw. Identification of a binding site for integrin $\alpha e\beta 7$ in the N- terminal domain of E-cadherin. *J. Biol. Chem.*, 271:30909–15, 1996.

[364] B. Kaur, F. Khwaja, E. Severson, S. Matheny, D. Brat, and E. VanMeir. Hypoxia and the hypoxia-inducible-factor pathway in glioma growth and angiogenesis. *Neuro-Oncol.*, 7:134–153, 2005.

[365] D. Kay and R. Welford. A multigrid finite element solver for the Cahn-Hilliard equation. *J. Comput. Phys.*, 212:288–304, 2006.

[366] P. Keller, F. Pampaloni, and E. Stelzer. Life sciences require the third dimension. *Curr. Op. Cell Biol.*, 18:117–124, 2006.

[367] T. Kelly, Y. Yan, R. L. Osborne, A. B. Athota, T. L. Rozypal, J. C. Colclasure, et al. Proteolysis of extracellular matrix by invadopodia facilitates human breast cancer cell invasion and is mediated by matrix metalloproteinases. *Clin. Exp. Metastasis*, 16(6):501–12, 1998.

[368] P. Kenny, G. Lee, and M. Bissell. Targeting the tumor microenvironment. *Front. Biosci.*, 12:3468–3474, 2007.

[369] K. Keren, Z. Pincus, G. M. Allen, E. L. Barnhart, G. Marriott, A. Mogilner, et al. Mechanism of shape determination in motile cells. *Nature*, 453(7194):475–80, 2008.

[370] K. Kerlikowske, A. Molinaro, I. Cha, B. M. Ljung, V. L. Ernster, K. Stewart, K. Chew, D. H. Moore 2nd, and F. Waldman. Characteristics associated with recurrence among women with ductal carcinoma in situ treated by lumpectomy. *J. Natl. Cancer Inst.*, 95(22):1692–702, 2003.

[371] J. F. R. Kerr, C. M. Winterford, and B. V. Harmon. Apoptosis. its significance in cancer and cancer therapy. *Cancer*, 73(8):2013–26, 1994.

[372] I. Kevrekidis, , C. Gear, J. Hyman, P. Kevrekidis, O. Runborg, and K. Theodoropoulos. Equation-free, coarse-grained multiscale computation: Enabling microscopic simulators to perform system-level analysis. *Comm. Math. Sci.*, 1:715–762, 2003.

[373] P. Kevrekidis, N. Whitaker, D. Good, and G. Herring. Minimal model for tumor angiogenesis. *Phys. Rev. E*, 73:061926, 2006.

[374] E. Khain and L. Sander. Generalized cahn-hilliard equation for biological applications. *Phys. Rev. E*, 77:051129, 2008.

[375] E. Khain, L. Sander, and C. Schneider-Mizell. The role of cell-cell adhesion in wound healing. *J. Stat. Phys.*, 128:209–218, 2007.

[376] S. Khan, M. Rogers, K. Khurana, M. Meguid, and P. Numann. Estrogen receptor expression in benign breast epithelium and breast cancer risk. *J. Natl. Canc. Inst.*, 90:37–42, 1998.

[377] S. Khan, A. Sachdeva, S. Naim, M. Meguid, W. Marx, H. Simon, et al. The normal breast epithelium of women with breast cancer displays an aberrant response to estra-

diol. *Canc. Epidemiol. Biomarkers Prev.*, 8:867–72, 1999.

[378] S. Kharait, S. Hautaniemi, S. Wu, A. Iwabu, D. A. Lauffenburger, and A. Wells. Decision tree modeling predicts effects of inhibiting contractility signaling on cell motility. *BMC Syst. Biol.*, 1:9ff, 2007.

[379] B. N. Kholodenko, O. V. Demin, G. Moehren, and J. B. Hoek. Quantification of short term signaling by the epidermal growth factor receptor. *J. Biol. Chem.*, 274(42):30169–81, 1999.

[380] J. Kim. Three-dimensional tissue culture models in cancer biology. *J. Biomol. Screening*, 15:365–77, 2005.

[381] J. Kim, K. Kang, and J. Lowengrub. Conservative multigrid methods for Cahn-Hilliard fluids. *J. Comput. Phys.*, 193:511–543, 2003.

[382] J. Kim, K. Kang, and J. Lowengrub. Conservative multigrid methods for ternary Cahn-Hilliard systems. *Comm. Math. Sci.*, 2:53–77, 2004.

[383] J. Kim and J. Lowengrub. Phase field modeling and simulation of three phase flows. *Int. Free Bound.*, 7:435–466, 2005.

[384] Y. Kim, M. Stolarska, and H. Othmer. A hybrid model for tumor spheroid growth in vitro i: Theoretical development and early results. *Math. Meth. App. Sci.*, 17:1773–1798, 2007.

[385] R. Kloner and R. Jennings. Consequences of brief ischemia: stunning, preconditioning, and their clinical implications: part 1. *Circulation*, 104:2981–2989, 2001.

[386] M. Knowles and P. Selby, editors. *Introduction to the Cellular and Molecular Biology of Cancer*. Oxford University Press, Oxford, UK, fourth edition, 2005.

[387] K. A. Knudsen, A. P. Soler, K. R. Johnson, and M. J. Wheelock. Interaction of α-actin with the cadherin/catenin cell-cell adhesion complex via α-catenin. *J. Cell. Biol.*, 130:66–77, 1995.

[388] A. G. Knudson. Mutation and cancer: statistical study of retinoblastoma. *Proc. Natl. Acad. Sci. USA*, 68(4):820–3, 1971.

[389] A. G. Knudson. Two genetic hits (more or less) to cancer. *Nat. Rev. Cancer*, 1(2):157–62, 2001.

[390] L. Kopfstein and G. Christofori. Metastasis: cell-autonomous mechanisms versus contributions by the tumor microenvironment. *Cell. Mol. Life Sci.*, 63:449–468, 2006.

[391] D. V. Krysko, T. V. Berghe, K. D'Herde, and P. Vandenabeele. Apoptosis and necrosis: Detection, discrimination and phagocytosis. *Methods*, 44:205–21, 2008.

[392] E. Kuhl and G. Holzapfel. A continuum model for remodeling in living structures. *J. Mater. Sci.*, 42:8811–8823, 2007.

[393] R. Kuiper, J. Schellens, G. Blijham, J. Beijnen, and E. Voest. Clinical research on antiangiogenic therapy. *Pharmacol. Res.*, 37:1–16, 1998.

[394] P. Kunkel, U. Ulbricht, P. Bohlen, R. F. M.A. Brockmann, D. Stavrou, M. Westphal, and K. Lamszus. Inhibition of glioma angiogenesis and growth in vivo by systemic treatment with a monoclonal antibody against vascular endothelial growth factor receptor-2. *Cancer Res.*, 61:6624–6628, 2001.

[395] L. Kunz-Schughart, J. P. Freyer, F. Hofstaedter, and R. Ebner. The use of 3-d cultures for high-throughput screening: The multicellular spheroid model. *J. Biomol. Screening*, 9:273–85, 2004.

[396] R. Küppers and R. Dalla-Favera. Mechanisms of chromosomal translocations in B cell lymphomas. *Oncogene*, 20(40):5580–94, 2001.

[397] A. Lal, C. Glazer, H. Martinson, H. Friedman, G. Archer, J. Sampson, and G. Riggins. Mutant epidermal growth factor receptor up-regulates molecular effectors of tumor invasion. *Cancer Res.*, 62:3335–3339, 2002.

[398] C. R. Lamb. Diagnosis of calcification on abdominal radiographs. *Vet. Rad. Ultrasound*, 32(5):211–20, 1991.

[399] O. T. Lampejo, D. M. Barnes, P. Smith, and R. R. Millis. Evaluation of infiltrating ductal carcinomas with a DCIS component: correlation of the histologic type of the in situ component with grade of the infiltrating component. *Semin. Diagn. Pathol.*, 11(3):215–22, 1994.

[400] K. Lamszus, P. Kunkel, and M. Westphal. Invasion as limitation to anti-angiogenic glioma therapy. *Acta Neurochir Suppl.*, 88:169–177, 2003.

[401] K. Landman and C. Please. Tumour dynamics and necrosis: Surface tension and stability. *IMA J. Math. Appl. Medicine Biol.*, 18:131–158, 2001.

[402] M. C. Lane, M. A. Koehl, F. WIlt, and R. Keller. A role for regulated secretion of apical extracellular matrix during epithelial invagination in the sea urchin. *Development*, 117(3):1049–60, 1993.

[403] H. Larjava, T. Salo, K. Haapasalmi, R. H. Kramer, and J. Heino. Expression of integrins and basement membrane components by wound keratinocytes. *J. Clin. Invest.*, 92(3):1425–35, 1993.

[404] D. A. Lauffenburger. Cell signaling pathways as control modules: complexity for simplicity? *Proc. Natl. Acad. Sci. USA*, 97(10):5031–3, 2000.

[405] C. Le Clainche and M. F. Carlier. Regulation of actin assembly associated with protrusion and adhesion in cell migration. *Physiol. Rev.*, 88(2):489–513, 2008.

[406] D. Lee, H. Rieger, and K. Bartha. Flow correlated percolation during vascular remodeling in growing tumors. *Phys. Rev. Lett.*, 96:058104, 2006.

[407] J. S. Lee, D. M. Basalyga, A. Simionescu, J. C. Isenburg, D. T. Sinionescu, and N. R. Vyavahare. Elastin calcification in the rate subdermal model is accompanied by upregulation of degradative and osteogenic cellular responses. *Am. J. Pathol.*, 168:490–8, 2006.

[408] S. Lee, S. K. Mohsin, S. Mao, S. G. Hilsenbeck, D. Medina, and D. C. Allred. Hormones, receptors, and growth in hyperplastic enlarged lobular units: early potential precursors of breast cancer. *Breast Canc. Res.*, 8(1):R6, 2006.

[409] S. Lehoux and A. Tedgui. Signal transduction of mechanical stresses in the vascular wall. *Hypertension*, 32(2):338–345, 1998.

[410] J. Less, T. Skalak, E. Sevick, and R. Jain. Microvascular architecture in a mammary carcinoma: branching patterns and vessel dimensions. *Cancer Res.*, 51:265–273, 1991.

[411] H. Levine and M. Nilsen-Hamilton. Angiogenesis- a biochemical/mathematical perspective. *Tutorials in Math. Biosci. III*, 1872:23–76, 2006.

[412] H. Levine, S. Pamuk, B. Sleeman, and M. Nilsen-Hamilton. Mathematical modeling of capillary formation and development in tumor angiogenesis: penetration into the stroma. *Bull. Math. Biol.*, 63:801–863, 2001.

[413] H. Levine and B. Sleeman. Modelling tumour-induced angiogenesis. In L. Preziosi, editor, *ancer modelling and simulation*, pages 147–184. Chapman&Hall/CRC, Boca Raton, Florida, 2003.

[414] H. Levine, B. Sleeman, and M. Nilsen-Hamilton. Mathematical modeling of the onset of capillary formation initiating angiogenesis. *J. Math. Biol.*, 42:195–238, 2001.

[415] H. Levine, M. Smiley, A. Tucker, and M. Nilsen-Hamilton. A mathematical model for the onset of avascular tumor growth in response to the loss of p53 function. *Cancer Informatics*, 2:163–188, 2006.

[416] H. Levine, A. Tucker, and M. Nilsen-Hamilton. A mathematical model for the role of cell signal transduction in the initiation and inhibition of angiogenesis. *Growth Factors*, 20:155–175, 2002.

[417] J. Li, P. Kevrekidis, C. Gear, and I. Kevrekidis. Deciding the nature of the coarse equation through microscopic simulations: The baby-bathwater scheme. *SIAM Review*, 49:469–487, 2007.

[418] X. Li, V. Cristini, Q. Nie, and J. Lowengrub. Nonlinear three-dimensional simulation of solid tumor growth. *Disc. Dyn. Contin. Dyn. Syst. B*, 7:581–604, 2007.

[419] S.-Y. Lin, W. Xia, J. C. Wang, K. Y. Kwong, and B. Spohn. β-Catenin, a novel prognostic marker for breast cancer: Its roles in Cyclin D1 expression and cancer progression. *Proc. Natl. Acad. Sci. USA*, 97(8):4262–6, 2000.

[420] L. Liotta and E. Kohn. The microenvironment of the tumour-host interface. *Nature*, 411:375–379, 2001.

[421] A. Lipton. Pathophysiology of Bone Metastases: How This Knowledge May Lead to Therapeutic Intervention. *J. Support. Oncol.*, 2(3):205–220, 2004.

[422] X. D. Liu, S. Osher, and T. Chan. Weighted essentially non-oscillatory schemes. *J. Comput. Phys.*, 115:200–212, 1994.

[423] B. Lloyd, D. Szczerba, M. Rudin, and G. Szekely. A computational framework for modeling solid tumour growth. *Phil. Trans. Roy. Soc. A*, 366:3301–3318, 2008.

[424] B. Lloyd, D. Szczerba, and G. Szekely. A coupled finite element model of tumor growth and vascularization. In N. Ayache, S. Ourselin, and A. Maeder, editors, *Medical image computing and computer-assisted intervention-MICCA 2007: 10th international conference*, volume 4792 of *Lecture Notes in Computer Science*, pages 874–881. Springer, New York, 2007.

[425] J. Lotem and L. Sachs. Epigenetics and the plasticity of differentiation in normal and cancer stem cells. *Oncogene*, 25(59):7663–7672, 2006.

[426] R. M. B. Loureiro and P. A. D'Amore. Transcriptional regulation of vascular endothelial growth factor in cancer. *Cytokine Growth Factor Rev.*, 16(1):77–89, 2005.

[427] J. Lowengrub, H. Frieboes, F. Jin, Y. Chuang, X. Li, P. Macklin, S. Wise, and V. Cristini. Nonlinear modeling of cancer: Bridging the gap between cells and tumors. *Nonlinearity*, 2010. in press.

[428] V. Lubarda and A. Hoger. On the mechanics of solids with a growing mass. *Int. J. Solids Structures*, 39:4627–4664, 2002.

[429] P. J. Lucio, M. T. Faria, A. M. Pinto, M. R. da Silva, M. E. Correia Jr., R. J. da Costa, and A. B. Parreira. Expression of adhesion molecules in chronic B-cell lymphoproliferative disorders. *Haematologica*, 83(2):104–11, 1998.

[430] B. Lustig, B. Jerchow, M. Sachs, S. Wiler, T. Pietsch, U. Karsten, M. van de Wetering, H. Clevers, P. M. Schlag, W. Birchmeier, and J. Behrens. Negative feedback loop of Wnt signaling through upregulation of conductin/axin2 in colorectal and liver tumors. *Mol. Cell. Biol.*, 22:1184–93, 2002.

[431] B. MacArthur and C. Please. Residual stress generation and necrosis formation in multi-cell tumour spheroids. *J. Math. Biol.*, 49:537–552, 2004.

[432] P. Macklin. Numerical Simulation of Tumor Growth and Chemotherapy. M.S. thesis, University of Minnesota School of Mathematics, September 2003.

[433] P. Macklin. *Toward Computational Oncology: Nonlinear Simulation of Centimeter-Scale Tumor Growth in Complex, Heterogeneous Tissues*. Ph.D. dissertation, University of California, Irvine Department of Mathematics, June 2007.

[434] P. Macklin, L. Carreras, J. Kim, S. Sanga, V. Cristini, and M. E. Edgerton. Mathematical analysis of histopathology indicates comparable oxygen uptake rates for quiescent and proliferating breast cancer cells in DCIS. (in preparation), 2009.

[435] P. Macklin, J. Kim, G. Tomaiuolo, M. E. Edgerton, and V. Cristini. Agent-Based Modeling of Ductal Carcinoma in Situ: Application to Patient-Specific Breast Cancer Modeling. In T. Pham, editor, *Computational Biology: Issues and Applications in Oncology*, chapter 4, pages 77–112. Springer, New York, NY, 2009.

[436] P. Macklin, J. Kim, G. Tomaiuolo, M. E. Edgerton, and V. Cristini. An agent-based cell model, with application to patient-specific ductal carcinoma in situ modeling. (in preparation), 2010.

[437] P. Macklin and J. Lowengrub. Evolving interfaces via gradients of geometry-dependent interior Poisson problems: Application to tumor growth. *J. Comput. Phys.*, 203:191–220, 2005.

[438] P. Macklin and J. Lowengrub. An improved geometry-aware curvature discretization for level set methods: Application to tumor growth. *J. Comput. Phys.*, 215:392–401, 2006.

[439] P. Macklin and J. Lowengrub. Nonlinear simulation of the effect of microenvironment on tumor growth. *J. Theor. Biol.*, 245:677–704, 2007.

[440] P. Macklin and J. Lowengrub. A new ghost cell/level set method for moving boundary problems: Application to tumor growth. *J. Sci. Comp.*, 35(2-3):266–99, 2008.

[441] P. Macklin, S. McDougall, A. Anderson, M. Chaplain, V. Cristini, and J. Lowengrub. Multiscale modeling and nonlinear simulation of vascular tumour growth. *J. Math. Biol.*, 58(4-5):765–98, 2009.

[442] A. D. C. Macknight, D. R. DiBona, A. Leaf, and M. C. Mortimer. Measurement of the composition of epithelial cells from the toad urinary bladder. *J. Membrane Biol.*, 6(2):108–26, 1971.

[443] S. Madsen, E. Angell-Petersen, S. Spetalen, S. Carper, S. Ziegler, and H. Hirschberg. Photodynamic therapy of newly implanted glioma cells in the rat brain. *Lasers Surg. Med.*, 38:540–548, 2006.

[444] S. Maggelakis and J. Adam. Mathematical model of prevascular growth of a spherical carcinoma. *Math. Comput. Modelling*, 13:23–38, 1990.

[445] E. Maher, F. Furnari, R. Bachoo, D. Rowitch, D. Louis, W. Cavenee, and R. De-Pinho. Malignant glioma: genetics and biology of a grave matter. *Genes Dev.*, 15:1311–1333, 2001.

[446] G. Majno and I. Joris. *Cells, Tissues, and Disease: Principles of General Pathology*. Oxford University Press, New York, second edition, 2004.

[447] A. G. Makeev, D. Maroudas, and I. G. Kevrekidis. 'Coarse' stability and bifurcation analysis using stochastic simulators: Kinetic Monte Carlo examples. *J. Chem. Phys.*, 116:10083–10091, 2002.

[448] A. G. Makeev, D. Maroudas, A. Z. Panagiotopoulos, and I. G. Kevrekidis. Coarse bifurcation analysis of kinetic Monte Carlo simulations: A lattice-gas model with lateral interactions. *J. Chem. Phys.*, 117:8229–8240, 2002.

[449] R. Malladi, J. A. Sethian, and B. C. Vemuri. Shape Modeling with Front Propagation: A Level Set Approach. *IEEE Trans. Pattern Anal. Mach. Intell.*, 17(2), 1995.

[450] R. Malladi, J. A. Sethian, and B. C. Vemuri. A fast level set based algorithm for topology-independent shape modeling. *J. Math. Imaging Vision*, 6(2-3):269–289, 1996.

[451] M. Malumbres and M. Barbacis. RAS oncogenes: the first 30 years. *Nat. Rev. Cancer*, 3(6):459–465, 2001.

[452] L. Malvern. *Introduction of the mechanics of a continuous medium*. Prentice Hall, Englewood Cliffs, 1969.

[453] D. Manoussaki, S. Lubkin, R. Vernon, and J. Murray. A mechanical model for the formation of vascular networks in vitro. *Acta Biotheor.*, 44:271–282, 1996.

[454] N. Mantzaris, S. Webb, and H. Othmer. Mathematical modeling of tumor-induced angiogenesis. *J. Math. Biol.*, 49:111–187, 2004.

[455] B. Marchant, J. Norbury, and J.A.Sherratt. Travelling wave solutions to a haptotaxis-dominated model of malignant invasion. *Nonlinearity*, 14:1653–1671, 2001.

[456] A. F. Maree, A. Jilkine, A. Dawes, V. A. Grieneisen, and L. Edelstein-Keshet. Polarization and movement of keratocytes: a multiscale modelling approach. *Bull. Math. Biol.*, 68(5):1169–1211, 2006.

[457] D. Martin and P. Colella. A cell-centered adaptive projection method for the incompressible Euler equations. *J. Comput. Phys.*, 163:271–312, 2000.

[458] M. Marusic, Z. Baizer, J. Freyer, and S. Vuk-Pavlovic. Analysis of growth of multicellular tumour spheroids by mathematical models. *Cell Prolif.*, 27:73–94, 1994.

[459] K. Matsumoto and T. Nakamura. Hepatocyte growth factor and the Met system as a mediator of tumor-stromal interactions. *Int. J. Cancer*, 119(3):477–483, 2006.

[460] B. McArthur and C. Please. Residual stress generation and necrosis formation in multicell tumor spheroids. *J. Math. Biol.*, 49:537–552, 2004.

[461] S. McDougall, A. Anderson, and M. Chaplain. Mathematical modelling of dynamic adaptive tumour-induced angiogenesis: Clinical applications and therapeutic targeting strategies. *J. Theor. Biol.*, 241:564–589, 2006.

[462] S. McDougall, A. Anderson, M. Chaplain, and J. Sherratt. Mathematical modelling of flow through vascular networks: implications for tumour-induced angiogenesis and chemotherapy strategies. *Bull. Math. Biol.*, 64:673–702, 2002.

[463] D. McElwain and L. Morris. Apoptosis as a volume loss mechanism in mathematical models of solid tumor growth. *Math. Biosci.*, 39:147–157, 1978.

[464] C. Medrek, G. Landberg, and K. Andersson, T adn Leandersson. Wnt-5a-CKIα signaling promotes β-Catenin/E-Cadherin complex formation and intercellular adhesion in human breast epithelial cells. *J. Biol. Chem.*, 284:10968–79, 2009.

[465] A. Menzel. Modelling of anisotropic growth in biological tissues- a new approach and computational aspects. *Biomech. Model. Mechanobiol.*, 3:147–171, 2005.

[466] R. Merks, S. Brodsky, M. Goligorksy, S. Newman, and J. Glazier. Cell elongation is key to in silico replication of in vitro vasculogenesis and subsequent remodeling. *Dev. Biol.*, 289:44–54, 2006.

[467] R. Merks and J. Glazier. Dynamic mechanisms of blood vessel growth. *Nonlinearity*, 19:C1–C10, 2006.

[468] R. Merks, E. P. A. Shirinifard, and J. Glazier. Contact-inhibited chemotaxis in de novo and sprouting blood-vessel growth. *PloS Comp. Biol.*, 4:e1000163, 2008.

[469] A. Merlo. Genes and pathways driving glioblastomas in humans and murine disease models. *Neurosurg. Rev.*, 26:145–158, 2003.

[470] N. Metropolis, A. Rosenbluth, M. Rosenbluth, A. Teller, and E. Teller. Equation of state calculations by fast computing machines. *J. Chem. Phys.*, 21:1087–1092, 1953.

[471] P. Michieli, C. Basilico, S. Pennacchietti, A. Maffè, L. Tamagnone, S. Giordano, A. Bardelli, and P. Comoglio. Mutant met mediated transformation is ligand-dependent and can be inhibited by hgf antagonists. *Oncogene*, 18:5221–5231, 1999.

[472] L. P. Middleton, G. Vlastos, N. Q. Mirza, S. Eva, and A. A. Sahin. Multicentric mammary carcinoma: evidence of monoclonal proliferation. *Cancer*, 94(7):1910–6, 2002.

[473] F. Milde, M. Bergdorf, and P. Koumoutsakos. A hybrid model for three-dimensional simulations of sprouting angiogenesis. *Biophys. J.*, 95:3146–3160, 2008.

[474] S. Mitran. *BEARCLAW a code for multiphysics applications with embedded boundaries: user's manuel*. Department of Mathematics, University of North Carolina, http://www.amath.unc.edu/Faculty/mitran/bearclaw.html, 2006.

[475] D. F. Moffat and J. J. Going. Three dimensional anatomy of complete duct systems in human breast: pathological and developmental implications. *J. Clin. Pathol.*, 49:48–52, 1996.

[476] A. Mogilner and L. Edelstein-Keshet. Regulation of actin dynamics in rapidly moving cells: a quantitative analysis. *Biophys. J.*, 83(3):1237–58, 2002.

[477] R. Montesano, K. Matsumoto, T. Nakamura, and L. Orci. Identification of a fibroblast-derived epithelial morphogen as hepatocyte growth factor. *Cell*, 67:901–908, 1991.

[478] J. Moreira and A. Deutsch. Cellular automaton models of tumor development: A critical review. *Adv. Complex Sys.*, 5:247–267, 2002.

[479] A. Morotti, S. Mila, P. Accornero, E. Tagliabue, and C. Ponzetto. K252a inhibits the oncogenic properties of met, the hgf receptor. *Oncogene*, 21:4885–4893, 2002.

[480] K. Morton and D. Mayers. *Numerical Solution of Partial Differential Equations*. Cambridge, Cambridge, UK, second edition, 2005.

[481] B. Mosadegh, W. Saadi, S. J. Wang, and N. L. Jeon. Epidermal growth factor promotes breast cancer cell chemotaxis in CXCL12 gradients. *Biotech. Bioeng.*, 100(6):1205–13, 2008.

[482] W. Mueller-Klieser. Multicellular spheroids: a review on cellular aggregates in cancer research. *J. Cancer Res. Clin. Oncol.*, 113:101–122, 1987.

[483] W. Mueller-Klieser. Three-dimensional cell cultures: from molecular mechanisms to clinical applications. *Am. J. Physiol. Cell Physiol.*, 273:C1109–C1123, 1997.

[484] W. Mueller-Klieser, J. Freyer, and R. Sutherland. Influence of glucose and oxygen supply conditions on the oxygenation of multicellular spheroids. *Br. J. Cancer*, 53:345–353, 1986.

[485] G. Müller and J.-J. Métois. *Crystal Growth: From Fundamentals to Technology*. Elsevier, 2004.

[486] W. Mullins and R. Sekerka. Morphological instability of a particle growing by diffusion or heat flow. *J. Appl. Phys.*, 34:323–329, 1963.

[487] G. R. Mundy. Metastasis to bone: causes, consequences and therapeutic opportunities. *Nat. Rev. Cancer*, 2(8):584–93, 2002.

[488] J. Murray and G. Oster. Cell traction models for generation of pattern and form in morphogenesis. *J. Math. Biol.*, 33:489–520, 1984.

[489] V. R. Muthukkaruppan, L. Kubai, and R. Auerbach. Tumor-induced neovascularization in the mouse eye. *J. Natl. Cancer Inst.*, 69(3):699–705, 1982.

[490] K. Nabeshima, T. Moriyama, Y. Asada, N. Komada, T. Inoue, H. Kataoka, A. Sumiyoshi, and M. Koono. Ultrastructural study of TPA-induced cell motility: human well-differentiated rectal adenocarcinoma cells move as coherent sheets via localized modulation of cell–cell adhesion. *Clin. Exp. Med.*, 13(6):499–508, 1995.

[491] M. Nagane, A. Levitzki, A. Gazit, W. Cavenee, and H. Huang. Drug resistance of human glioblastoma cells conferred by a tumor-specific mutant epidermal growth factor receptor through modulation of bcl-x l and caspase-3-like proteases. *Proc. Natl. Acad. Sci. USA*, 95:5724–5729, 1998.

[492] H. Naganuma, R. Kimurat, A. Sasaki, A. Fukamachi, H. Nukui, and K. Tasaka. Complete remission of recurrent glioblastoma multiforme following local infusions of lymphokine activated killer cells. *Acta Neurochir.*, 99:157–160, 1989.

[493] J. Nagy. The ecology and evolutionary biology of cancer: A review of mathematical models of necrosis and tumor cell diversity. *Math. Biosci. Eng.*, 2:381–418, 2005.

[494] M. N. Nakatsu, R. C. A. Sainson, J. N. Aoto, K. L. Taylor, M. Aitkenhead, S. Prez-del Pulgard, P. M. Carpenter, and C. C. W. Hughes. Angiogenic sprouting and capillary lumen formation modeled by human umbilical vein endothelial cells (HUVEC) in fibrin gels: the role of fibroblasts and Angiopoietin-1. *Microvasc. Res.*, 66:102–112, 2003.

[495] M. A. H. Navarrete, C. M. maier, R. Falzoni, L. G. d. A. Quadros, E. C. Baracat, and A. C. P. Nazário. Assessment of the proliferative, apoptotic, and cellular renovation indices of the human mammary epithelium during the follicular and luteal phases of the menstrual cycle. *Breast Cancer Res.*, 7:R306–13, 2005.

[496] C. Nelson and M. Bissell. Of extracellular matrix, scaffolds, and signaling: tissue architecture regulates development, homeostasis, and cancer. *Annu. Rev. Cell Dev. Biol.*, 22:287–309, 2006.

[497] P. Netti, L. Baxter, Y. Boucher, R. Skalak, and R. Jain. Time dependent behavior of interstitial fluid pressure in solid tumors: Implications for drug delivery. *Cancer Res.*, 55:5451–5458, 1995.

[498] A. Neville, P. Matthews, and H. Byrne. Interactions between pattern formation and domain growth. *Bull. Math. Biol.*, 68:1975–2003, 2006.

[499] G. Ngwa and P. Maini. Spatio-temporal patterns in a mechanical model for mesenchymal morphogenesis. *J. Math. Biol.*, 33:489–520, 1995.

[500] M. Nichols and T. Foster. Oxygen diffusion and reaction kinetics in the photodynamic therapy of multicell tumour spheroids. *Phys. Med. Biol.*, 39:2161–2181, 1994.

[501] R. Nishikawa, X. Ji, R. Harmon, C. Lazar, G. Gill, W. Cavenee, and H. Huang. A mutant epidermal growth factor receptor common in human glioma confers enhanced tumorigenicity. *Proc. Natl. Acad. Sci. USA*, 91:7727–7731, 1994.

[502] J. Nor, J. Christensen, J. Liu, M. Peters, D. Mooney, R. Strieter, and P. Polverini. Upregulation of bcl-2 in microvascular endothelial cells enhances intratumoral angiogenesis and accelerates tumor growth. *Cancer Res.*, 61:2183–2188, 2001.

[503] M. A. Nowak, N. L. Komarova, A. Sengupta, J. V. Prasad, I.-M. Shih, B. Vogelstein, and C. Lengauer. The role of chromosomal instability in tumor initiation. *Proc. Natl. Acad. Sci. USA*, 99(25):16226–16231, 2002.

[504] J. O'Connor, A. Jackson, G. Parker, and G. Jayson. Dce-mri biomarkers in the clinical evaluation of antiangiogenic and vascular disrupting agents. *Br. J. Cancer*, 96:189–195, 2007.

[505] K. Oda, Y. Matsuoka, A. Funahashi, and H. Kitano. A comprehensive pathway map of epidermal growth factor receptor signaling. *Mol. Syst. Biol.*, 1, 2005.

[506] T. Ohtake, I. Kimijima, T. Fukushima, M. Yasuda, K. Sekikawa, S. Takenoshita, and R. Abe. Computer-assisted complete three-dimensional reconstruction of the mammary ductal/lobular systems. *Cancer*, 91:2263–72, 2001.

[507] B. Øksendal. *Stochastic Differential Equations: An Introduction with Applications*. Springer, New York, 6th edition, 2007.

[508] M. Orme and M. Chaplain. Two-dimensional models of tumour angiogenesis and anti-angiogenesis strategies. *Math. Med. Biol.*, 14:189–205, 1997.

[509] S. Osher and R. Fedkiw. Level Set Methods: An Overview and Some Recent Results. *J. Comput. Phys.*, 169(2):463–502, 2001.

[510] S. Osher and R. Fedkiw. *Level Set Methods and Dynamic Implicit Surfaces*. Springer, New York, NY, 2002.

[511] S. Osher and J. Sethian. Fronts propagating with curvature-dependent speed: algorithms based on hamilton-jacobi formulation. *J. Comput. Phys.*, 79:12, 1988.

[512] H. Othmer and A. Stevens. Aggregration, blowup, and collapse: the abc's of taxis in reinforced random walks. *Siam. J. Appl. Math.*, 57:1044–1081, 1997.

[513] H. G. Othmer, S. R. Dunbar, and W. Alt. Models of dispersal in biological systems. *J. Math. Biol.*, 26:263–298, 1988.

[514] M. Owen, T. Alarcón, P. Maini, and H. Byrne. Angiogenesis and vascular remodeling in normal and cancerous tissues. *J. Math. Biol.*, 58:689–721, 2009.

[515] M. R. Owen, H. M. Byrne, and C. E. Lewis. Mathematical modelling of the use of macrophages as vehicles for drug delivery to hypoxic tumour sites. *J. Theor. Biol.*, 226(4):377–91, 2004.

[516] T. Padera, B. Stoll, J. Tooredman, D. Capen, E. di Tomaso, and R. Jain. Cancer cells compress intratumour vessels. *Nature*, 427:695, 2004.

[517] D. Page, T. Anderson, and G. Sakamoto. *Diagnostic Histopathology of the Breast*. Churchill Livingstone, New York, 1987.

[518] D. L. Page, W. D. Dupont, L. W. Rogers, and M. Landenberger. Intraductal carcinoma of the breast: follow-up after biopsy only. *Cancer*, 49(4):751–8, 1982.

[519] S. Paget. The distribution of secondary growths in cancer of the breast. *Lancet*, 133(3421):571–573, 1889.

[520] S. Paku. First step of tumor-related angiogenesis. *Lab. Invest.*, 65:334–346, 1991.

[521] D. Palmieri, C. E. Horak, J.-H. Lee, D. O. Halverson, and P. S. Steeg. Translational approaches using metastasis suppressor genes. *J. Bioenerg. Biomembr.*, 38(3-4):151–161, 2006.

[522] E. Palsson and H. Othmer. A model for individual and collective cell movement in dictyostelium discoideum. *Proc. Nat. Acad. Sci. USA*, 97:10338–10453, 2000.

[523] S. Pamuk. Qualitative analysis of a mathematical model for capillary formation in tumor angiogenesis. *Math. Models Meth. Appl. Sci.*, 13:19–33, 2003.

[524] P. Panorchan, M. S. Thompson, K. J. Davis, Y. Tseng, K. Konstantopoulos, and D. Wirtz. Single-molecule analysis of cadherin-mediated cell-cell adhesion. *J. Cell Sci.*, 119:66–74, 2006.

[525] W. Pao, T. Y. Wang, G. J. Riely, et al. KRAS mutations and primary resistance of lung adenocarcinomas to gefitinib or erlotinib. *PLoS Med.*, 2:e17, 2005.

[526] S. Parnuk. A mathematical model for capillary formation and development in tumor angiogenesis: A review. *Chemotherapy*, 52:35–37, 2006.

[527] S. Patan, S. Tanda, S. Roberge, R. Jones, R. Jain, and L. Munn. Vascular morphogenesis and remodeling in a human tumor xenograft: blood vessel formation and growth after ovariectomy and tumor implantation. *Circ. Research*, 89:732–739, 2001.

[528] N. Patani, B. Cutuli, and K. Mokbel. Current management of DCIS: a review. *Breast Cancer Res. Treat.*, 111(1):1–10, 2008.

[529] A. Patel, E. Gawlinski, S. Lemieux, and R. Gatenby. A cellular automaton model of early tumor growth and invasion: The effects of native tissue vascularity and increased anaerobic tumor metabolism. *J. Theor. Biol.*, 213:315–331, 2001.

[530] N. Paweletz and M. Knierim. Tumor-related angiogenesis. *Crit. Rev. Oncol. Hematol.*, 9:197–242, 1989.

[531] S. Peirce. Computational and mathematical modeling of angiogenesis. *Microcirculation*, 15(8):739–751, 2008.

[532] S. Pennacchietti, P. Michieli, M. Galluzzo, S. Giordano, and P. Comoglio. Hypoxia promotes invasive growth by transcriptional activation of the met protooncogene. *Cancer Cell*, 3:347–361, 2003.

[533] C. Peskin. The immersed boundary method. *Acta Numer.*, 11:479–517, 2002.

[534] C. S. Peskin. Flow patterns around heart valves: A numerical method. *J. Comput. Phys.*, 10(2):252–71, 1972.

[535] J. Peterson, G. Carey, D. Knezevic, and B. Murray. Adaptive finite element methodology for tumour angiogenesis modelling. *Int. J. Num. Meth. Eng.*, 69:1212–1238, 2007.

[536] G. Pettet, C. Please, M. Tindall, and D. McElwain. The migration of cells in multicell tumor spheroids. *Bull. Math. Biol.*, 63:231–257, 2001.

[537] M. Plank and B. Sleeman. A reinforced random walk model of tumour angiogenesis and anti-angiogenic strategies. *Math. Med. Biol.*, 20:135–181, 2003.

[538] M. Plank and B. Sleeman. Lattice and non-lattice models of tumour angiogenesis. *Bull. Math. Biol.*, 66:1785–1819, 2004.

[539] C. Please, G. Pettet, and D. McElwain. A new approach to modeling the formation of necrotic regions in tumors. *Appl. Math. Lett.*, 11:89–94, 1998.

[540] C. Please, G. Pettet, and D. McElwain. Avascular tumour dynamics and necrosis. *Math. Models Appl. Sci.*, 9:569–579, 1999.

[541] N. Poplawski, U. Agero, J. Gens, M. Swat, J. Glazier, and A. Anderson. Front instabilities and invasiveness of simulated avascular tumors. *Bull. Math. Biol.*, 71:1189–1227, 2009.

[542] L. Postovit, M. Adams, G. Lash, J. Heaton, and C. Graham. Oxygen-mediated regulation of tumor cell invasiveness. involvement of a nitric oxide signaling pathway. *J. Biol. Chem.*, 277:35730–35737, 2002.

[543] J. Pouysségur, F. Dayan, and N. Mazure. Hypoxia signalling in cancer and approaches to enforce tumour regression. *Nature*, 441:437–443, 2006.

[544] F. Prall. Tumour budding in colorectal carcinoma. *Histopathology*, 50:151–162, 2007.

[545] M. Preusser, H. Heinzl, E. Gelpi, K. Schonegger, C. Haberler, P. Birner, C. Marosi, M. hegi, T. Gorlia, and J. Hainfellner. Histopathologic assessment of hot-spot microvessel density and vascular patterns in glioblastoma: Poor observer agreement limits clinical utility as prognostic factors: a translational research project of the european organization for research and treatment of cancer brain tumor group. *Cancer*, 107:162–170, 2006.

[546] L. Preziosi. *Cancer Modelling and Simulation*. Chapman and Hall/CRC, London, 2003.

[547] L. Preziosi and S. Astanin. Modelling the formation of capillaries. In A. Quarteroni, L. Formaggia, and A. Veneziani, editors, *Complex Systems in Biomedicine*. Springer, Milan, 2006.

[548] L. Preziosi and A. Tosin. Multiphase modeling of tumor growth and extracellular matrix interaction: Mathematical tools and applications. *J. Math. Biol.*, 58:625–656, 2009.

[549] A. Pries, B. Reglin, and T. Secomb. Structural adaptation and stability of microvascular networks: functional roles of adaptive responses. *Am. J. Physiol. Heart Circ. Physiol.*, 281:H1015–H1025, 2001.

[550] A. Pries, B. Reglin, and T. Secomb. Structural adaptation of vascular networks: the role of pressure response. *Hypertension*, 38:1476–1479, 2001.

[551] A. Pries and T. Secomb. Control of blood vessel structure: insights from theoretical models. *Am. J. Physiol. Heart Circ. Physiol.*, 288:1010–1015, 2005.

[552] A. Pries and T. Secomb. Modeling structural adaptation of microcirculation. *Microcirculation*, 15(8):753–64, 2008.

[553] A. Pries, T. Secomb, and P. Gaehtgens. Structural adaptation and stability of microvascular networks: theory and simulations. *Am. J. Physiol. Heart Cir. Physiol.*, 275:H349–H360, 1998.

[554] W. C. Prozialeck, P. C. Lamar, and D. M. Appelt. Differential expression of E-cadherin, N-cadherin and beta-catenin in proximal and distal segments of the rat nephron. *BMC Physiol.*, 4(10), 2004.

[555] V. Quaranta, K. Rejniak, P. Gerlee, and A. Anderson. Invasion emerges from cancer cell adaptation to competitive microenvironments: Quantitative predictions from multiscale mathematical models. *Sem. Cancer Biol.*, 18(5):338–48, 2008.

[556] V. Quaranta, A. Weaver, P. Cummings, and A. Anderson. Mathematical modeling of cancer: The future of prognosis and treatment. *Clinica Chimica Acta*, 357:173–179, 2005.

[557] C. M. Quick, W. L. Young, E. F. Leonard, S. Joshi, E. Gao, and T. Hashimoto. Model of structural and functional adaptation of small conductance vessels to arterial hypotension. *Am. J. Physiol. Heart Circ. Physiol.*, 279(4):H1645–H1653, 2000.

[558] K. C. Quon and A. Berns. Haplo-insufficiency? Let me count the ways. *Genes Dev.*, 15(22):2917–21, 2001.

[559] A. Ramanathan, C. Wang, and S. Schreiber. Perturbational profiling of a cell-line model of tumorigenesis by using metabolic measurements. *PNAS*, 102:5992–5997, 2005.

[560] I. Ramis-Conde, M. Chaplain, and A. Anderson. Mathematical modelling of cancer cell invasion of tissue. *Math. Comp. Model.*, 47:533–545, 2008.

[561] I. Ramis-Conde, D. Drasdo, A. Anderson, and M. Chaplain. Modeling the influence of the e-cadherin-beta-catenin pathway in cancer cell invasion: A multiscale approach. *Biophys. J.*, 95:155–165, 2008.

[562] A. Rätz, A. Ribalta, and A. Voigt. Surface evolution of elastically stressed films under deposition by a diffuse interface model. *J. Comput. Phys.*, 214:187–208, 2006.

[563] K. Rejniak. A single-cell approach in modeling the dynamics of tumor microregions. *Math. Biosci. Eng.*, 2:643–655, 2005.

[564] K. Rejniak. An immersed boundary framework for modeling the growth of individual cells: An application to the early tumour development. *J.Theor. Biol.*, 247:186–204, 2007.

[565] K. Rejniak and A. Anderson. A computational study of the development of epithelial acini: 1. sufficient conditions for the formation of a hollow structure. *Bull. Math. Biol.*, 70:677–712, 2008.

[566] K. Rejniak and A. Anderson. A computational study of the development of epithelial acini: Ii. necessary conditions for structure and lumen stability. *Bull. Math. Biol.*, 70:1450–1479, 2008.

[567] K. Rejniak and R. Dillon. A single cell-based model of the ductal tumor microarchitecture. *Comp. Math. Meth. Med.*, 8(1):51–69, 2007.

[568] K. Rennstam and I. Hedenfalk. High-throughput genomic technology in research and clinical management of breast cancer. molecular signatures of progression from benign epithelium to metastatic breast cancer. *Breast Canc. Res.*, 8(4):213ff, 2006.

[569] B. Ribba, T. Alarcón, K. Marron, P. Maini, and Z. Agur. The use of hybrid cellular automaton models for improving cancer therapy. In B. C. P.M.A. Sloot and A. Hoekstra, editors, *ACRI, LNCS*, pages 444–453. Springer, Berlin, 2004.

[570] B. Ribba, O. Saut, T. Colin, D. Bresch, E. Grenier, and J. P. Boissel. A multiscale mathematical model of avascular tumor growth to investigate the therapeutic benefit of anti-invasive agents. *J. Theor. Biol.*, 243(4):532–41, 2006.

[571] A. Ridley, M. Schwartz, K. Burridge, R. Firtel, M. Ginsberg, G. Borisy, J. Parsons, and A. Horwitz. Cell migration: Integrating signals from front to back. *Science*, 302:1704–1709, 2003.

[572] E. Robinson, K. Zazzali, S. Corbett, and R. Foty. α5b1 integrin mediates strong tissue cohesion. *J. Cell. Sci.*, 116:377–386, 2003.

[573] E. Rofstad and E. Halsør. Hypoxia-associated spontaneous pulmonary metastasis in human melanoma xenographs: involvement of microvascular hotspots induced in hypoxic foci by interleukin. *Br. J. Cancer*, 86:301–308, 2002.

[574] E. Rofstad, H. Rasmussen, K. Galappathi, B. Mathiesen, K. Nilsen, and B. Graff. Hypoxia promotes lymph node metastasis in human melanoma xenografts by up-regulating the urokinase-type plasminogen activator receptor. *Cancer Res.*, 62:1847–1853, 2002.

[575] J. Rohzin, M. Sameni, G. Ziegler, and B. Sloane. Pericellular ph affects distribution and secretion of cathepsin b in malignant cells. *Cancer Res.*, 54:6517–6625, 1994.

[576] T. Roose, S. J. Chapman, and P. Maini. Mathematical models of avascular tumor growth. *SIAM Review*, 49:179–208, 2007.

[577] T. Roose, P. Netti, L. Munn, Y. Boucher, and R. Jain. Solid stress generated by spheroid growth using a linear poroelastic model. *Microvascular Res.*, 66:204–212, 2003.

[578] B. Rubenstein and L. Kaufman. The role of extracellular matrix in glioma invasion: A cellular potts model approach. *Biophys. J.*, 95:5661–5680, 2008.

[579] J. Rubenstein, J. Kim, T. Ozawa, K. Zhang, M. Westphal, D. Deen, and M. Shuman. Anti-vegf antibody treatment of glioblastoma prolongs survival but results in increased vascular cooption. *Neoplasia*, 2:306–314, 2000.

[580] K. Rygaard and M. Spang-Thomsen. Quantitation and gompertzian analysis of tumor growth. *Breast Cancer Res. Treat.*, 46:303–312, 1997.

[581] Y. Saad and M. Schultz. Gmres: A generalized minimal residual algorithm for solving nonsymmetric linear systems. *SIAM J. Sci. Stat. Comput.*, 7:856–869, 1986.

[582] E. Sahai. Mechanisms of cancer cell invasion. *Curr. Opin. Genet. Dev.*, 15:87–96, 2005.

[583] T. Sairanen, R. Szepesi, M.-L. Karjalainen-Lindsberg, J. Saksi, A. Paetau, and P. J. Lindsberg. Neuronal caspase-3 and PARP-1 correlate differentially with apoptosis and necrosis in ischemic human stroke. *Acta Neuropathologica*, 118(4):541–52, 2009.

[584] G. Sakamoto. Infiltrating carcinoma: major histological types. In D. Page and T. Anderson, editors, *Diagnostic Histopathology of the Breast*. Churchill-Livingstone, London, 1987.

[585] M. E. Sanders, P. A. Schuyler, W. D. Dupont, and D. L. Page. The natural history of low-grade ductal carcinoma in situ of the breast in women treated by biopsy only

revealed over 30 years of long-term follow-up. *Cancer*, 103(12):2481–4, 2005.

[586] S. Sanga, M. E. Edgerton, P. Macklin, and V. Cristini. From receptor dynamics to directed cell motion: A predictive multiscale model of cell motility in complex microenvironments. in press, 2009.

[587] S. Sanga, H. Frieboes, X. Zheng, R. Gatenby, E. Bearer, and V. Cristini. Predictive oncology: a review of multidisciplinary, multiscale in silico modeling linking phenotype, morphology and growth. *NeuroImage*, 37:S120–S134, 2007.

[588] S. Sanga, J. Sinek, H. Frieboes, M. Ferrari, J. Fruehauf, and V. Cristini. Mathematical modeling of cancer progression and response to chemotherapy. *Expert Rev. Anticancer Ther.*, 6:1361–1376, 2006.

[589] B. Sansone, P. D. Santo, M. Magnano, and M. Scalerandi. Effects of anatomical constraints on tumor growth. *Phys. Rev. E*, 64:21903, 2002.

[590] B. Sansone, M. Scalerandi, and C. Condat. Emergence of taxis and synergy in angiogenesis. *Phys. Rev. Lett.*, 87:128102, 2001.

[591] M. Santini, G. Rainaldi, and P. Indovina. Apoptosis, cell adhesion and the extracellular matrix in three-dimensional growth of multicellular tumor spheroids. *Crit. Rev. Oncol. Hematol.*, 36:75–87, 2000.

[592] M. Sarntinoranont, F. Rooney, and M. Ferrari. Interstitial stress and fluid pressure within a growing tumor. *Ann. Biomed. Eng.*, 31:327–335, 2003.

[593] J. Satulovsky, R. Lui, and Y. L. Wang. Exploring the control circuit of cell migration by mathematical modeling. *Biophys. J.*, 94(9):3671–83, 2008.

[594] N. Savill and P. Hogeweg. Modeling morphogenesis: From single cells to crawling slugs. *J. Theor. Biol.*, 184:229–235, 1997.

[595] J. L. Scarlett, P. W. Sheard, G. Hughes, E. C. Ledgerwood, H.-K. Ku, and M. P. Murphy. Changes in mitochondrial membrane potential during staurosporine-induced apoptosis in Jurkat cells. *FEBS Letters*, 475(3):267–72, 2000.

[596] J. Schlessinger. Ligand-induced, receptor-mediated dimerization and activation of EGF receptor. *Cell*, 110(6):669–72, 2002.

[597] K. Schmeichel, V. Weaver, and M. Bissel. Structural cues from the tissue microenvironment are essential determinants of the human mammary epithelial cell phenotype. *J. Mammary Gland Biol. Neoplasia*, 3:201–213, 1998.

[598] L. S. Schulman and P. E. Seiden. Statistical mechanics of a dynamical system based on conway's game of life. *J. Stat. Phys.*, 19(3):293–314, 1978.

[599] E. Seftor, P. Meltzer, D. Kirshmann, J. Pe'er, A. Maniotis, J. Trent, R. Folberg, and M. Hendrix. Molecular determinants of human uveal melanoma invasion and metastasis. *Clin. Exp. Metastasis*, 19:233–246, 2002.

[600] M. J. Seidensticker and J. Behrens. Biochemical interactions in the wnt pathway. *Biochim. Biophys. Acta*, 1495:168–82, 2000.

[601] B. Selam, U. A. Kayisli, J. A. Garcia-Velasco, and A. Arici. Extracellular matrix-dependent regulation of FAS ligand expression in human endometrial stromal cells. *Biol. Reprod.*, 66(1):1–5, 2002.

[602] G. L. Semenza. HIF-1, O_2, and the 3 PHDs: How animal cells signal hypoxia to the nucleus. *Cell*, 107(1):1–3, 2001.

[603] G. Serini, D. Ambrosi, E. Giraudo, A. Gamba, L. Preziosi, and F. Bussolino. Modeling the early stages of vascular network assembly. *EMBO J.*, 22:1771–1779, 2003.

[604] S. Setayeshgar, C. Gear, H. Othmer, and I. Kevrekidis. Application of coarse integration to bacterial chemotaxis. *SIAM Multiscale Model. Sim.*, 4:307–327, 2005.

[605] J. A. Sethian. *Level Set Methods and Fast Marching Methods*. Cambridge University Press, New York, NY, 1999.

[606] J. A. Sethian and P. Smereka. Level set methods for fluid interfaces. *Ann. Rev. of Fluid Mech.*, 35(1):341–372, 2003.

[607] M. Shannon and B. Rubinsky. The effect of tumor growth on the stress distribution in tissue. *Adv. Biol. Heat Mass Transfer*, 231:35–38, 1992.

[608] N. Sharifi, B. T. Kawasaki, E. M. Hurt, and W. L. Farrar. Stem Cells in Prostate Cancer: Resolving the Castrate-Resistant Conundrum and Implications for Hormonal Therapy. *Cancer Biol. Ther.*, 5(8):910–906, 2006.

[609] C. J. Sherr. Cancer Cell Cycles. *Science*, 274(5293):1672–1677, 1996.

[610] J. Sherratt. Traveling wave solutions of a mathematical model for tumor encapsulation. *SIAM J. Appl. Math.*, 60:392–407, 1999.

[611] J. Sherratt and M. Chaplain. A new mathematical model for avascular tumour growth. *J. Math. Biol.*, 43:291–312, 2001.

[612] A. N. Shiryaev. *Probability*. Springer, New York, NY, 2nd edition, 1995.

[613] B. I. Shraiman. Mechanical feedback as a possible regulator of tissue growth. *Proc. Natl. Acad. Sci. USA*, 102(9):3318–23, 2005.

[614] C.-W. Shu and S. Osher. Efficient implementation of essentially non-oscillatory shock-capturing schemes. *J. Comput. Phys.*, 77:439–471, 1988.

[615] C.-W. Shu and S. Osher. Efficient implementation of essentially non-oscillatory shock capturing schemes, II. *J. Comput. Phys.*, 83:32–78, 1989.

[616] D. Shweiki, A. Itin, D. Soffer, and E. Keshet. Vascular endothelial growth factor induced by hypoxia may mediate hypoxia-initiated angiogenesis. *Nature*, 359:843–845, 1992.

[617] A. Sierra. Metastases and their microenvironments: linking pathogenesis and therapy. *Drug Resist. Updates*, 8:247–257, 2005.

[618] S. A. Silver and F. A. Tavassoli. Ductal carcinoma in situ with microinvasion. *Breast J.*, 4(5):344–8, 1998.

[619] M. J. Silverstein. Predicting residual disease and local recurrence in patients with ductal carcinoma in situ. *J. Natl. Cancer Inst.*, 89(18):1330–1, 1997.

[620] M. J. Silverstein. Recent advances: diagnosis and treatment of early breast cancer. *BMJ*, 314(7096):1736ff, 1997.

[621] M. J. Silverstein. Ductal carcinoma in situ of the breast. *Annu. Rev. Med.*, 51:17–32, 2000.

[622] P. T. Simpson, J. S. Reis-Filho, T. Gale, and S. R. Lakhani. Molecular evolution of breast cancer. *J. Pathol.*, 205(2):248–54, 2005.

[623] J. Sinek, H. Frieboes, X. Zheng, and V. Cristini. Two-dimensional chemotherapy simulations demonstrate fundamental transport and tumor response limitations involving nanoparticles. *Biomedical Microdevices*, 6:297–309, 2004.

[624] J. Sinek, S. Sanga, X. Zheng, H. Frieboes, M. Ferrari, and V. Cristini. Predicting drug pharmacokinetics and effect in vascularized tumors using computer simulation. *J. Math. Biol.*, 58:485–510, 2009.

[625] S. Skinner. Microvascular architecture of experimental colon tumors in the rat. *Cancer Res.*, 50:2411–2417, 1990.

[626] V. I. F. Slettenaar and J. L. Wilson. The chemokine network: A target in cancer biology? *Adv. Drug Deliv. Rev.*, 58(8):962–974, 2006.

[627] K. Smallbone, R. Gatenby, R. Gillies, P. Maini, and D. Gavaghan. Metabolic changes during carcinogenesis: Potential impact on invasiveness. *J. Theor. Biol.*, 244:703–713,

2007.

[628] K. Smallbone, R. Gatenby, and P. Maini. Mathematical modelling of tumour acidity. *J. Theor. Biol.*, 255:106–112, 2008.

[629] K. Smallbone, D. Gavaghan, R. Gatenby, and P. Maini. The role of acidity in solid tumor growth and invasion. *J. Theor. Biol.*, 235:476–484, 2005.

[630] K. Smallbone, D. Gavaghan, P. Maini, and J. M. Brady. Quiescence as a mechanism for cyclical hypoxia and acidosis. *J. Math. Biol.*, 55:767–779, 2007.

[631] S. A. A. Sohaib and R. H. Reznek. MR imaging in ovarian cancer. *Canc. Img.*, 7(Special Issue A):S119–29, 2007.

[632] V. Spencer, R. Xu, and M. Bissell. Extracellular matrix, nuclear and chromatin structure, and gene expression in normal tissues and malignant tumors: a work in progress. *Adv. Cancer Res.*, 97:275–294, 2007.

[633] T. A. Springer. Adhesion receptors of the immune system. *Nature*, 346(6283):425–34, 1990.

[634] P. Steeg. Angiogenesis inhibitors: motivators of metastasis? *Nature Med.*, 9:822–823, 2003.

[635] A. Stein, T. Demuth, D. Mobley, M. Berens, and L. Sander. A mathematical model of glioblastoma tumor spheroid invasion in a three-dimensional in vitro experiment. *Biophys. J.*, 92:356–365, 2007.

[636] M. S. Steinberg and M. Takeichi. Experimental specification of cell sorting, tissue spreading, and specific spatial patterning by quantitative differences in cadherin expression. *Proc. Natl. Acad. Sci. USA*, 91:206–9, 1994.

[637] A. Stephanou, S. McDougall, A. Anderson, and M. Chaplain. Mathematical modelling of flow in 2d and 3d vascular networks: Applications to anti-angiogenic and chemotherapeutic drug strategies. *Math. Comput. Model.*, 41:1137–1156, 2005.

[638] A. Stephanou, S. McDougall, A. Anderson, and M. Chaplain. Mathematical modelling of the influence of blood rheological properties upon adaptative tumour-induced angiogenesis. *Math. Comput. Model.*, 44:96–123, 2006.

[639] J. Stewart, P. Broadbridge, and J. Goard. Symmetry analysis and numerical modelling of invasion by malignant tumour tissue. *Nonlinear Dyn.*, 28:175–193, 2002.

[640] C. Stokes and D. Lauffenburger. Analysis of the roles of microvessel endothelial cell random motility and chemotaxis in angiogenesis. *J. Theor. Biol.*, 152:377–403, 1991.

[641] P. C. Stomper and F. R. Margolin. Ductal carcinoma in situ: the mammographer's perspective. *Am. J. Roentgenology*, 162:585–91, 1994.

[642] E. Stott, N. Britton, J. Glazier, and M. Zajac. Simulation of benign avascular tumour growth using the potts model. *Math. Comput. Model.*, 30:183–198, 1999.

[643] D. Stupack and D. Cheresh. Get a ligand, get a life: Integrins, signaling and cell survival. *J. Cell. Sci.*, 115:3729–3738, 2002.

[644] C. Sun and L. Munn. Lattice-boltzmann simulation of blood flow in digitized vessel networks. *Comp. and Math. Appl.*, 55:1594–1600, 2008.

[645] S. Sun, M. Wheeler, M. Obeyesekere, and C. P. Jr. A deterministic model of growth factor-induced angiogenesis. *Bull. Math. Biol.*, 67:313–337, 2005.

[646] S. Sun, M. Wheeler, M. Obeyesekere, and C. P. Jr. Multiscale angiogenesis modeling using mixed finite element methods. *Multiscale Model. Simul.*, 4:1137–1167, 2005.

[647] X.-F. Sun and H. Zhang. Clinicopathological significance of stromal variables: angiogenesis, lymphangiogenesis, inflammatory infiltration, MMP and PINCH in colorectal carcinomas. *Mol. Cancer*, 5:43, 2006.

[648] K. Sundfor, H. Lyng, and E. Rofstad. Tumour hypoxia and vascular density as predictors of metastasis in squamous cell carcinoma of the uterine cervix. *Br. J. Cancer*, 78:822–827, 1998.

[649] M. Sussman, P. Smereka, and S. Osher. A level set approach for computing solutions to incompressible two-phase flow. *J. Comput. Phys.*, 114(1):146–159, 1994.

[650] R. Sutherland. Cell and environment interactions in tumor microregions: the multicell spheroid model. *Science*, 240:177–184, 1988.

[651] R. Sutherland, J. Carlsson, R. Durand, and J. Yuhas. Spheroids in cancer research. *Cancer Res.*, 41:2980–2994, 1981.

[652] K. Swanson, C. Bridge, J. Murray, and E. A. Jr. Virtual and real brain tumors: Using mathematical modeling to quantify glioma growth and invasion. *J. Neuro. Sci.*, 216:1–10, 2003.

[653] L. A. Taber. An optimization principle for vascular radius including the effects of smooth muscle tone. *Biophys. J.*, 74(1):109–114, 1998.

[654] P. J. Tannis, O. E. Nieweg, R. A. Valdés Olmos, and B. B. R. Kroon. Anatomy and physiology of lymphatic drainage of the breast from the perspective of sentinel node biopsy. *J. Am. Coll. Surg.*, 192(3):399–409, 2001.

[655] Y. Tao and M. Chen. An elliptic-hyperbolic free boundary problem modelling cancer therapy. *Nonlinearity*, 19:419–440, 2006.

[656] Y. Tao, N. Yoshida, and Q. Guo. Nonlinear analysis of a model of vascular tumour growth and treatment. *Nonlinearity*, 17:867–895, 2004.

[657] M. J. Terol, M. Tormo, J. A. Martinez-Climent, I. Marugan, I. Benet, A. Ferrandez, A. Teruel, R. Ferrer, and J. Garcia-Conde. Soluble intercellular adhesion molecule-1 (s-ICAM-1/s-CD54) in diffuse large B-cell lymphoma: association with clinical characteristics and outcome. *Ann. Oncol.*, 14(3):467–74, 2003.

[658] R. Thomlinson and L. Gray. The histological structure of some human lung cancers and the possible implications of radiotherapy. *Br. J. Cancer*, 9:539–549, 1955.

[659] B. Thorne, A. Bailey, and S. Peirce. Combining experiments with multi-cell agent-based modeling to study biological tissue patterning. *Briefings in Bioinformatics*, 8:245–257, 2007.

[660] M. Tindall, C. Please, and M. Peddie. Modelling the formation of necrotic regions in avascular tumours. *Math. Biosci.*, 211:34–55, 2008.

[661] S. Tong and F. Yuan. Numerical simulations of angiogenesis in the cornea. *Microvasc. Res.*, 61:14–27, 2001.

[662] A. Tosin. Multiphase modeling and qualitative analysis of the growth of tumor cords. *Networks Heterogen. Media*, 3:43–84, 2008.

[663] A. Tosin, D. Ambrosi, and L. Preziosi. Mechanics and chemotaxis in the morphogenesis of vascular networks. *Bull. Math. Biol.*, 68:1819–1836, 2006.

[664] P. Tracqui. Biophysical models of tumor growth. *Rep. Prog. Phys.*, 72:056701, 2009.

[665] U. Trottenberg, C. Oosterlee, and A. Schüller. *Multigrid*. Academic Press, New York, 2005.

[666] C. Truesdell and R. Toupin. Classical field theories. In S. Flugge, editor, *Handbuch der Physik, Vol III/I*. Springer-Verlag, Berlin, 1960.

[667] S. Turner and J. Sherratt. Intercellular adhesion and cancer invasion: A discrete simulation using the extended potts model. *J. Theor. Biol.*, 216:85–100, 2002.

[668] B. Tysnes and R. Mahesparan. Biological mechanisms of glioma invasion and potential therapeutic targets. *J. Neurooncol.*, 53:129–147, 2001.

[669] P. Vajkoczy, M. Farhadi, A. Gaumann, R. Heidenreich, R. Erber, A. Wunder, J.C., M. M. Tonn, and G. Breier. Microtumor growth initiates angiogenic sprouting with simultaneous expression of vegf, vegf receptor-2, and angiopoietin-2. *J. Clin. Invest.*, 109:777–785, 2002.

[670] L. van Kempen, D. Ruiter, G. van Muijen, and L. Coussens. The tumor microenvironment: a critical determinant of neoplastic evolution. *Eur. J. Cell. Biol.*, 82:539–548, 2003.

[671] I. van Leeuwen, C. Edwards, M. Ilyas, and H. Byrne. Towards a multiscale model of colorectal cancer. *World Gastroenterol.*, 13:1399–1407, 2007.

[672] V. V. Vasko and M. Saji. Molecular mechanisms involved in differentiated thyroid cancer invasion and metastasis. *Curr. Opin. Oncol.*, 19(1):11–17, 2007.

[673] P. Vaupel, H. Haugland, T. Nicklee, A. Morrison, and D. Hedley. Hypoxia-inducible factor-1 alpha is an intrinsic marker for hypoxia in cervical cancer xenografts. *Cancer Res.*, 61:7394–7398, 2001.

[674] R. Vernon, J. Angello, M. Iruela-Arispe, and T. Lane. Reorganization of basement membrane matrices by cellular traction promotes the formation of cellular networks in vitro. *Lab. Invest.*, 66:536–547, 1992.

[675] E. Villa-Cuesta, E. Gonz/'alez-P/'erez, and J. Modolell. Apposition of *iroguois* expressing and non-expressing cells leads to cell sorting and fold formation in *Drosphila* imaginal wing disc. *BMC Devel. Biol.*, 7(106), 2007.

[676] B. Vollmayr-Lee and A. Rutenberg. Stresses in growing soft tissues. *Acta Biomaterialia*, 2:493–504, 2006.

[677] J. von Neumann. *Theory of Self-Replicating Automata*. University of Illinois Press, 1966. Edited by Arthur W. Burks.

[678] C. Walker and G. Webb. Global existence of classical solutions for a haptotaxis model. *SIAM J. Math. Anal.*, 38(5):1694–1713, 2007.

[679] T. Walles, M. Weimer, K. Linke, J. Michaelis, and H. Mertsching. The potential of bioartificial tissues in oncology research and treatment. *Onkologie*, 30:388–394, 2007.

[680] R. Wang, L. Jinming, K. Lyte, N. K. Yashpal, F. Fellows, and C. G. Goodyer. Role for $\beta 1$ integrin and its associated $\alpha 3$, $\alpha 5$, and $\alpha 6$ subunits in development of the human fetal pancreas. *Diabetes*, 54:2080–9, 2005.

[681] Z. Wang, L. Zhang, J. Sagotsky, and T. Deisboeck. Simulating non-small cell lung cancer with a multiscale agent-based model. *Theor. Biol. Med. Model.*, 4:50, 2007.

[682] J. Ward and J. King. Mathematical modelling of avascular tumour growth. *IMA J. Math. Appl. Medicine Biol.*, 14:36–69, 1997.

[683] J. Ward and J. King. Mathematical modelling of avascular-tumour growth ii: modelling growth saturation. *Math. Med. Biol.*, 16:171–211, 1999.

[684] J. Ward and J. King. Modelling the effect of cell shedding on avasacular tumour growth. *J. Theor. Med.*, 2:155–174, 2000.

[685] J. Ward and J. King. Mathematical modelling of drug transport in tumour multicell spheroids and monolayer cultures. *Math. Biosci.*, 181:177–207, 2003.

[686] R. Wcislo and W. Dzwinel. Particle based model of tumor progression stimulated by the process of angiogenesis. In J. Adam and N. Bellomo, editors, *Computational Science - ICCS 2008*, pages 177–186. Springer, Heidelberg, 2008.

[687] A. M. Weaver. Invadopodia: specialized cell structures for cancer invasion. *Clin. Exp. Metastasis*, 23(2):97–105, 2006.

[688] C. Wei, M. Larsen, M. P. Hoffman, and K. M. Yamada. Self-organization and branching morphogenesis of primary salivary epithelial cells. *Tissue Eng.*, 13(4):721–35, 2007.

[689] O. D. Weiner, W. A. Marganski, L. F. Wu, S. J. Altschuler, and M. W. Kirschner. An actin-based wave generator organizes cell motility. *PLoS Biol*, 5(9):e221, 08 2007.

[690] S. R. Wellings, H. M. Jensen, and R. G. Marcum. An atlas of subgross pathology of the human breast with special reference to possible precancerous lesions. *J. Natl. Cancer Inst.*, 55(2):231–73, 1975.

[691] A. Wells, B. Harms, A. Iwabu, L. Koo, K. Smith, L. Griffith, et al. Motility signaled from the EGF receptor and related systems. *Meth. Mol. Biol.*, 327:159–77, 2006.

[692] A. Wells, J. Kassis, J. Solava, T. Turner, and D. A. Lauffenburger. Growth factor-induced cell motility in tumor invasion. *Acta Oncol.*, 41(2):124–30, 2002.

[693] M. Welter, K. Bartha, and H. Rieger. Emergent vascular network inhomogeneities and resulting blood flow patterns in a growing tumor. *J. Theor. Biol.*, 250:257–80, 2008.

[694] M. Welter, K. Bartha, and H. Rieger. Hot spot formation in tumor vasculature during tumor growth in an arterio-venous-network environment. arXiv.org ¿ q-bio ¿ arXiv:0801.0654v2, 2008.

[695] N. Wentzensen, S. Vinokurova, and M. von Knebel Doeberitz. Systematic review of genomic integration sites of human papillomavirus genomes in epithelial dysplasia and invasive cancer of the female lower genital tract. *Canc. Res.*, 64(11):3878–84, 2004.

[696] K. Wiesenfeld and F. Moss. Stochastic resonance and the benefits of noise: from ice ages to crayfish and squids. *Nature*, 373:33, 1995.

[697] H. S. Wiley, S. Y. Shvartsman, and D. A. Lauffenburger. Computational modeling of the EGF-receptor system: a paradigm for systems biology. *Trends Cell. Biol.*, 13(1):43–50, 2003.

[698] S. Wise, J. Kim, and J. Lowengrub. Solving the regularized, strongly anisotropic Cahn-Hilliard equation by an adaptive nonlinear multigrid method. *J. Comput. Phys.*, 226:414–446, 2007.

[699] S. Wise, J. Lowengrub, and V. Cristini. An adaptive algorithm for simulating solid tumor growth using mixture models. in prep.

[700] S. Wise, J. Lowengrub, H. Frieboes, and V. Cristini. Three-dimensional multispecies nonlinear tumor growth– i. model and numerical method. *J. Theor. Biol.*, 253:524–543, 2008.

[701] E. K. Wolf, A. C. Smidt, and A. E. Laumann. Topical sodium thiosulfate therapy for leg ulcers with dystrophic calcification. *Arch. Dermatol.*, 144(12):1560–2, 2008.

[702] K. Wolf and P. Friedl. Molecular mechanisms of cancer cell invasion and plasticity. *Br. J. Dermatology*, 154:11–15, 2006.

[703] K. Wolf, R. Müller, S. Borgmann, E.-B. Bröcker, and P. Friedl. Amoeboid shape change and contact guidance: T-lymphocyte crawling through fibrillar collagen is independent of matrix remodeling by MMPs and other proteases. *Blood*, 102(9):3262–9, 2003.

[704] J. Wu and S. Cui. Asymptotic behavior of solutions of a free boundary problem modeling the growth of tumors with stokes equations. *Discr. Contin. Dyn. Sys.*, 24(2):625–51, 2009.

[705] J. Wu, F. Zhou, and S. Cui. Simulation of microcirculation in solid tumors. *IEEE/ICME Int. Conf. on Complex Med. Eng.*, pages 1555–1563, 2007.

[706] M. Wurzel, C. Schaller, M. Simon, and A. Deutsch. Cancer cell invasion of brain tissue: guided by a prepattern? *J. Theor. Medicine*, 6:21–31, 2005.

[707] Y. Xiong, P. Rangamani, B. Dubin-Thaler, M. Sheetz, and R. Iyengar. A three-dimensional stochastic spatio-temporal model of cell spreading. *Nat. Proc.*, 2007. Available from Nature Proceedings: http://10.1038/npre.2007.62.2.

[708] R. Xu, V. Spencer, and M. Bissell. Extracellular matrix-regulated gene expression requires cooperation of swi/snf and transcription factors. *J. Biol. Chem.*, 282:14992–14999, 2007.

[709] S. Xu. Hopf bifurcation of a free boundary problem modeling tumor growth with two time delays. *Chaos Solitons Fractals*, 41(5):2491–4, 2009.

[710] Y. Xu and R. Gilbert. Some inverse problems raised from a mathematical model of ductal carcinoma in situ. *Math. Comp. Model.*, 49(3-4):814–28, 2009.

[711] H. Yamaguchi, J. Wyckoff, and J. Condeelis. Cell migration in tumors. *Curr. Op. Cell Biol.*, 17:559–564, 2005.

[712] K. Yamauchi, M. Yang, P. Jiang, M. Xu, N. Yamamoto, H. Tsuchiya, K. Tomita, A. R. Moossa, M. Bouvet, and R. M. Hoffman. Development of real-time subcellular dynamic multicolor imaging of cancer-cell trafficking in live mice with a variable-magnification whole-mouse imaging system. *Canc. Res.*, 66:4028–4214, 2006.

[713] S. Young and R. Hill. Effects of reoxygenation of cells from hypoxic regions of solid tumors: anticancer drug sensitivity and metastatic potential. *J. Natl. Cancer Inst.*, 82:338–339, 1990.

[714] S. Young, R. Marshall, and R. Hill. Hypoxia induces dna overreplication and enhances metastatic potential of murine tumor cells. *Proc. Natl. Acad. Sci. USA*, 85:9533–9537, 1988.

[715] J. Yu, J. Rak, B. Coomber, D. Hicklin, and R. Kerbel. Effect of p53 status on tumor response to antiangiogenic therapy. *Science*, 295:1526–1528, 2002.

[716] A. Zagorska and J. Dulak. HIF-1: the knowns and unknowns of hypoxia sensing. *Acta Biochimica Polonica*, 51(3):563–585, 2004.

[717] D. Zagzag, A. R., M. Greco, H. Yee, J. Holash, S. Wiegand, S. Zabski, G. Yancopoulos, and M. Grumet. Vascular apoptosis and involution in gliomas precede neovascularization: a novel concept for glioma growth and angiogenesis. *Lab. Invest.*, 80:837–849, 2000.

[718] M. Zajac, G. Jones, and J. Glazier. Model of convergent extension in animal morphogenesis. *Phys. Rev. Lett.*, 85:2022–2025, 2000.

[719] M. H. Zaman, R. D. Kamm, P. Matsudaira, and D. A. Lauffenburger. Computational model for cell migration in three-dimensional matrices. *Biophys. J.*, 89(2):1389–97, 2005.

[720] A. Zetterberg, O. Larsson, and K. G. Wilman. What is the restriction point? *Curr. Opin. Cell Biol.*, 7(6):835–842, 1995.

[721] L. Zhang, C. Athale, and T. Deisboeck. Development of a three-dimensional multiscale agent-based tumor model: simulating gene-protein interaction profiles, cell phenotypes and multicellular patterns in brain cancer. *J. Theor. Biol.*, 244:96–107, 2007.

[722] L. Zhang, C. Strouthos, Z. Wang, and T. Deisboeck. Simulating brain tumor heterogeneity with a multiscale agent-based model: Linking molecular signatures, phenotypes and expansion rate. *Math. Comp. Model.*, 49:307–319, 2009.

[723] L. Zhang, Z. Wang, J. Sagotsky, and T. Deisboeck. Multiscale agent-based cancer modeling. *J. Math. Biol.*, 58(4-5):545–59, 2009.

[724] G. Zhao, J. Wu, S. Xu, M. Collins, Q. Long, C. Koenig, Y. Jiang, J. Wang, and A. Padhani. Numerical simulation of blood flow and interstitial fluid pressure in solid

tumor microcirculation based on tumor-induced angiogenesis. *Mech. Sinica*, 23:477–483, 2007.

[725] X. Zheng, S. Wise, and V. Cristini. Nonlinear simulation of tumor necrosis, neovascularization and tissue invasion via an adaptive finite-element/level-set method. *Bull. Math. Biol.*, 67:211–259, 2005.

[726] F. Zhou and S. Cui. Bifurcation for a free boundary problem modeling the growth of multi-layer tumors. *Nonlinear Analysis Theory Meth. Appl.*, 68:2128–2145, 2008.

[727] F. Zhou, J. Escher, and S. Cui. Well-posedness and stability of a free boundary problem modeling the growth of multi-layer tumors. *J. Diff. Eq.*, 244:2909–2933, 2008.

[728] D. Zipori. The mesenchyme in cancer therapy as a target tumor component, effector cell modality and cytokine expression vehicle. *Cancer Metastasis Rev.*, 25(3):459–467, 2006.